DIII–D RESEARCH OPERATIONS

ANNUAL REPORT

OCTOBER 1, 1996
THROUGH
SEPTEMBER 30, 1997

GENERAL ATOMICS

GA–A22827
UC–420

DIII–D RESEARCH OPERATIONS ANNUAL REPORT TO THE U.S. DEPARTMENT OF ENERGY

OCTOBER 1, 1996 THROUGH SEPTEMBER 30, 1997

by
PROJECT STAFF

Work prepared under
Department of Energy
Contract No. DE-AC03-89ER51114
W-7405-ENG-48 and DE-AC05-96OR22464

GENERAL ATOMICS PROJECTS 3466, 3467, 3470, 3473
DATE PUBLISHED: OCTOBER 1998

DISCLAIMER

This report has been reproduced
directly from the best available copy.

Available to DOE and DOE contractors from the
Office of Scientific and Technical Information
P.O. Box 62
Oak Ridge, TN 37831
Prices available from (615) 576-8401,
FTS 626-8401.

Available to the public from the
National Technical Information Service
U.S. Department of Commerce
5285 Port Royal Rd.
Springfield, VA 22161

TABLE OF CONTENTS

LIST OF FIGURES

LIST OF TABLES

1. DIII–D NATIONAL PROGRAM OVERVIEW

The DIII–D National Program is a multi-institutional fusion science research program funded by the U.S. Department of Energy (DOE), and operated by General Atomics (GA). Major research responsibilities are shared by GA, the Lawrence Livermore National Laboratory (LLNL), the Oak Ridge National Laboratory (ORNL), Princeton Plasma Physics Laboratory (PPPL), and groups at the University of California campuses at Los Angeles (UCLA), Irvine (UCI), and San Diego (UCSD). In addition, a large number of U.S. and international collaborators contribute focused scientific and operational expertise. A comprehensive list of collaborators is given in Table 1-1.

TABLE 1-1
DIII–D PROGRAM COLLABORATORS

National Laboratories	Universities	International Laboratories
ANL	Cal Tech	Academia Sinica (China)
INEL	Columbia U.	Cadarache (France)
LANL	Hampton U.	CCFM (Canada)
LLNL	Johns Hopkins U.	Culham (England)
ORNL	Lehigh	FOM (Netherlands)
PNL	MIT	Frascati (Italy)
PPPL	Moscow State U.	Ioffe (Russia)
SNLA	RPI	IPP (Germany)
SNLL	U. Maryland	JAERI (Japan)
	U. Texas	JET (EC)
	U. Washington	KAIST (Korea)
Industry Collaborators	U. Wisconsin	Keldysh Inst. (Russia)
CompX	UCB	KFA (Germany)
CPI (Varian)	UCI	Kurchatov (Russia)
GA	UCLA	Lausanne (Switzerland)
Gycom	UCSD	NIFS (Japan)
Orincon	Ohio State University	TRINITI (Russia)
FARTECH		Southwestern Inst. (China)
		Tsukuba U. (Japan)

1.1. THE DIII–D MISSION

Development of the scientific basis of the fusion energy source for future generations represents a grand challenge for science and offers the prospect of great benefits for mankind. The

strategy for the recently restructured U.S. Fusion Energy Sciences Program focuses on innovation and scientific discovery, strengthens the program's ties to other fields of science, positions the United States to continue playing a meaningful role in the world fusion energy effort within available resources, and preserves the basis for an expanded U.S. Fusion Energy Program when national needs require.

Significant advances have occurred recently in tokamak research. Techniques for producing high temperature plasmas have become routine and reproducible, measurements of plasma internal magnetic and electric fields are now routinely available during experiments, and methods for controlling the plasma current and pressure profiles are being deployed. Transport barriers have reduced ion energy transport to neoclassical levels, plasma pressures have reached magnetohydrodynamic (MHD) theoretical limits, current drive by neoclassical bootstrap currents and radio frequency (rf) current drive are at theoretical levels, and divertor operation with active particle pumping and radiative power dissipation has been demonstrated and modeled with numerical codes. These experimental advances have been observed in discharges for short periods and generally in isolation. However, by using such advances to help build understanding of the underlying processes, tokamak research is developing a capability for truly theory-based discharge manipulation, which is fairly mature in some areas and less so in others.

Within this context, the DIII–D Program mission goal is

> ***To establish the scientific basis for the optimization of the tokamak approach to fusion energy production.***

''Optimization'' means experimentally demonstrating performance parameters at the theoretically predicted limits for the tokamak confinement system and achieving to the greatest degree possible an integrated, steady-state demonstration of optimized performance that projects to an attractive fusion power system. ''Scientific'' means developing a solid understanding of the underlying physical principles and incorporating it into useful predictive modeling tools. The integrated optimization sought and the scientific basis established will allow the definition of optimal paths to fusion energy using the tokamak approach.

The DIII–D Program mission seeks to develop and exploit fusion science to the betterment of the fusion energy goal: demonstrated, scaleable plasma performance; backed up by a firm, comprehensive theoretical model; and achieved in a total configuration that is attractive as an eventual power plant concept. In DIII–D we quantify this goal as sustaining for 10 s a plasma with 5% beta (the ratio of plasma to magnetic field pressure).

The Advanced Tokamak (AT) has been the basic organizing thrust of the DIII–D research program for several years. The AT is now recognized, partially because of early DIII–D successes in this area, as potentially making possible a variety of attractive near-term development steps for magnetic fusion energy. In implementing the new DIII–D Research Plan, we will continue along this path and pursue AT science and integrated performance optimization as the most promising direction for determining the highest potential of the tokamak. Advancing and benchmarking modeling tools will go hand-in-hand with these investigations.

The DIII–D National Program will support the six near-term objectives established by the U.S. fusion community. Primary contributions will be made to two of these objectives:

- Marked progress in scientific understanding and optimization of toroidal plasmas, and
- Improved integrated modeling based on theory and experiments;

as well as secondary, but significant, contributions to the other four objectives:

- Participation in international collaboration to study burning plasma physics and related fusion technologies.
- Strengthened general science and education and connection to other scientific communities.
- Evaluation of several nontokamak fusion approaches.
- Marked progress in understanding technologies and materials for fusion power.

In the newly restructured U.S. Fusion Energy Science Program, DIII–D is called upon "to move toward full, maximally productive utilization, including some upgrades, as a user facility to pursue the rich science to be gained." The role of DIII–D is to advance fusion science, to lead the development of tokamak improvements, to link to our international partners, and to provide critical physics R&D for International Thermonuclear Experimental Reactor (ITER). The plasma physics issues being addressed in DIII–D are aimed at maturing the tokamak knowledge base for future applications, whether tokamaks or alternate concepts. The plasma science also has applications to a wider and broader scientific understanding of natural plasma phenomena, application to other branches of science, and industrial application.

1.2. SUMMARY OF THE 1997 DIII–D EXPERIMENT CAMPAIGN

The main goals of the DIII–D experiments in 1997 were, by extending and integrating the understanding of fusion science, to make progress in the tokamak concept improvements as delineated in the DIII–D Long Range Plan and to make substantial contributions to urgently needed R&D for the ITER Engineering Design Activity. For these purposes, we modified the top divertor to include pumping with baffling of high triangularity shaped plasmas and brought into operation two megawatt-level-gyrotrons for electron cyclotron heating (ECH) and off-axis current drive. The elements of the DIII–D experimental program and its objectives are organized into five topical areas: Stability and Disruption Physics, Transport and Turbulence Physics, Divertor and Boundary Physics, Wave-Particle Physics, and Integrated Fusion Science and Innovative Concept Improvement. The resulting DIII–D fusion science accomplishments are described in detail in this report. Here we give an overview of these and highlight a few.

Substantial progress was made on physics characterization of the two major upgrades to enhance the long-term DIII–D mission: high Triangularity, pumped divertor; and 110 GHz steerable ECH system.

The new high-triangularity (δ), upper pumped, baffled divertor expanded the density range for AT operation. The steady-state density during ELMing H–mode was reduced in the closed (upper) divertor configuration compared to the open (lower) divertor, and the density was further reduced by the pump, achieving a figure of merit, n_e/I_p, of 2.5 (10^{19} m^{-3}/MA). With the pumped and baffled upper single-null divertor, core ionization was reduced substantially (as indicated by

reduced midplane pressure and H-alpha), and partial detachment was observed to occur at ~20% lower line-average density. Also during this "AT+D campaign" the double-null design shape was produced totally under the control of the isoflux control algorithm. Preliminary results indicated similar VH–mode performance in these lower triangularity discharges compared to past higher triangularity reference VH–mode discharges.

ECH experiments with two 110-GHz gyrotrons demonstrated effective electron heating and central current drive. ECH system was operated reliably with power up to 1.2 MW for up to 2.0 s. ECH deposition location is controlled by the steerable antennas, in agreement with ray tracing predictions. The internal loop voltage analysis with motional Stark effect (MSE) diagnostic yielded the central ECCD of 170 kA, which is in agreement with using TORAY code prediction and is similar to the fast wave current drive (FWCD) efficiency (0.03×10^{20} A/W/m^2).

Several paths to extend high performance duration have been explored: internal transport barrier control; benign ELMs; high-l_i; and radiative I–mode.

Slow increase in power during high performance phase of L–mode edge negative central shear (NCS) discharges was used to expand TB slowly and to extend duration of high performance. Strongly negative magnetic shear allowed formation of transport barriers in four transport channels (density, electron and ion temperature, plasma rotation). This shot (92664) showed the steepest internal ion temperature gradient yet seen in a DIII–D discharge, about 300 keV/m, which is bigger by a factor of 2 to 3 than the edge ion temperature gradient in H–mode. In addition, the E×B shearing rate of 2×10^6/s is about 4 times greater than the previous DIII–D record value. The discharge was limited by MHD activities (3/2 modes or sawtooth).

With pumping, ELMing (H–mode edge) NCS discharges achieved $\beta_N \cdot H$ of ~7 for 1 s, where $\beta_N \equiv \beta/(I/aB)$ and H is the ratio of energy confinement to the prediction of ITER–89P L–mode scaling. However, experiments were performed to reduce the impact of ELMs on the plasma through modification of the stability threshold by increasing squareness of the discharge shape. With square plasmas, ELMs were observed to be small and rapid, and the edge pressure gradient was maintained at the first regime ballooning stability limit, as expected. An internal thermal barrier with ELMing H–mode was also demonstrated with the square plasma.

The high-l_i scenario affords edge control by reducing the edge current density. Experiment using the elongation ramp technique obtained $\beta_N \leq 4.5$ with $l_i = 1.4$ to 1.7. The stability of these discharges were limited by low-n MHD modes as q_{min} dropped near 1 rather than large ELMs (X-events). These data are consistent with the $\beta_N \sim 4\ l_i$ operational limit observed for other high-performance discharges (e.g., L– and H–mode edge NCS).

Radiative mantle discharges with enhanced confinement have been obtained in DIII–D. Modest increase in confinement was observed with neon puffing in inner-wall limited discharges (H89P up to 1.5 with $P_{rad}/P_{in} \sim 0.7$ and $n_e/n_G \sim 0.7$), results similar to RI–mode in TEXTOR. More importantly, neon puffing in diverted upper single-null (USN) discharges yielded energy confinement similar to VH–mode but with much higher density, leading to $\beta_N \cdot H$ of ~7 for 0.8 s only limited by premature termination of NBI pulse.

DIII–D has continued strong contributions in all research areas of ITER urgent R&D: disruption mitigation; divertor detachment physics; density limit physics; H–mode power threshold; H–mode core confinement; and finite-β effect.

Disruption experiments indicated the halo current fraction is related to vertical instability growth rates. Since the vertical instability growth rate is predicted to be low in ITER, halo currents on ITER are expected to be significantly lower than predicted by the multimachine halo current database. Methane "killer" pellets provided a well-controlled resistive termination of plasma current without driving runaways, compared with neon killer pellets. These experimental results were used to benchmark the killer pellet radiation model (KPRAD). This model predicts a factor 4 reduction in the local disruption forces in ITER.

H–mode power threshold scaling is different for forward and reverse B_t direction. Although the neoclassical model by Hinton and Staebler fails to predict the B_t scaling, it predicts correct sign changes of gas puff and X-point effects. Sawtooth power can be substantial in P_{th} scaling, and its effects need to be included when interpreting the H–mode power threshold scaling database. Nonsawtooth triggered transitions show weak but positive B_T scaling. Sawtooth triggered L–H transitions show almost linear B_T scaling. Experiments with varying triangularity and plasma density were carried out and contributed to the H–mode edge and ELM/pedestal databases. Energy loss per ELM was found proportional to the change in the pedestal pressure. The pedestal width does not scale with temperature (e.g., gyroradius). A dimensionless pressure scaling predicts favorable edge pedestal temperature (T^{PED} = 5 keV) for ITER.

Divertor studies were highlighted by 2–D spatial distribution of recombination and plasma flow with new plasma flow measurements in detached and attached plasmas.

Density limit studies successfully reproduced the last year's results with more detailed characterization of the termination. Experiment with normal gas fueling exceeded the Greenwald limit (first on DIII–D), and documented MARFEs near Greenwald limit. Double-null configuration has higher gas puff density limit (H–L back transition) than in the single-null configuration.

In the core confinement area, perturbative experiments with ECH modulation tested various theory-based transport models. Preliminary analysis indicates that the Itoh model agrees with the electron response to the modulation, while the IFS/PPPL model agrees with the ion response. The detailed data have been made available to the modeling community. The DIII–D nondimensional (ρ_*) scaling experiment was performed to improve the local transport comparison with JET and Alcator C–Mod along ρ_* scaling path.

In the area of finite β effects, the neoclassical tearing mode stability limit was increased by modifying the plasma shape and current density profile. High triangularity yielded a modest improvement in normalized beta for onset of the 3/2 mode. Maintaining $q(0)$ above 1, eliminating sawteeth, and inducing weak negative magnetic shear increased the threshold for the 3/2 mode.

The national DIII–D program continued to develop new resources and capabilities. A large number of improved diagnostic capabilities implemented before the 1997 campaign led to better physics understanding. One of the highlights in these improvements was the new two-view MSE system which gave direct measurements of E_r and more accurate determination of q-profiles. The remote experiment environment (REE) was demonstrated by conducting DIII–D Physics Run (one day of Helium Campaign) from a remote experimental site (LLNL).

2. FUSION SCIENCE

2.1. CONFINEMENT AND TRANSPORT

This section of the annual report covers work from the Transport and Fluctuations topical area.

2.1.1. CORE TRANSPORT AND CORE FLUCTUATIONS

Two key issues in physics of formation and extension of core transport barriers were the focus of the work in this area this year. First, we attempted to extend the duration of the core barrier phase by tailoring the increase of neutral beam power. The basic idea was to refrain from increasing the input power too rapidly in order to give the transport barrier time to expand; barrier expansion is slow because the diffusivities inside the barrier region are quite small. Second, we studied the effect of strong negative magnetic shear on the formation of a core electron transport barrier and were able to demonstrate such an electron barrier could be created. In general, ion thermal and angular momentum transport barriers are the easiest to create while electron thermal transport barriers are much more difficult to obtain.

As is illustrated in Figs. 2-1 and 2-2, by stepping up the neutral beam heating power at appropriate times, the barrier can be formed in the 2.5 MW injection phase and then expanded

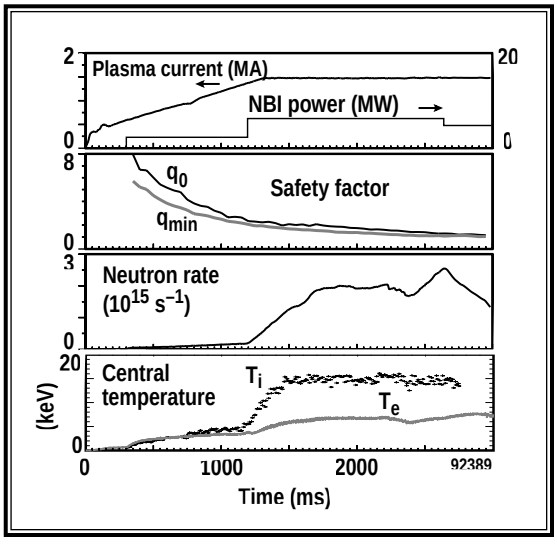

Fig. 2-1. Time evolution of the plasma current, NBI power, central and minimum values of the safety factor (q_0 and q_{min}), neutron rate, and central ion and electron temperatures during an NCS discharge with central toroidal magnetic field of 2.1 T.

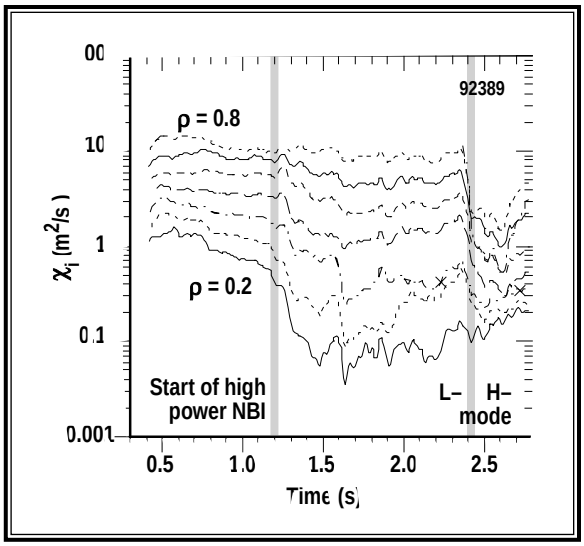

Fig. 2-2. Time and spatial dependence of the ion thermal diffusivity during a time interval bracketing the start of high power NBI. The separate curves are associated with different locations in the plasma separated by 0.1 in ρ space. In this discharge, the NBI is increased from 2.5 to 7.5 MW at t = 1200 ms. Note that the value of χ_i decreases over most of the plasma radius. The plasma current was 1.5 MA and central toroidal magnetic field was 2.1 T.

when the high power phase begins. The ion thermal diffusivity decreases inside $\rho = 0.3$ in the lower power phase, indicating the presence of the transport barrier, and the region of decrease broadens after the power is stepped up. An L-to-H transition late in the shot produces a further decrease in χ_i. A well-formed core ion thermal and angular momentum transport barrier persists for about 1.5 s, with indication of a barrier in the very core for at least 0.5 s before that.

As is shown in Fig. 2-3, the initial barrier formation takes place in a stepwise fashion. Although the steps are quite reproducible from shot to shot, they do not seem to correlate with simple feature of the current profile. For example, there is not a good correlation with either the central q value or the minimum q value passing through integer values. On the other hand, the good reproducibility strongly suggests that they are correlated with a plasma parameter that is similarly reproducible. This might be some other feature of the current profile.

The stepwise formation of the core barrier does correlate with changes in the density fluctuation amplitude seen in the plasma with FIR scattering, as is illustrated in Fig. 2-4. The characteristic wiggles in the electron temperature measured with electron cyclotron emission (ECE) correlate very well with the steps in the ion temperature of the type shown in Fig. 2-3. Many of

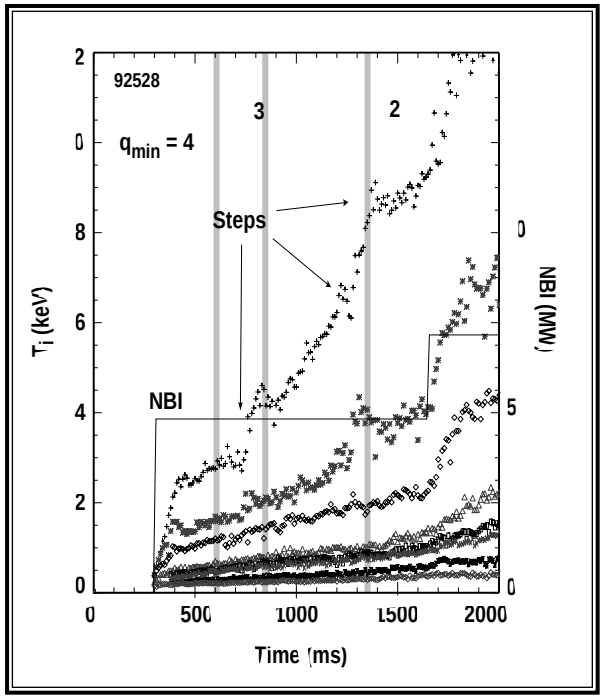

Fig. 2-3. Time evolution of the ion temperature at numerous radii spanning from near the magnetic axis to within 10 cm of the edge during a discharge with plasma current of 1.6 MA and toroidal magnetic field 2.1 T. Note the step-like jumps in the local temperature at various locations in the plasma core. The steps are not generally correlated with times when the minimum value of the safety factor, q_{min}, crosses through low order rational values (m/n < 5), some of which are shown by the gray bars.

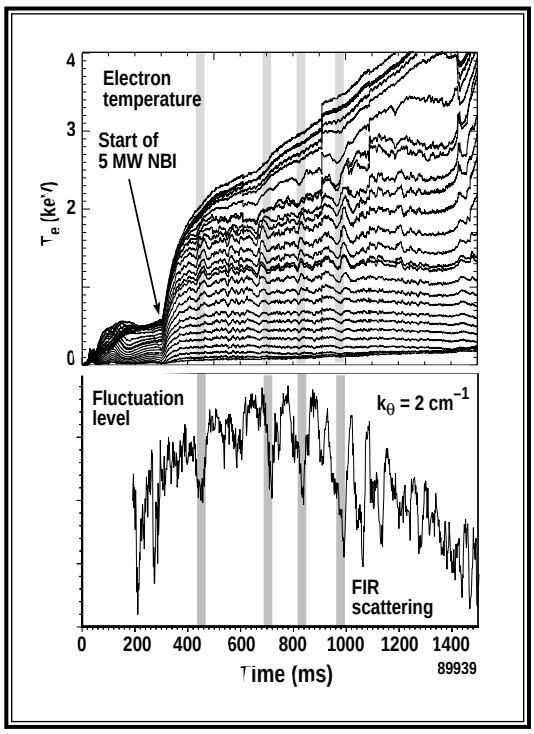

Fig. 2-4. Time evolution of the electron temperature measured at numerous positions from the center outward to the edge, separated by approximately 2 cm, and the interior fluctuation level measured via far-infrared scattering during the low power phase. The time sequence illustrated here is compiled from four consecutive discharges with adjacent time extents. The discontinuities in T_e at 600, 900, and 1100 ms are attributed to slight differences in the discharges. The discharges were nominally identical, with plasma current of 1.6 MA and toroidal magnetic field of 2.1 T.

these features also correlate with the transient decrease in density fluctuations. The connection between density fluctuation reduction and confinement improvement is consistent with the E×B shear stabilization hypothesis which has been used to explain the formation of core and edge transport barriers.

A key puzzle for theories of core transport barrier formation is the difficulty that many machines have had in producing electron thermal transport barriers compared to the relative ease with which ion thermal and angular momentum transport barriers are produced. If one takes a somewhat simplistic view of total turbulence stabilization by E×B shear, for example, then one would expect similar improvements in both transport channels. The experimental observation of significant differences suggests that additional processes are influencing electron thermal transport over and above those modes which are subject to E×B shear stabilization. Speculation has centered on electron temperature gradient-driven turbulence which has too short a spatial scale for the observed E×B shearing rates to affect it.

Based on observations on JT–60U of electron thermal transport barriers in shots with strongly negative magnetic shear, an experiment was performed on DIII–D to see whether such barriers could be produced here also. As is shown in Figs. 2-5 and 2-6, strong negative shear does allow the production of electron thermal barriers. The reduction in the inferred diffusivities in all the transport channels at about the same physical location shown in Fig. 2-6 clearly demonstrates the presence of transport barriers in all four transport channels. A notable difference with the JT–60U results is that the transport barrier is located well inside the minimum in q at the times shown in Figs. 2-5 and 2-6.

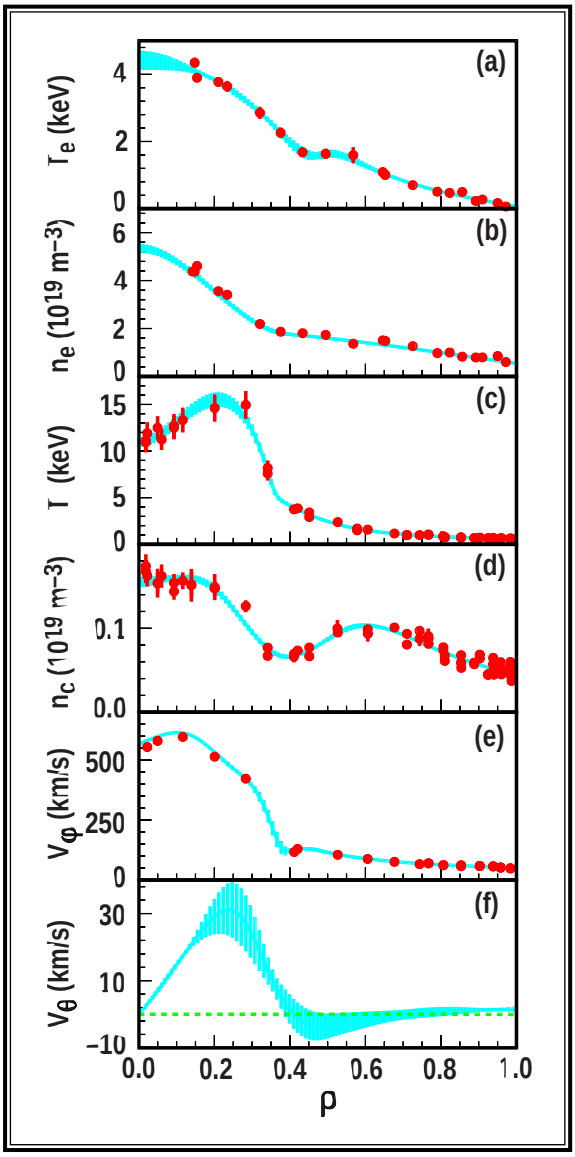

Fig. 2-5. Profiles of plasma parameters at 1000 ms in shot 92664 during the initial current ramp, showing transport barriers in all four transport channels. Notice the extremely steep ion temperature and carbon rotation gradients. (a) Electron temperature, (b) electron density, (c) ion temperature, (d) carbon density, (e) carbon toroidal rotation, (f) carbon poloidal rotation. Basic conditions are toroidal field 2.14 T and plasma current 1.2 MA, dI_p/dt = 0.9 MA/s, beam power 7.5 MW in an upper single-null divertor (SND) with ∇B drift away from the X–point. For quantities that are not consistent on a flux surface (v_ϕ and v_θ), plots are along the outer midplane of the plasma. Vertical bars show error in input data and in spline fits.

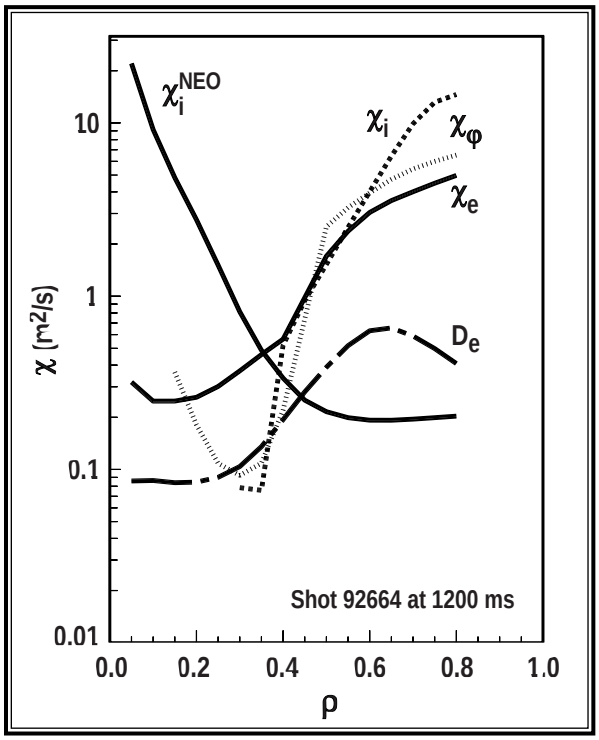

Fig. 2-6. Ion thermal diffusivity χ_i, electron thermal diffusivity χ_e, angular momentum diffusivity χ_ϕ, and electron particle diffusivity D_e determined from power balance analysis for shot 92664 at 1200 ms. This calculation was done using a time-dependent transport analysis with the TRANSP code. Also shown is the Chang-Hinton neoclassical predictions for the ion thermal diffusivity. Note that all the diffusivities show a rapid decrease near $\rho = 0.4$ demonstrating the presence of a transport barrier in all four transport channels.

2.1.2. PARTICLE TRANSPORT

The key experiment in the particle transport area on 1997 involved impurity transport in plasma with core transport barriers. Earlier work on DIII–D in core barrier discharges has demonstrated that electron particle transport in these plasmas could be at the neoclassical level. One of the key predictions of neoclassical impurity transport theory is the preferential peaking impurity densities. This peaking increases as the charge *Z* of the impurity ion increases.

An experiment was conducted to compare the impurity and electron density profiles for various impurities (helium, carbon, neon) in a discharge with a clear core particle transport barrier. The time history of the formation and sustainment of the core transport barrier in this discharge is illustrated in Fig. 2-7. This was one of the types of discharges discussed in the last section which had a core barrier which lasted about 1.5 s. This was long enough for the injected impurities to come to steady state. As is shown in Fig. 2-8, the helium density profile shows no peaking relative to the electron density profile while the peaking is greater for carbon and greater still for neon. This trend is what is expected from neoclassical theory; however, calculations show that the anomalous transport rates needed to quantitatively match the results are still about 5 times the neoclassical rates. The lack of peaking of the helium density relative to electron density shows, for example, that helium exhaust in an AT fusion reactor will be limited by the pumping at the plasma edge rather than the transport in the core.

2.1.3. H–MODE PHYSICS

An active campaign of H–mode experiments and analysis produced several significant results in 1997. (1) The width of the H–mode edge transport barrier was shown to increase with the beta-poloidal at the top of the H–mode edge pedestal, contrary to simple theoretical argument which predicted a scaling with poloidal gyroradius. (2) Work on the H–mode power threshold moved back from the global empiricism associated with ITER scaling needs to more detailed examination of the effect of local parameters, such as the ∇B drift.

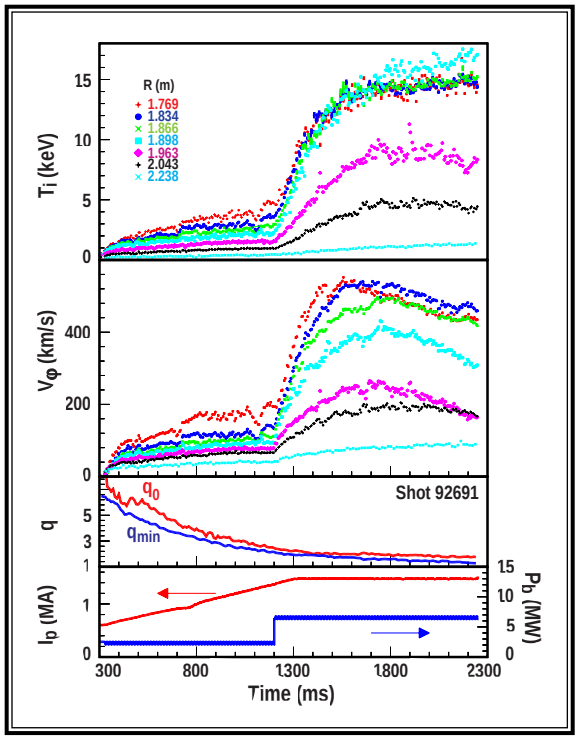

Fig. 2-7. Core ion barriers form in stepwise fashion even at 2.5 MW input power.

Because of the controversy over using theory-based transport models to predict the confinement time in ITER, considerable work was done this year on the structure of the H–mode edge pedestal and how the width of this pedestal scales with plasma parameters. The theory-based models, at present, are totally unable to cope with the physics of the edge transport barrier; accordingly, they use the values at the top of the pedestal as boundary conditions for their calculation. In order to project to future machines accurately, an accurate predictive capability for this pedestal value must be developed.

Extensive studies have shown that a highly sheared radial electric field E_r exists in the H–mode edge transport barrier and considerable theoretical and experimental work suggests that the sheared E_r causes the improved confinement. Because of the complexity of turbulent transport, a predictive model for the height and width of the H–mode transport barrier does not yet exist; the goal of the work was to investigate these empirically.

In order to predict the pedestal density and temperature for various machines, a model was developed which contained several parts. First, work on DIII–D in 1996 has shown that there is a very good correlation between the line-averaged density in H–mode and the density at the top of the H–mode pedestal. Accordingly, if we had a way to predict the pedestal pressure, then the temperature could be derived from that and the density. Theoretically, one expects a limit on the edge pressure gradient dP/dr to be set by infinite-*n* ideal ballooning modes. Since the pressure at the top of the pedestal can be written as $P = \delta \times dP/dr$, a means of predicting the transport barrier width Δ

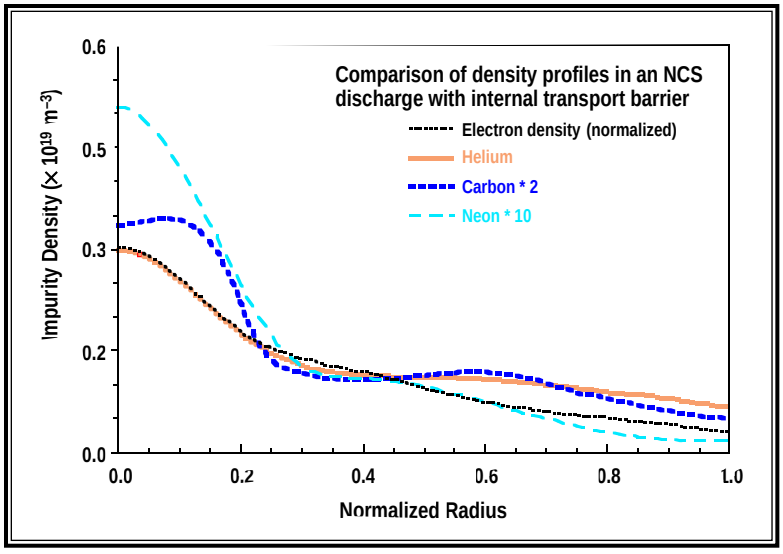

Fig. 2-8. Impurity-dependent accumulation in discharges with an internal transport barrier shows that neoclassical transport is becoming important in these plasmas.

would finish the problem. This is the reason why the studies focused separately on the functional dependence of δ and dP/dr.

For typical conditions, the pedestal values of the electron and ion temperature are comparable. Measurements of both the main ion and the C^{6+} profiles indicate that the edge ion pressure gradient is 50% to 100% of the electron pressure gradient for deuterium plasmas. The studies show that the limiting edge pressure gradient scales with magnetic shear $\hat{s}$ and edge safety factor q in a manner consistent with ballooning mode theory. However, the measured values are typically a factor of 1.5 to 2 above the predictions of the theory for simple edge current density profiles. Calculations done using edge current density profiles consistent with the measured pressure gradients have shown that the edge of these plasmas has access to the second stable ballooning region, indicating that there should be no limit on the edge pressure gradient. It may be that some other mechanism, such as medium-*n* ballooning modes, limits the gradient or that additional physics must be added to the theory of infinite-*n* ballooning modes. One can use the observed pressure gradient scaling, calibrated against experiment, to predict pressure gradients for other machines.

An edge parameter database has been established to look for correlations between the width of the edge pressure pedestal and other edge parameters. The width has a significant correlation only with plasma current, edge pedestal pressure, edge temperature and edge density gradient. Unfortunately, there is also a strong correlation between plasma current and edge density gradient; thus, one of these parameter is probably redundant. By looking not only at the measured values of Δ at a particular time but also at the whole time history during several discharges, it appears that the best empirical relation is

$$\delta / R \propto \left(\beta_p^{ped}\right)^{0.4} ,$$

where R is the device major radius and β_p^{ped} is the poloidal beta value at the top of the pedestal. This scaling is illustrated in Fig. 2-9. Note that the R in this relation is inserted simply to make the left-hand side dimensionless. As long as one scales along a dimensionally similar path, any machine dimension could be used in place of R.

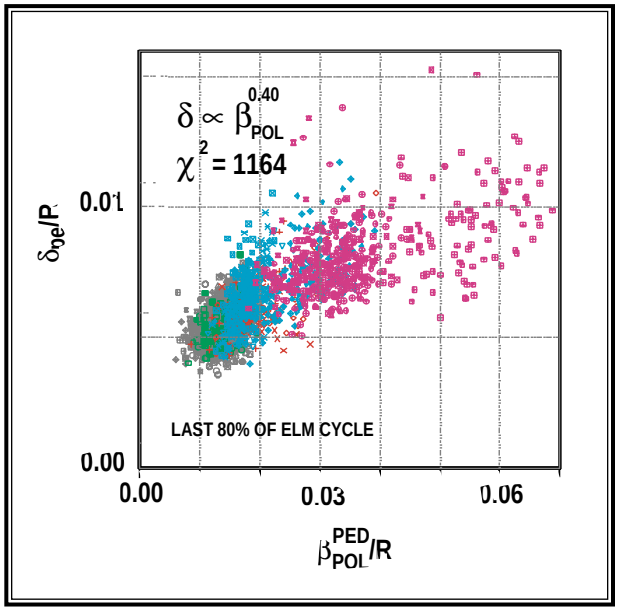

Fig. 2-9. Scaling of edge pedestal width δ with pedestal β_P.

The work on H–mode power thresholds returned to studies of local edge parameters across the L-to-H transition in 1997 after spending several years providing more global information for ITER. Although the key physics of the transport and fluctuation reduction at the L-to-H transition involves the sheared E×B flow at the plasma edge,

studies are now more focused on the plasma conditions needed to start the generation of the edge electric field. We have a number of empirical observations on what machine parameters influence the H–mode power threshold; the key question now is the connection between these control knobs and the actual edge plasma conditions.

One control knob that makes a factor of 2 or 3 difference in the power threshold is the direction of the ion ∇B drift relative to the X–point in SND. As is illustrated in Fig. 2-10, changing the drift from toward to away from the X–point raises the threshold substantially. Because of early work by Hinton and later Hinton and Staebler, we are interested in looking at the connections between poloidal temperature asymmetries just outside the separatrix, caused by neoclassical effects, and the process which triggers the formation of the electric field. An experiment was done this year to study plasma edge conditions for shots with the ∇B drift away from the X–point. The results of this are being combined with earlier detailed edge measurements for cases with the ∇B drift towards the X–point.

As part of this experiment, we also repeated some of our earlier work on the effect of divertor pumping and gas puffing on the H–mode power threshold. In earlier work with the ∇B drift towards the X–point, pumping raised the power threshold while a lower X–point or gas puffing lowered it. Carreras and co-workers at ORNL showed that, because of changes in the scrapeoff layer (SOL), pumping actually increased the density of deuterium neutrals inside the separatrix while gas puffing lowered it. In the present work, as is shown in Fig. 2-10, the sign of the effect is the opposite: a lower X–point and gas puffing raised it. The opposite sign of these effects is consistent with the theoretical ideas, because the sign of the effect of the poloidal asymmetries on the H–mode power threshold reverses when the ∇B drift is reversed.

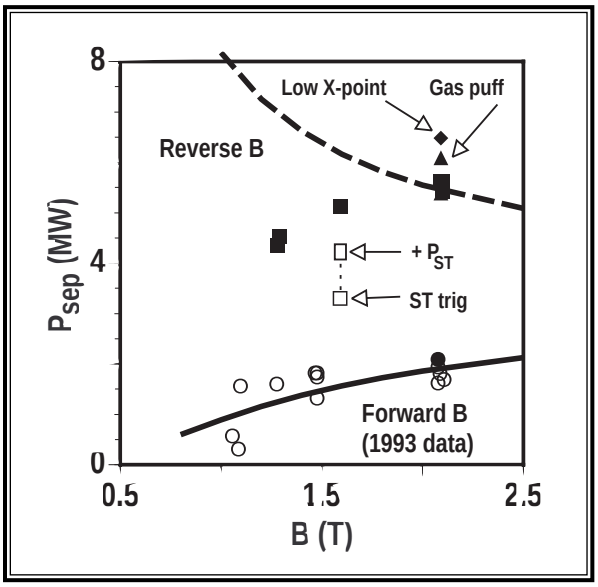

Fig 2-10. Power crossing the separatrix P_{sep} needed to trigger the L-to-H transition in discharges with the ion grad-B drift towards the X–point (Forward B) and away from the X–point (Reverse B) as a function of the magnitude of the toroidal magnetic field BT. Notice that the power required increases substantially. Notice also that the power required increases further when the X–point height above the floor is decreased (Low X–point) or when the gas puff is increased. Finally, all of the Reverse B data except the open square are for transitions where there are no sawtooth oscillations on the plasma. The open square is a sawtooth triggered transition, demonstrating that the sawtooth heat pulse lowers the auxiliary power needed for the transition substantially.

Another effect, made extremely obvious this year, was the effect of sawtooth heat pulses in triggering the L-to-H transition. As is shown in Fig. 2-10, when these triggered the transition, the plasma only required about half as much auxiliary heating to reach H–mode. Processes like this need to be included in the projections for future devices, since some AT modes operate without sawteeth. At present, H–mode power threshold projections for these devices are based on data sets from machines where the transitions almost always have a sawtooth trigger.

2.1.4. NONDIMENSIONAL TRANSPORT STUDIES

The key nondimensional transport work this year involved determining the scaling of local and global transport with the safety factor q. Combining this with the collisionality, beta and gyroradius work done in previous years allows one to determine the size scaling of confinement using data from a single machine. When converted into engineering variables, this gives a global confinement scaling very similar to ITER–93H, but with a more favorable scaling with input power. This suggests that energy confinement in ITER will be better than predicted by the ITER–93H values.

The q scaling experiments were done in two different ways. First, by adjusting the level and timing of NBI heating during the initial phase of the discharge, q was changed by a constant factor while leaving all other nondimensional parameters essentially the same. This method of scaling also insures that the magnetic shear is not changed. The second technique changes the q at the plasma edge while keeping the central q value the same. This is the technique that is usually used when determining the current scaling of confinement. Magnetic shear is not constant in a scan like this.

When q was changed by a constant factor of 1.4, the thermal energy confinement time changed by a factor equivalent to a q scaling of $q^{-2.42\pm0.31}$. As is shown in Fig. 2-11, the changes in the local diffusivities are consistent with this change in global confinement. The change in the one fluid diffusivity is equivalent to a q scaling of $q^{2.3\pm0.64}$.

The scan performed with constant q at the plasma center is more complex to interpret. The global thermal confinement scaling in this case is equivalent to $q^{-1.43\pm0.23}$. This weaker

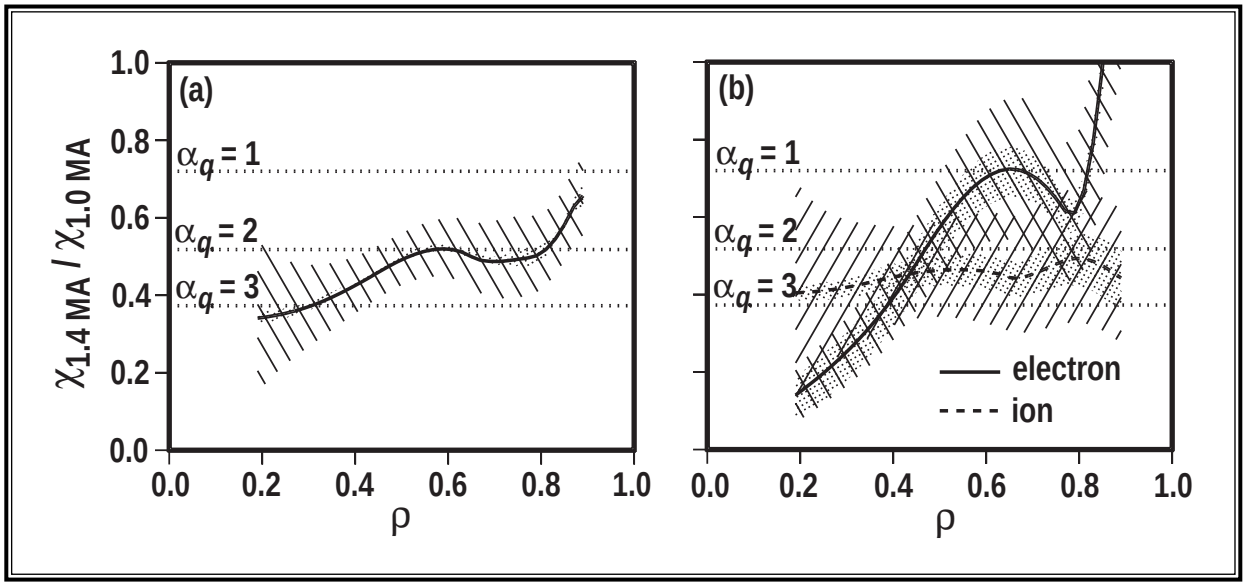

Fig. 2-11. (a) Ratio of effective thermal diffusivities for the 1.4 and 1.0 MA H–mode discharges with fixed magnetic shear. The lined shading indicates the standard deviation of the random error, while the dotted shading indicates the potential effect of systematic error. (b) Ratio of ion and electron thermal diffusivities for the 1.4 and 1.0 MA H–mode discharges with fixed magnetic shear. The lined shading indicates the standard deviation of the random error, while the dotted shading indicates the potential effect of systematic error.

dependence was mainly due to the different way the local value of q changed between the two scans. As is shown in Fig. 2-12, the change in electron and ion thermal diffusivities can be compared to the change expected from just the change in q alone, based on the results shown in Fig. 2-11. The ion thermal diffusivity changes are accounted for by the q change, but the electron thermal diffusivity change is much different than that expected from just the change in q. If this is due to a dependence of electron thermal diffusivity on magnetic shear, then electron heat transport increases with increasing magnetic shear for $\hat{s} < 1$.

By combining the present q scaling results with the beta, collisionality, and gyroradius work done over the last several years, one can produce a complete global confinement scaling. Assuming a power law form for the scaling relation, the dimensionless parameter scaling studies for H–mode plasmas on DIII–D can be summarized as

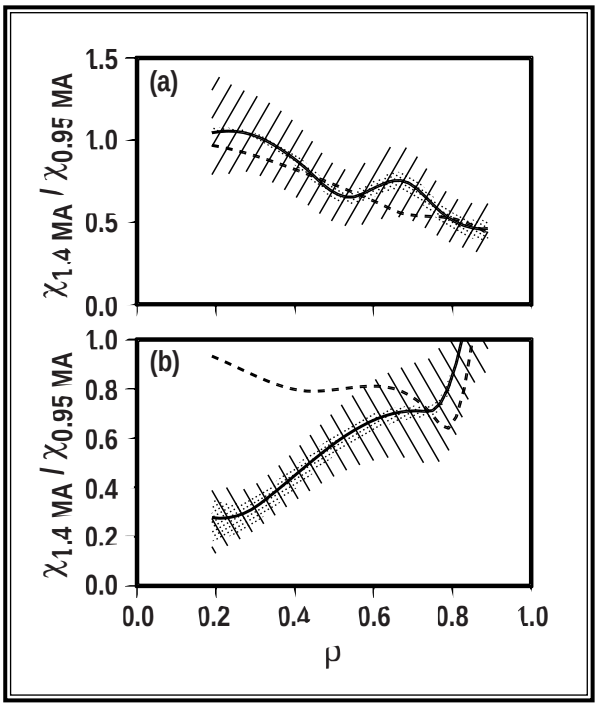

Fig. 2-12. Ratio of (a) ion thermal diffusivities, and (b) electron thermal diffusivities for the 1.4 and 0.95 MA H–mode discharges with fixed q_0. The dashed lines show the expected change in the ratios due to the measured q dependence in Fig. 2.1-11(b).

$$B\tau_{th} \propto \rho_*^{-3.15\pm0.2}\,\beta^{0.03\pm0.13}\,\nu^{-0.42\pm0.03}\,q_{95}^{-1.43\pm0.23} \quad .$$

Converting this dimensionless parameter scaling relation to physical parameters gives

$$\tau_{th} \propto I^{0.84\pm0.16}\,B^{0.39\pm0.21}\,n^{0.18\pm0.07}\,P^{-0.41\pm0.06}\,L^{2.00\pm0.24} \quad ,$$

where L represents the physical size scaling needed to make the scaling relation dimensionally correct. Thus, it can be seen that the dimensionless scaling approach yields a definite prediction for the size scaling of confinement from single machine experiments.

This scaling relation can be compared to the ITER–93H scaling, which is

$$\tau_{ITER-93H} = 0.036 I^{1.06}\,B^{0.32}\,n_{19}^{0.17}\,P^{-0.67}\,R^{1.9}\,a^{-0.11}\,A^{0.41}\,\kappa^{0.66} \quad .$$

A comparison of the two equations finds that the B, n and size scalings agree to within one standard deviation while the difference in the I scaling is only a little larger than one standard deviation. The main difference is in the power scaling, where the dimensionless parameter scalings on DIII–D produce a much weaker power degradation. This discrepancy is partly due to the

strong unfavorable beta scaling implicit in ITER–93H which was not observed in the beta scaling experiment. Since the expected heating power in ITER is 30 times that used in the DIII–D experiment, this weaker power degradation will result in more optimistic predictions for ITER than the ITER–93H results.

2.1.5. TEST OF THEORY-BASED TRANSPORT MODELS

This working group was created in 1997 in order to provide detailed, quantitative, definitive experimental tests of the so-called "theory-based" transport models which have been developed in the past several years. (A theory-based transport model is one in which the functional forms of the transport coefficients are based on theoretical models; the purists in this area allow no free parameters which can be calibrated against experiment.)

For the past two years, there has been an active, world-wide effort to test the predictions of these models against measured profiles from steady-state tokamak discharges. This work has been organized by the ITER Expert Group on Confinement Database and Modeling. A number of DIII–D physicists have played a major role in this area, either providing data or developing and testing models. As part of this work, it has become clear that theory-based models which contain rather different fundamental transport processes can all give about equally good matches to the experimental results. Accordingly, it was obvious that different experimental tests needed to be devised in order to really be able to distinguish the various models and decide which one(s) are incorrect. (A fundamental theorem of inductive logic states that a theory can never be proven but can only be shown to be incorrect by demonstrating that it does not agree with the data.)

Since steady-state discharges could not provide discrimination between the various models, it was natural to turn to ideas based on time-dependent transport studies. An experiment was devised which involved off-axis heating of the plasma with modulated ECH. The various theoretical models were used to calculate what the electron and ion thermal responses should be, so that it was clear that the responses would be big enough to measure and that the theoretical predictions would be distinct enough to discriminate among the theories. Calculations showed that several of the theories could be differentiated by their predictions of the amplitude and phase of the temperature modulation.

As is shown in Figs. 2-13 and 2-14, the results were somewhat unexpected. Although the various theories predict different phases of the modulation on axis when the plasma was heated at the half radius, they each predict that the phase would be the same for ion temperature and electron temperature. Experimentally, the ion and electron temperature modulations are out of phase. Accordingly, ITG-based theories (such as the GLF23 and IFS/PPPL) model can match the ion response, but not the electron. Theories without critical gradients (such as Itoh-Itoh-Fukuyama) match the electron response but not the ion. Accordingly, we are left with a puzzle which requires more experimental work to sort out.

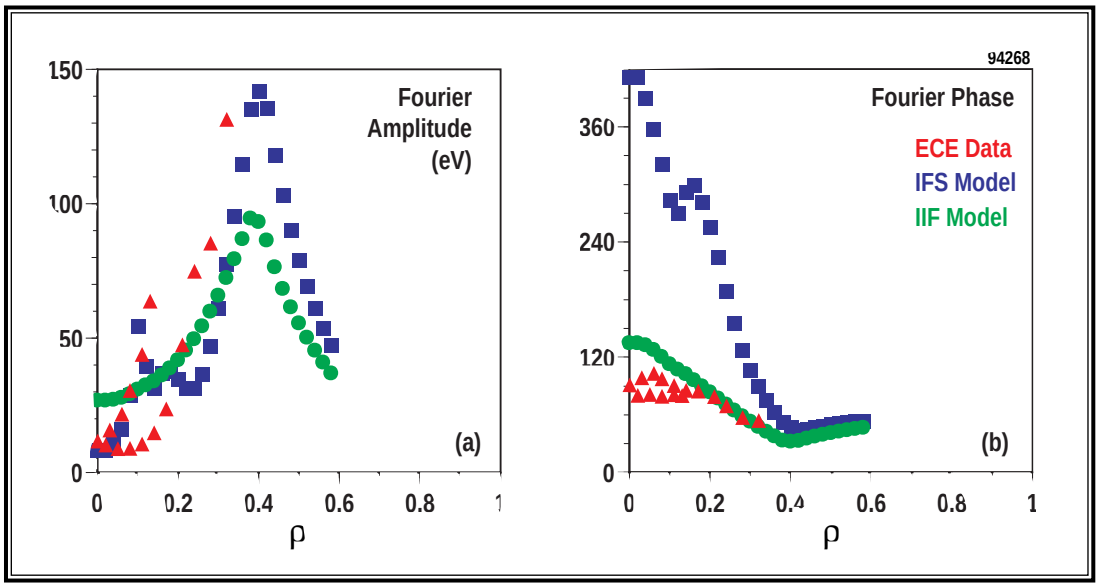

Fig. 2-13. The electron channel modulation is better described by the Itoh model.

2.2. STABILITY AND DISRUPTION PHYSICS

2.2.1. INTRODUCTION

Several experiments performed in 1997 were aimed at improving our understanding of the instabilities that limit AT discharges, particularly discharges with internal transport barriers. The goals were to raise the maximum stable beta in these discharges and to prolong the duration of the high performance phase toward steady state. These experiments were enhanced by the use of

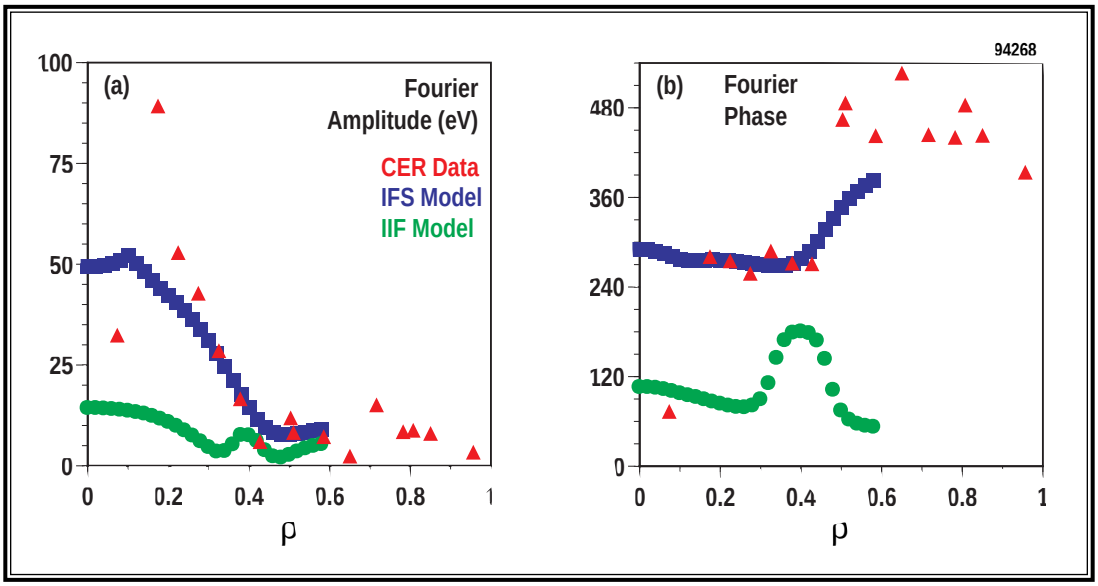

Fig. 2-14. The ion channel modulation is better described by the IFS/PPPL model.

improved plasma control algorithms and several new or upgraded diagnostics. Internal transport barriers have been observed in many tokamaks with negative or weakly positive central magnetic shear. To date, however, the duration of the transport barrier is generally limited to about 1 to 2 energy confinement times. In discharges with an L–mode edge, excessive pressure peaking in the core drives internal magnetohydrodynamic (MHD) instabilities which recent evidence indicates are probably ideal kink modes. Recently, the internal transport barrier has been sustained for more than 1 s by reducing the heating power and magnitude of the negative magnetic shear. Performance in H–mode edge discharges is typically limited by edge-localized instabilities, and recent simulations show that bootstrap current can play an important role in allowing the edge pressure gradient to reach the stability limit for low-n ballooning/kink modes. In experiments this year, the amplitude of the edge-localized modes and their impact on the temperature profile was varied over a wide range by altering the discharge shape, consistent with stability calculations. A conducting wall can raise the stability limit for low-n ideal kink modes, as demonstrated in experiments this year. The more slowly growing "resistive wall mode" was also observed in qualitative agreement with predictions. Neoclassically destabilized tearing modes can cause a reduction of the stable beta well below the ideal MHD limit in long-pulse discharges. However, recent experiments show that the threshold for these metastable modes can be significantly improved by avoiding triggering mechanisms such as sawteeth.

2.2.2. DIAGNOSTICS AND PLASMA CONTROL

Several new capabilities this year have allowed more accurate plasma control and equilibrium reconstruction, both of which are crucial to MHD stability experiments. These include upgrades to the motional Stark effect (MSE) and magnetic diagnostic systems, and the "isoflux" algorithm for discharge shape control.

The upgraded 35-channel MSE system is now used routinely for between-shot equilibrium reconstructions to yield q-profiles which are corrected for the radial electric field of the plasma. The addition of a second viewing angle allows determination of the radial electric field directly from MSE data, and the electric field profile obtained in this way agrees well with measurements by the charge exchange recombination diagnostic. Accurate reconstruction of the q-profiles also yields accurate pressure profiles in high beta plasmas, even in the absence of direct measurements of the pressure. In addition, an array of eight magnetic probes was installed on the new upper divertor baffle to improve plasma shape control and equilibrium reconstruction in the vicinity of the upper X–point.

The newly developed "isoflux" control scheme with real-time equilibrium reconstructions has been used to accurately produce a wide range of plasma shapes including crescent shaped discharges with indentations up to 0.15, the first time such a shape had been made in DIII–D. The plasma control system solves the Grad-Shafranov equilibrium equation in real time, using a modification of the EFIT code's algorithm which takes advantage of the fact that the experimental equilibrium changes by only a small amount during the time required to execute one iteration of the algorithm. The difference between the calculated and desired positions of the plasma boundary is then used to control the poloidal field coils. The use of a full equilibrium solution provides greater flexibility than algorithms based on regression analysis of equilibria similar to the desired shape and makes the shape control more robust to changes in the internal profiles.

2.2.3. STABILITY WITH ENHANCED CORE

High-performance discharges with an internal transport barrier and L–mode edge are generally limited by disruptions to low values of normalized beta, $\beta_N \leq 2.5$. Improving the maximum beta or the duration of high performance requires an understanding of this instability. Both ideal and resistive stability calculations for plasmas with negative central shear predict that the maximum stable beta decreases with peaking of the pressure profile, in good agreement with experiment. Detailed ECE profile data has recently been obtained during such disruptions which indicates an ideal mode structure, peaked in the region of large pressure gradient (Fig. 2-15). Similar disruptions have now also been observed in discharges with a broad, H–mode edge pressure profile, but at significantly higher normalized beta ($\beta_N \sim 4$) as expected with the broader pressure profile. These results suggest that the predicted ideal stability boundary has now been approached in plasmas with a wide range of pressure profile peaking.

In addition to the disruption precursor, bursts of MHD activity localized near the magnetic axis have been observed in many negative central shear discharges with peaked pressure profiles. These were identified with a resistive interchange mode destabilized in the negative shear region, and did not appear to play a direct role in the disruption. However, in some recent discharges in DIII–D and JET, the disruption occurs after the rotation of this mode slows to the frequency of the usual disruption precursor, leading to the speculation that coupling of the central resistive interchange mode to the ideal kink mode at larger minor radius may contribute to destabilization of the kink mode.

Disruptions driven by pressure peaking can be avoided either by controlling the central pressure to remain below the stability limit or by broadening the pressure profile. In some recent discharges with strong pressure peaking ($p(0)/\langle p \rangle \geq 6$), the internal instability was postponed allowing internal transport barriers to be sustained for more than 1 s (greater than five energy confinement times). The improvement in pulse length was achieved by reducing the magnitude of negative magnetic shear and lowering the neutral beam power and, hence, central fueling. Ideal stability analysis suggests that in this case, the disruption resulted not simply from peaking of the pressure profile, but also from the minimum of the q-profile

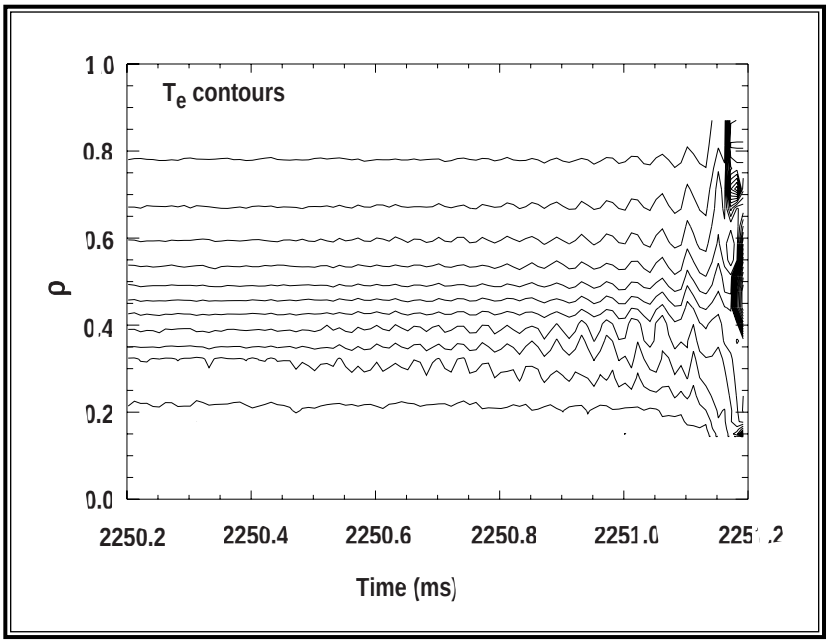

Fig. 2-15. Contours of electron temperature versus time and normalized minor radius during the precursor to a pressure-peaking disruption. In-phase motion across the entire profile indicates an ideal MHD mode structure.

decreasing toward unity as the current density profile evolves in the absence of active profile control. Here the calculated unstable mode is an ideal kink with strong m/n = 1/1 and 2/1 components, in qualitative agreement with experimental observations.

We have also begun experiments on expanding the radius of the negative shear region as a technique to expand the transport barrier radius and thus to broaden the pressure profile. With the use of H–mode transitions early in the current ramp to help raise the electron temperature and slow the inward diffusion of current, negative central shear profiles with a normalized radius r/a = 0.7 have been obtained.

2.2.4. EDGE STABILITY

High-performance plasmas with a large (H–mode) edge pressure gradient are often limited by instabilities with toroidal mode numbers n ~ 2 to 4 which begin near the plasma edge. These ballooning/kink instabilities driven by the steep edge pressure gradient can penetrate inward as far as r/a ~ 0.5, making it difficult to establish or sustain an internal transport barrier.

In an experiment earlier this year, crescent-shaped discharges with indentations up to 0.15 were produced using a new control scheme based on a real-time equilibrium fitting algorithm. Indentation into a “bean” or “crescent” shape is predicted to improve access to the second stable regime for ballooning modes, potentially improving the beta limit. Good energy confinement was observed, with up to a factor of 3 enhancement over the ITER–89P L–mode scaling, but the normalized beta limit of 3.5 to 4.5 had little dependence on indentation. Stability analysis shows that these discharges have access to the second stable regime over most of their volume, as predicted, and are stable to ideal n = 1 and n = 2 modes. However, the performance is limited by edge localized instabilities with n ≥ 4, similar to those seen in VH–mode discharges. Improvement of the edge stability is needed in order to make better use of the improved ballooning stability in the interior.

Recent simulations and analysis of experimental discharges show that the bootstrap current associated with the increasing pressure gradient helps to open access to the second ballooning stability regime near the edge, allowing the pressure gradient to continue to rise. At smaller minor radius the pressure gradient reaches the ideal ballooning limit, which may also help to steepen the edge pressure gradient. Further increases in the edge pressure gradient destabilize low-n kink-ballooning modes, with n = 3 modes predicted to be more unstable than the n = 1 and high-n modes as observed in experiments. The radial width of the unstable modes is calculated to expand with the width of the large pressure gradient region at the edge (Fig. 2-16), suggesting that the resulting performance degradation may depend on the form of the edge pressure profile.

Recent experiments have explored discharge shaping as one approach to control pressure gradients and stability at the edge and sustain high performance. Increasing the “squareness” of the discharge [Fig. 2-17(a)] leads to a narrowing or elimination of the second stable region for ballooning modes at the edge and lowers the first regime limit on the pressure gradient. Consistent with these expectations, ELMs are observed to become smaller and more rapid as the squareness increases with a weaker perturbation of the electron temperature profile [Fig. 2-17(b)]. At very high squareness, the ELMs suddenly shift to a very rapid, low amplitude

mode; this transition appears correlated with the disappearance of the second regime access. A weak internal transport barrier has been maintained during steady, high frequency ELMs in such discharges; but so far, the global beta limit and energy confinement are not significantly improved over standard H–mode.

2.2.5. WALL STABILIZATION

High beta discharges with negative central shear require a conducting wall for stabilization of low-n kink modes. An experiment was carried out this year to demonstrate wall stabilization and to characterize the theoretically predicted "resistive wall modes." These slowly rotating instabilities can become unstable in the presence of a real wall with finite conductivity when beta is above the no-wall stability limit but below the limit for an ideally conducting wall. Rotation of the plasma relative to the wall is predicted to help stabilize them.

For a clear experimental demonstration of wall stabilization, a large margin between the ideal MHD stability limits with and without a conducting wall is desired. We have calculated

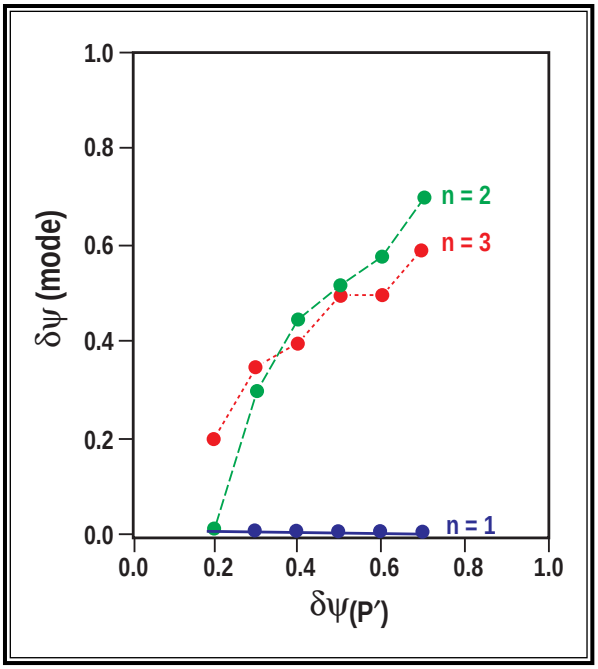

Fig. 2-16. Calculated stability of edge-driven kink-ballooning modes. Mode width $\delta\Psi_{mode}$ increases with the edge pressure pedestal width $\delta\Psi_{p'}$. Toroidal mode numbers n = 2 and 3 are more unstable than n = 1.

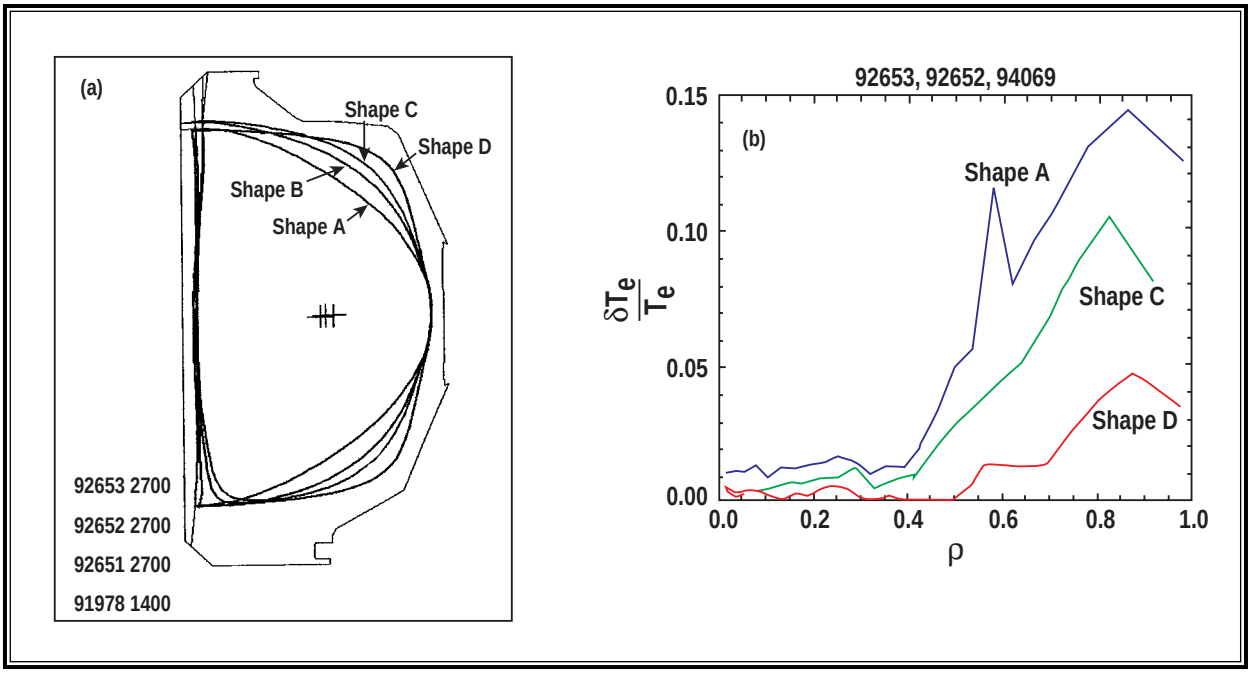

Fig. 2-17. (a) Increasing plasma squareness leads to (b) reduced amplitude of the electron temperature perturbation due to ELMs.

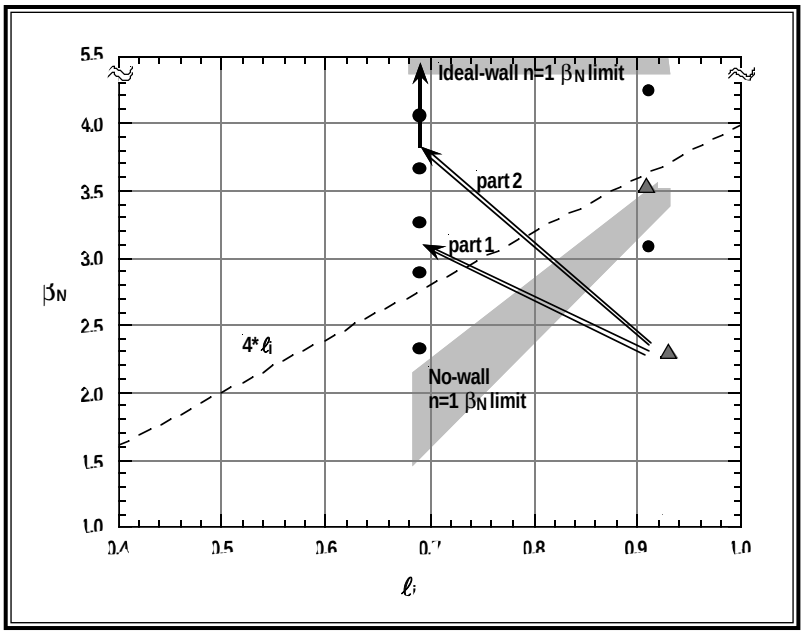

Fig. 2-18. Calculated n = 1 ideal kink mode beta limit increases with internal inductance ℓ_i in the absence of a conducting wall. The largest difference from the cases where the wall-stabilized beta limit for the n = 1 external kink is more than double the limit without a wall, in equilibria with strongly negative central shear (q_0 = 3.8 and q_{min} = 2.1) and a shape compatible with the new divertor configuration. These H–mode equilibria are predicted to be stable to n = 1 modes up to β_N = 8.8 with an ideal wall at the location of the DIII–D wall, while the no-wall beta limit is about 3.6. Further calculations suggested the use of similar plasmas but with very low internal inductance (Fig. 2-18) in order to reduce the no-wall ideal beta limit and make it easier to exceed this limit, as well as to provide strong coupling to the vacuum vessel wall. These plasmas were produced in the experiment by current ramping techniques.

At least one discharge, with a relatively modest normalized beta of 2.7, is calculated to be 30% to 40% above the ideal MHD limit without a conducting wall (Fig. 2-19). Beta remains above the no-wall limit for about 200 ms which is much longer than the wall penetration time of a few milliseconds, indicating that plasma rotation must be helping to maintain the wall

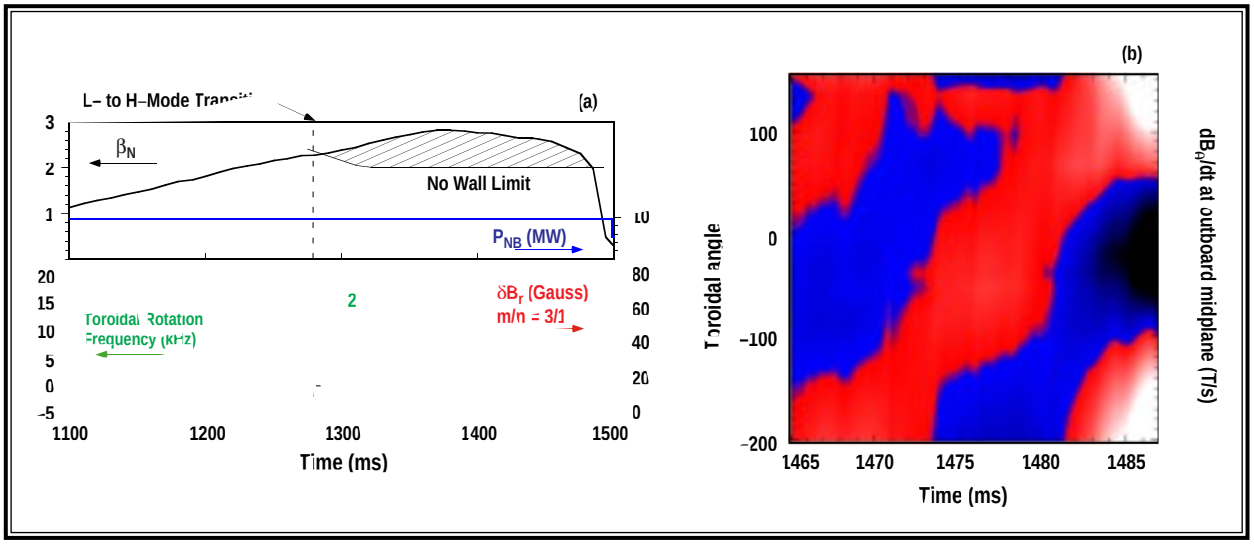

Fig. 2-19. (a) Wall-stabilized discharge remains above the calculated no-wall beta limit for about 200 ms, with normalized beta up to 40% greater than the no-wall limit. (b) Growth of a slowly rotating m/n = 3/1 mode begins when the plasma rotation at the q = 3 surface decreases below 1 kHz.

stabilization. Careful analysis of the magnetic and ECE data shows instabilities that are qualitatively consistent with the expected resistive wall mode. During the wall-stabilized time, a very slowly rotating n = 2 mode appears, coinciding with contraction of the core transport barrier and consequent slowing of the plasma rotation. ECE temperature profiles show no evidence of islands associated with this mode, consistent with expectations for a resistive wall mode. As the rotation of the $q = 3$ surface decreases to less than 1 kHz a very slowly rotating n = 1 mode grows and leads to a minor disruption, consistent with loss of rotational stabilization. These instabilities rotate and grow on a time scale comparable to the magnetic penetration time of the vessel wall, as expected for the resistive wall mode.

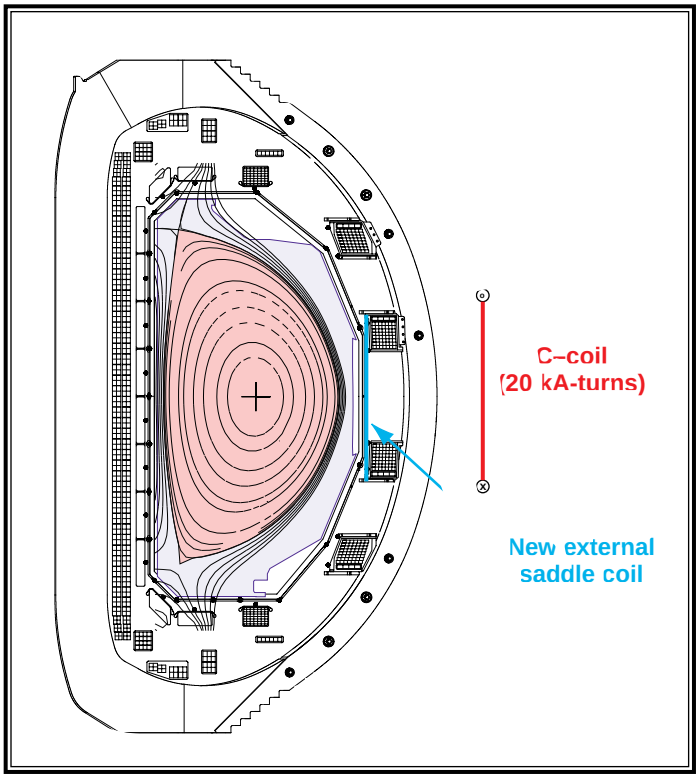

Fig. 2-20. A set of six new midplane saddle loops, matched to the existing C–coil segments, will aid in the detection and control of resis-

In the future, we plan to develop active stabilization of resistive wall modes, using feedback controlled external nonaxisymmetric coils. As a first step toward this goal, a set of six new saddle loop sensors has been designed and will soon be installed (Fig. 2-20). These consist of equally spaced rectangular loops along the outboard midplane, with toroidal and poloidal angular widths matching the C–coil segments. They will be mounted outside the vacuum vessel but inside the toroidal and poloidal field coils, in order to detect radial magnetic field perturbations that penetrate the vacuum vessel wall such as the resistive wall mode. These saddle loops will be used for resistive wall mode detection and, ultimately, for stabilization through feedback control of the C–coil.

2.2.6. NEOCLASSICAL TEARING MODES

The beta limit in long-pulse ITER-like discharges in DIII–D is believed to be set by neoclassically destabilized tearing modes, where destabilization requires a large pressure gradient, low collisionality, and a finite-amplitude seed island. The seed island may be produced, for example, by a sawtooth crash. Experiments in the last few years have shown that in low collisionality plasmas, the threshold in beta for neoclassical tearing modes can be as much as a factor of 2 below the ideal stability limit, which is of concern for ITER and DIII–D steady-state AT scenarios. A three-day experimental campaign this year focused on the influence of discharge shape and current density profile on resistive and ideal stability limits with emphasis on neoclassically destabilized tearing modes. The experiment included scans of collisionality and $q(0)$ in high and low

triangularity single-null plasmas, making use of DIII–D's unique capability for divertor pumping in both high triangularity (upper-null) and low triangularity (lower-null) configurations to control the density. Preliminary analysis indicates that the 2/1 neoclassical tearing mode's threshold in beta increases with triangularity. Maintaining $q(0)$ greater than 1 also significantly improved stability to the 3/2 and 2/1 modes (Fig. 2-21), evidently by eliminating sawteeth as a source of "seed islands" to trigger metastable modes. These observations are consistent with earlier DIII–D and JET experiments in which normalized beta near three was sustained in the absence of sawteeth.

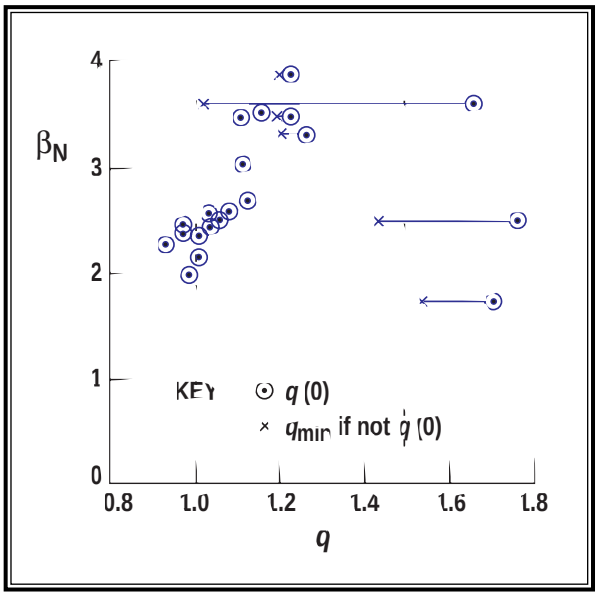

Fig. 2-21. The threshold in beta for onset of m/n = 3/2 neoclassical tearing modes increases when q_{min} is greater than 1, eliminating sawteeth.

2.2.7. DISRUPTIONS

Considerable progress was made in the disruption research area during FY97. Experiments and analysis in the area of disruption characterization, mitigation, and runaway electron generation led to new insights in these areas and provided valuable input for some of the ongoing disruption issues critical to the ITER design. Much of our effort this year was spent developing codes and models and benchmarking against our experimental results. The validated codes were then available for application to ITER.

In one set of experiments, vertical displacement events (VDEs) were triggered in ITER-like single-null discharges. By varying the current profile, plasma beta, and vertical elongation, we successfully produced a wide variation in the vertical stability growth rates (from 40 to 250 rad/s) and demonstrated a significant correlation between increasing vertical instability growth rate and increasing peak poloidal halo current amplitude. The dependence has been compared with an analytic model of halo currents and the agreement is excellent. Considerable progress was also made in the characterization of the disruptive heat flux. Using the Poynting flux method of measuring electromagnetic energy flows, IR TV measurements of conducted energy flow, and bolometric measurements of radiation gives a reasonably accurate energy balance for all types of disruptions (statistically to about 15%), and a very accurate (to better than 5%) account in high energy DND negative central shear (NCS) discharges. Analysis of disruptive heat flux profiles in these different disruptions has yielded interesting results. High density disruptions lead to very in/out asymmetric heat flux deposition while high beta disruptions show relatively symmetric in/out flux deposition. However, large toroidal asymmetries in the peak heat flux (between 3:1 and 10:1) are observed in the high beta disruptions. Disruptions of high performance NCS discharges lead to very broad flux distributions on the floor which lowers the heat flux relative to the normally peaked distributions in other disruption types.

As part of our mitigation program, we are trying to explain the rapid core cooling and runaway electron production observed during "killer" pellet injection. A numerical code that simulates the killer pellet radiation and resulting processes (KPRAD) was developed and has been successful at predicting the rapid cooling of the plasmas. In addition, the simulation code also predicts two new mechanisms for generation of runaway electrons. The first is the slideaway of hot tail electrons due to the extremely rapid cooling of the bulk electrons. Because the temperature drops so rapidly due to the impurity radiation, a portion of the original Maxwellian tail (>12 T_e) has insufficient collisional coupling to the bulk electrons and can cross over the critical energy and runaway. This mechanism has also been confirmed using a full kinetic Fokker-Planck code (CQL3D). The code also indicates that the high radiation rates are sufficient to produce steep pressure gradients during the pellet ablation that result in instabilities that transport hot electrons in the plasma core into the colder outer region where they can then runaway.

2.3. DIVERTORS AND EDGE PHYSICS

The divertor research in the past year has investigated the physical processes that are necessary to reduce the exhaust heat flux and minimize sputtering of the walls and divertor. New hardware has been installed in the upper divertor, so our experiments have been a combination of detailed physics experiments in the lower divertor with an extensive diagnostic set, along with a more empirical approach using the closed upper divertor. These two divertors [Fig. 2-22 (open lower divertor) and Fig. 2-23 (closed upper divertor)] have allowed us to compare single-null operation with either open or closed divertors.

A new emphasis in the current experiments has been the measurement and control of plasma and impurity flows in the SOL and divertor. New diagnostics have been installed in the lower divertor to measure flow as described in Section 2.3.1. The new divertor has been used to control the density in high-triangularity discharges (Section 2.3.2) and results similar to those obtained in the LSN open divertor have been obtained. Both gas puffing and pellets have been used in density limit experiments (Section 2.3.3). Experiments to enrich impurities have been carried out in open divertors with preliminary studies in the closed divertor. Substantial argon enrichment in the lower divertor has been observed (Section 2.3.4). The behavior of ELM has been characterized in

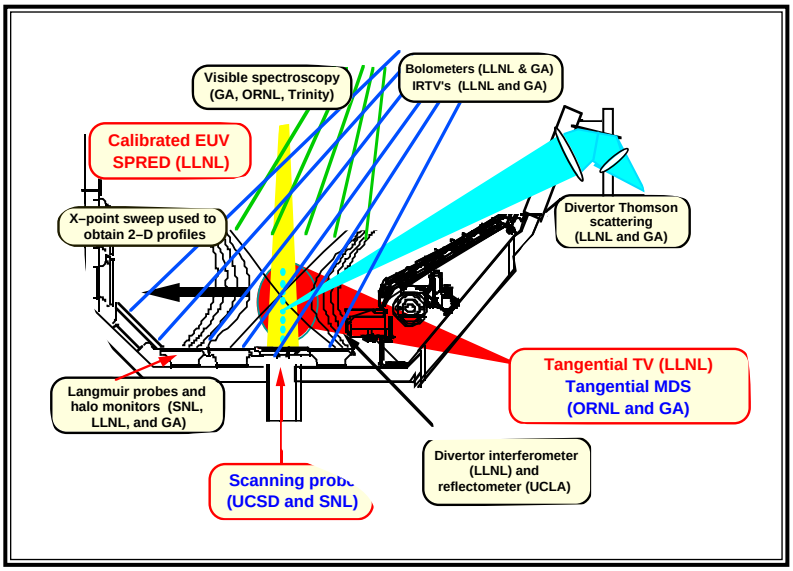

Fig. 2-22. The open lower divertor with an extensive set of diagnostics. Flow measurements are carried out with Mach probes on the scanning probe and tangentially viewing spectroscopy.

several operating regimes as discussed in Section 2.3.5. Finally, the DiMES erosion probe has measured very small net erosion in the private flux region and at the separatrix in detached plasmas (Section 2.3.6).

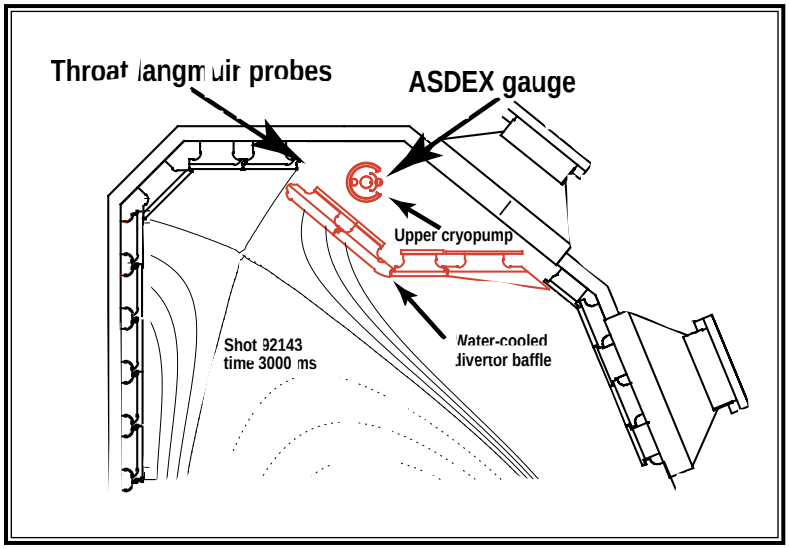

Fig. 2-23. The closed upper divertor and cryopump. Langmuir probes at the pump entrance are used to measure the incident ion flux, and the ASDEX gauge

2.3.1. DETACHED DIVERTOR EXPERIMENTS: 1–D AND 2–D RECOMBINATION

Research to measure the plasma conditions in the divertor during radiative divertor (RD) operation continued this year. The experiments were focused on two physics objectives: (1) to confirm, by direct measurement of the strongest radiating lines of deuterium and carbon, the relative contributions of these radiating constituents to the total radiated power; and (2) to determine the role of deuterium recombination in the physics of RD operation.

Direct measurement of the C IV line at 1550A and the deuterium Lyman$_\alpha$ line at 1216A were made with the divertor SPRED diagnostic. The instrument was upgraded this year to include a grating capable of producing spectra in the range from 170 to 1700A (previous capability was limited to 100 to 1100A). Using a line of sight along the divertor leg, so that both the outer strike point and the region near the X–point were visible to the SPRED, agreement was obtained between the bolometer radiated power and the total inferred from SPRED. During RD operation, carbon accounted for 80% of the total and deuterium produced the remaining 20%. 2–D visible imagery again showed that the carbon radiation was located near the X–point — the deuterium was from near the strike point. This direct measurement of the lines containing the majority of the radiated power agrees with the conclusions from previous measurements of weaker, short wavelength lines and radiative collisional modeling.

The new grating in the SPRED also allowed ratios of line intensity from Lyman$_\alpha$ and Lyman$_\beta$ to be calculated during RD operation. Collisional radiative modeling indicates that for plasmas in which radiation from neutrals is dominated by collisional excitation processes, this ratio monotonically increases from 40 to 70 as the electron temperature decreases from 8 to 1 eV. For a plasma in which radiation from neutrals is dominated by neutrals coming from recombination of ions, this ratio is in the range 3 to 4 for similar temperatures. Measurements of this intensity ratio in the outer divertor leg versus time are shown in Fig. 2-24 for a plasma with strong deuterium gas puffing starting at 1.9 s and radiative divertor operation starting at approximately 2.5 s. During the attached H–mode phase, collisional excitation accounts for most of the deuterium emission. During the detached RD operation, half of the radiation from deuterium is due to

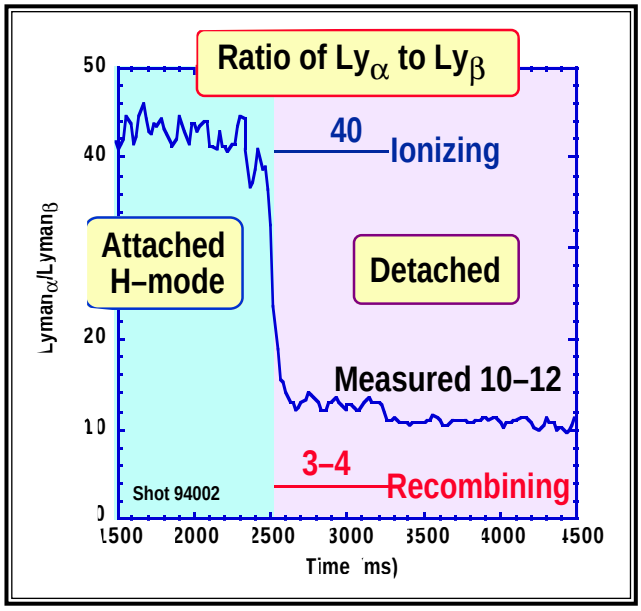

Fig. 2-24. Ratio of Lyman$_\alpha$ to Lyman$_\beta$ in the outer leg of a plasma in which strong deuterium puffing began at 1.9 s and radiative divertor operation began at 2.5 s. The significant decrease in the ratio at the onset of RD operation is indicative of an increase in deuterium recombination in the detached outer leg.

recombination assuming the plasma is optically thin. Work will continue next year to determine the validity of this assumption.

The 2–D distributions of the recombination regions were obtained with the tangentially viewing visible camera system (TTV). Dual cameras were used simultaneously this year and the ratio of Balmer$_\alpha$ and Balmer$_\gamma$ radiation was calculated for each pixel in the image. Data from a shot similar to that used with the SPRED analysis is shown in Fig. 2-25. The fraction of the Balmer$_\alpha$ emission which is attributed to recombination is shown in false color (red regions indicate nearly 100% emission from recombination). The calculations assumed that the plasma electron temperature was T_e = 1 eV throughout; future analysis will involve the 2–D temperature profile measured by divertor Thomson scattering with the TTV images to more accurately define the recombination regions. The initial results show strong recombination near the inner strike point during attached ELMing H–mode indicating that the inner leg is actually partially detached. During RD operation, recombination emission is observed all along the outer leg near the separatrix consistent with the Thomson measurements of low temperature (T_e = 1 to 2 eV). Recombination falls off farther out in the SOL consistent with the model of partially detached divertors in which the plasma remains attached to the target plate in the far outer SOL regions of the outer leg and is detached near the separatrix strike point.

Ion and Impurity Flows in Attached and Detached Plasmas. Spectroscopic measurements of impurity flows in the lower divertor of DIII–D have been performed using a set of five quasi-tangential viewchords aligned parallel to the normal direction of the toroidal magnetic field. Fiducials for measuring Doppler shifts (i.e., the unshifted line positions) are determined from fitting the line profile data from the seven vertical viewchords of the Multichordal Divertor Spectrometer. In Fig. 2-26, both the tangential viewchords (mapped onto a poloidal plane) and the vertical viewchords are overlaid on a representative MHD flux plot of a lower, SND configuration.

From Doppler shifts of C II and C III spectral lines, flows of carbon ions along the magnetic field lines of both the inner and outer divertor legs have been determined. Flows are normal, i.e., directed toward the target plate, except in a band adjacent to the outer separatrix where reversal is observed. The assumption of equal carbon and deuteron temperatures implies that normal carbon flows in the outer leg are 0.3 to 0.7 of the deuteron sound speed; the normally flowing ions in the inner leg and the reversed-flowing group in the outer leg achieve speeds that are near sonic. In discharges with strong gas puffing, impurity flow velocities are observed to

increase significantly in the outer leg with the onset of detachment. Spectroscopic signatures of the flow cases cited above (namely no flow, normal flow, and the combination of normal and reverse flow) are illustrated in Fig. 2-27 by lineshapes of a C II transition observed from three different views.

Parallel Flows. The UCSD/SNL team performed first measurements of the parallel flow of background plasma in the DIII–D tokamak divertor using a fast scanning Mach probe. The measured parallel flow patterns feature complex behavior such as reverse flow, stagnant flow, and large scale convection. For detached discharges, the measurements confirm predictions of convective flow towards the divertor target plate at near sound speed over large regions in the divertor as shown in Fig. 2-28(a) and 2-28(b) as circles. For attached discharges with low divertor recycling, the plasma velocity and Mach number increase monotonically towards the plate as shown in Fig. 2-28(a) and 2.3-7(b) as diamonds. For attached discharges with high divertor recycling, we have observed flow reversal (i.e., away from the target plate) in a thin region around the outer separatrix as shown in Fig. 2-28(c) and 2-28(d), thereby confirming the existence of a mechanism by which impurities can be transported away from the divertor target plates. The convected heat flux to the divertor target plate using probe, was compared to the total heat flux measured by IR cameras [Lasnier (1998), Hill (1991)] at the probe position. It is found that for detached discharges, the convected heat flux is 30×10^4 W/m^2 or ~80% of the total heat flux. For attached discharges, the convected heat flux is 23×10^4 W/m^2 (or less than 30% of the total) explaining most of the heat flux to the target plates by conduction. The main features of the measurements have been

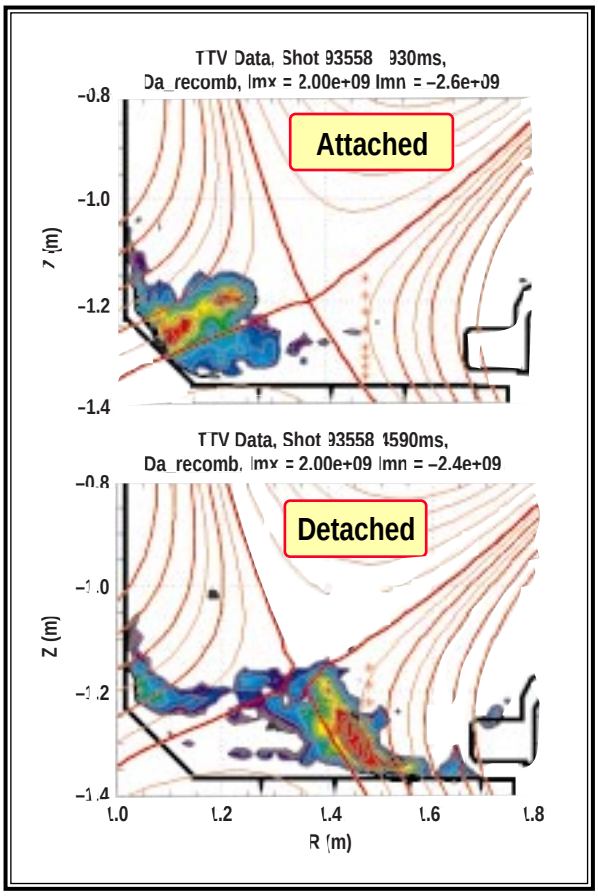

Fig. 2-25. 2–D distributions (flase color) of the Balmer$_\alpha$ emission attributable to recombination in the attached and detached phases of the discharge. Red regions indicate nearly 100% emission from recombination. T_e = 1 eV was assumed in the calculations.

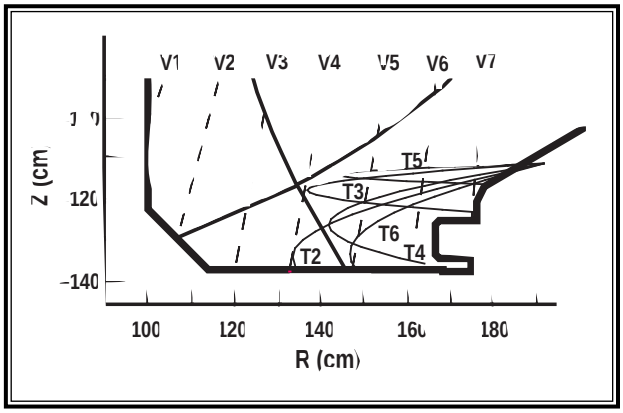

Fig. 2-26. Schematic of the visible spectrometer views with respect to the separatrix for the static configuration studies. The vertical views are shown as dashed lines (V1–V7). The projection of the tangential views on a poloidal plane are shown as solid lines (T2–T6).

reproduced by modeling with the 2–D fluid code UEDGE. UEDGE can reproduce measurements of flow reversal at the separatrix, followed by flow towards the plate above the separatrix and by stagnant flow near the X–point are shown in Fig. 2-29(a). Measurements of steady plasma acceleration towards the plate during attached divertor operation are also reproduced [Fig. 2-29(b)] and convective flow over a large divertor volume can be seen in the simulation shown in Fig. 2-29(c) 2-29(d) for two vertical cuts at the strike point radius (R_{OSP}) and 5 cm inside ($R_{OSP} - 5$ cm).

2.3.2. EXPERIMENTS WITH THE NEW CLOSED DIVERTOR

We have used the new upper baffle and cryopump to control the density in high-triangularity tokamak discharges. As show in Fig. 2-30, active density control was observed when we moved the strike point close to the pump aperture. This figure also shows the pumpout of the density after a density increase with a gas puff.

Experiments have also started to compare the difference between operation in open and closed divertors. We have found that the density at which detachment occurs with deuterium puffing is reduced about 20% with the new baffle divertor. So far, we have not observed any large differences in core confinement with two divertors. The UEDGE code predicts a 3× reduction in the core ionization in SN with the upper baffle. Core ionization has been estimated with a tangentially viewing array of H-alpha chords and also a transport analysis of the detailed edge profiles. These measurements are in rough quantitative agreement with the model.

2.3.3. H–MODE DENSITY LIMIT EXPERIMENTS

We have succeeded in significantly exceeding the Greenwald density limit [Greenwald (1988)] ($\bar{n}_e \geq 1.5 \times n_{GW}$, $n_{GW} = I_p/\pi a^2$) with good energy confinement ($\tau_E \geq 1.1 \times \tau_E^{ITER-93H}$) using pellet injection and

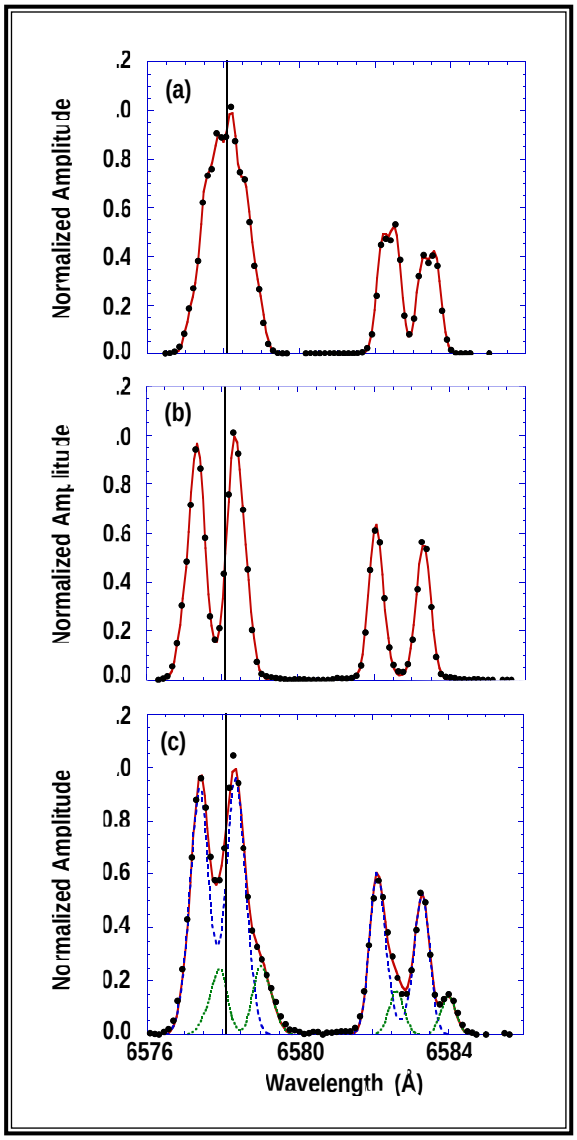

Fig. 2-27. Lineshapes of the $^2S–^2P$ transitions of C II observed from three different views: (a) along V4 which passes close to the X–point. The line at 6578.1 A is located near the center of the unshifted short-wavelength component of the doublet. (b) Along T6 where the blue shift indicates flow toward the target plate. (c) Along T3 which intercepts one group of ions flowing toward the target and a second group near the separatrix group flowing away from the target (red-shifted component).

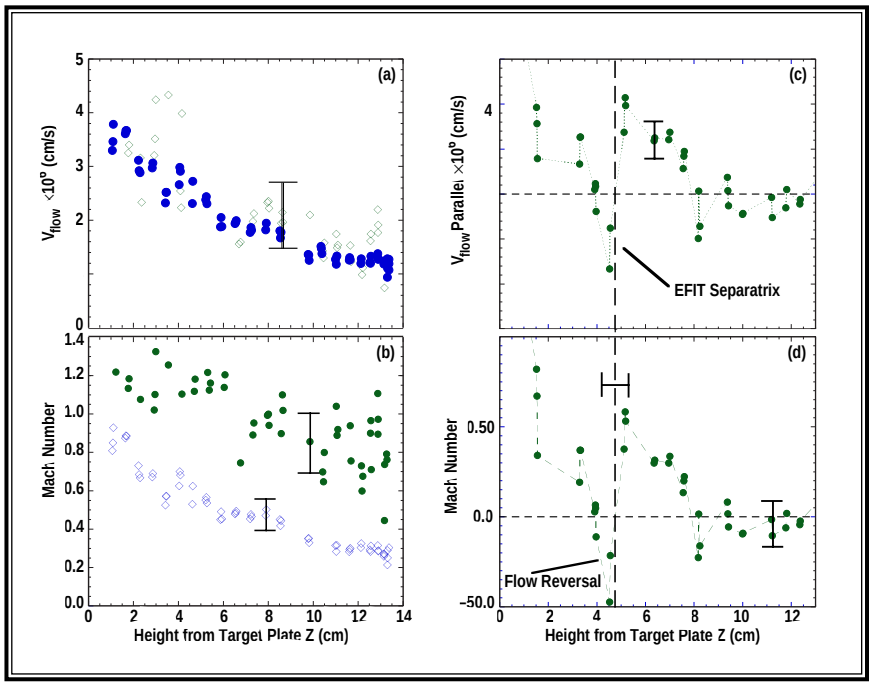

Fig. 2-28. Flow velocity (a)–(c) and Mach number (b)–(d) are shown versus height from the divertor plate for attached (diamonds) and detached (solid circles) discharges. Flow reversal can be observed in a 1 cm wide region (d) near the separatrix for a high recycling attached discharge. The plasma flows away from the target plate at 1×10^6 cm/s (c).

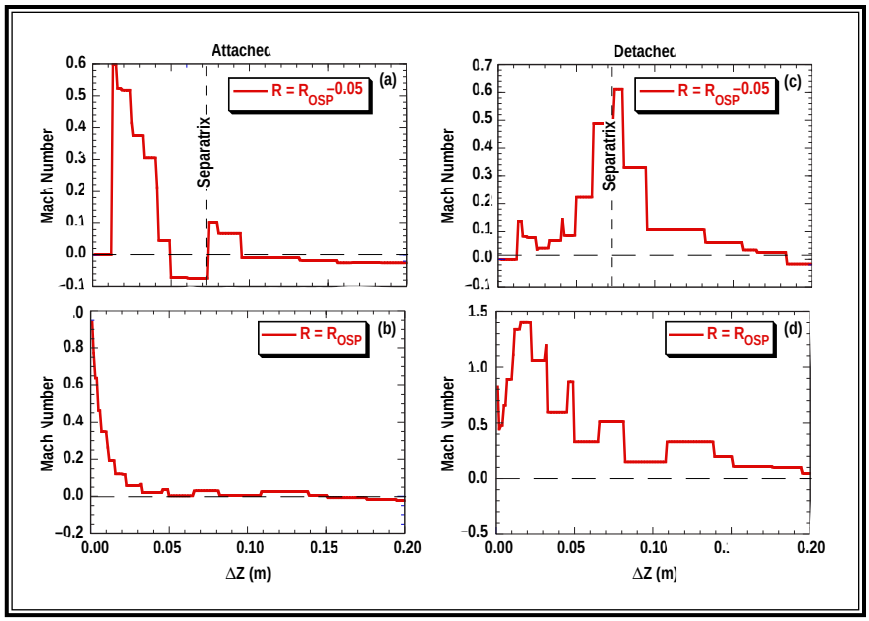

Fig. 2-29. Mach number from UEDGE modeling for attached (a)–(b) andd detached (c)–(d) discharges. The data is presented along two vertical cuts; one located at the outer strike point (OSP) radius (b)–(d) and the other along a cut 5 cm inside the OSP (a)–(c).

divertor pumping. One of these discharges is shown below in Fig. 2-31.

Greenwald scaling has presented a challenge to the plasma physics community because theories predict additional dependencies, e.g., heating power (P_{heat}) and impurity concentration (n_Z/n_e). These theories indicate that several distinct processes exist which can limit density in either the core, edge, or divertor plasma. These processes include divertor detachment (which can lead to divertor collapse), particle confinement and fueling limits, MARFE formation, and MHD activity.

When the divertor temperature reaches a few electron volts, partial divertor detachment (PDD) is observed and the plasma pressure and ion current near the divertor strike point drop. Experimentally [Petrie (1997)], the divertor thermally collapses and H–mode confinement is

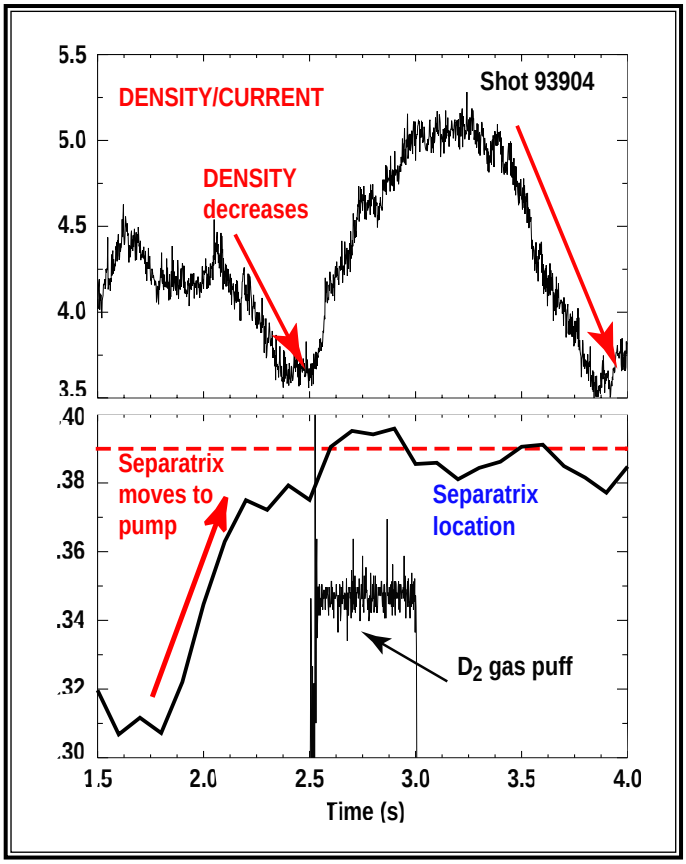

Fig. 2-30. Density control has been demonstrated with the upper baffle and cryopump. The density decreases when the strike point is moved towards the pump aperture. The density decays after a deuterium gas puff has been injected.

lost if the density is increased after the onset of partial detachment. We bypassed [Maingi (1997)] divertor collapse as a density limiting process by particle source profile control. The SOL n_e was maintained below the divertor collapse limit with divertor pumping, and the ratio of $\bar{n}_e$ to SOL n_e was increased with pellet fueling. This allowed us to maintain divertor temperature above the detachment threshold. Because PDD is the first step toward total detachment and an ensuing density limit, we investigated the heating power dependence of separatrix parameters at PDD onset. We determined [Maingi (1998)] that the upstream separatrix density (n_e^{sep}) above the outer midplane increases with the SOL power (P_{SOL}):

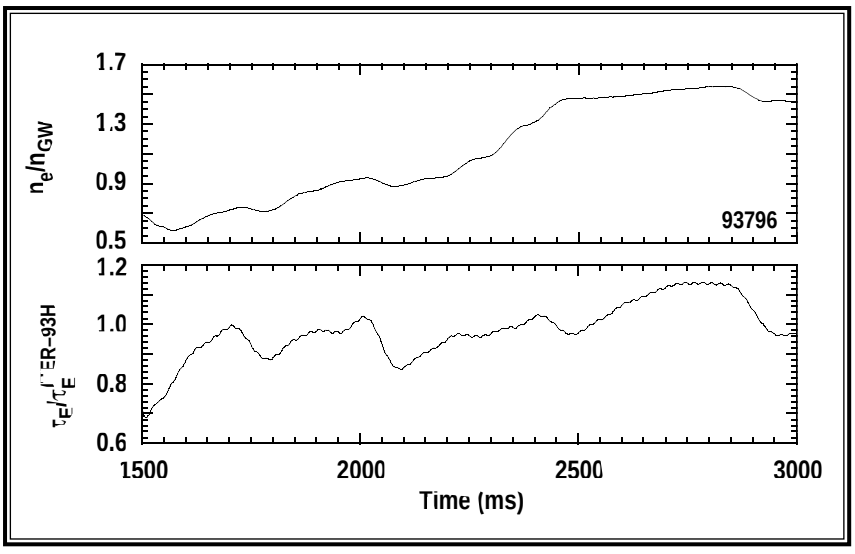

Fig. 2-31. Line-averaged density well above the Greenwald limit is maintained for several confinement times while the confinement is above the H–mode scaling.

$n_e^{sep} \sim P_{SOL}^{0.8}$. This observation is in contrast to the line-average density at PDD onset which is independent of heating power. In addition, the upstream SOL temperature at PDD onset (T_e^{sep}) increases with P_{SOL}: $T_e^{sep} \sim P_{SOL}^{0.6}$. These dependencies are comparable to the ones predicted by the Borass model: $n_e^{sep} \sim P_{SOL}^{0.7}$ .and $T_e^{sep} \sim P_{SOL}^{0.3}$. This work corroborates the physics of the Borass model which predicts a PDD onset limit for ITER above the Greenwald density limit for standard density profile assumptions.

A reduction in particle confinement time as $\bar{n}_e$ approaches n_{GW} was proposed [Greenwald (1988)] as the mechanism behind the Greenwald limit. However, we observed [Maingi (1997)] no correlation between the particle confinement time and n_e/n_{GW} for pellet-fueled discharges. We observed a stronger than linear plasma current dependence of the density decay time following pellet injection. In addition, pellet fueling efficiency was found to decrease with heating power. At high B_t with heating power near the L–H confinement transition limit, pellets produced H–L transitions which rapidly ejected the pellet density in <10 ms. Access to high density was achieved by operating at low B_t, giving more margin over the L–H threshold.

We compared edge plasma parameters at MARFE formation to those predicted by models and found semiquantitative agreement. We have also derived [Mahdavi (1997)] an edge density limit which scales as $(I_p^{0.96}/a^{1.9}) * (P_{heat} R)^{0.17} (n_Z/n_e)^{-0.1}$, i.e., comparable to Greenwald scaling. This limit was obtained by examining MARFE onset requirements in the presence of the ITER–89P energy confinement scaling. In practice, MARFEs were avoided by low edge safety factor operation and divertor pumping.

We found that MHD modes can be destabilized at densities as low as $\bar{n}_e/n_{GW} \sim 0.8$ during pellet fueling; the cause is unclear. MHD activity was observed over a wide heating power range but was avoidable at $P_{heat} < 3$ MW. By operating at reduced heating power ($\beta_N < 1.7$), we have suppressed these modes.

By studying each process and selecting conditions to avoid it, we have achieved H–mode discharges at $\bar{n}_e/n_{GW} \sim 1.5$ for up to 600 ms. These discharges were ELM-free, and owing to impurity accumulation and low central heat deposition, ended in a central radiative collapse — neutral beam heat deposition becomes hollow during the high density phase. Future studies will focus on using pellets to trigger ELMs and pellet fueling from the high-field side.

2.3.4. DIVERTOR IMPURITY ENRICHMENT EXPERIMENTS

Analysis of induced SOL experiments (so-called “puff and pump” experiments) has shown that the divertor enrichment of argon can be increased by a factor of 3 by inducing a strong main ion flow in the SOL through simultaneous D_2 gas injection at the midplane and divertor exhaust. In fact, the best enrichment values (~17) are of sufficient magnitude that a radiative divertor solution with the primary radiator being argon in the divertor plasma can now be considered possible.

While the induced SOL flow has a strong effect on argon, neon and helium enrichment is less affected with improvements ~80% and <20%, respectively. Analysis shows that this *Z*-dependence results from a combination of both neutral physics (ionization mean-free path) and ion transport in the divertor (frictional drag versus thermal gradient force). Furthermore, detailed particle measurements made possible by the direct measurement of impurity densities in several reservoirs indicate reasonable particle balance for helium throughout the duration of the discharge. Conversely, while the total input of neon is balanced by total exhaust by the end of a discharge, particle balance is not observed during the course of the discharge. A significant wall inventory with a short release time (~10 ms) is surmised. A paper by M.R. Wade et al., "Impurity Enrichment Studies Using Induced SOL Flow in DIII–D," which includes the analysis results and interpretation of the results, has been submitted to the Nuclear Fusion journal.

These experiments were made possible by the implementation and improvement of several diagnostic capabilities over the past year. Significant progress was made in using the DIII–D CER system in measuring the absolute content of neon and argon in the core region. For neon, the primary advance was experimental determination of the proper excitation rates needed to compute the neon impurity densities. It was found that the effect of excited neutrals within the beam on the excitation rate of the NeX 11–10 transition by the beam must be included. The results of this study are reported in a paper by D.G. Whyte et al., "Measurement and Verification of Z_{eff} Radial Profiles Using Charge-Exchange Recombination Spectroscopy on DIII–D." For argon, the primary improvement was the identification of spectral lines (both in the visible and VUV) excited via CER. Using theoretical CER cross sections, $Ar^{+16,+17,+18}$ densities can be determined from the DIII–D CER and midplane SPRED systems. A new method of detecting the K_α line using "notched" soft x-ray filters was also developed and a prototype system tested. Based on the results of this system, a full array has now been prepared and installed on DIII–D. Also, the Penning gauge system in the lower pumping plenum was upgraded to allow measurement of argon partial pressures.

2.3.5. DIVERTOR EROSION

Net erosion rates of carbon target plates have been measured in situ for the DIII–D lower divertor. The principal method of obtaining this data is the DiMES probe, which inserts and retracts graphite samples from the DIII–D lower divertor floor. Recent experiments have focused on comparing erosion at the outer strike point (OSP) during two different divertor plasma conditions: attached (T_e > 40 eV) ELMing plasmas, and detached (T_e < 2 eV) ELMing plasmas. For the attached cases, the net erosion rates of carbon exceed 10 cm/exposure-year (i.e., loss of plate thickness expected in a continuous year of plasma exposure), even with incident heat flux <1 MW/m^2. This rate is unacceptable for a power-producing magnetic fusion device. Modeling of the divertor erosion has been performed using the measured divertor plasma characteristics and the REDEP erosion model. Measurements and modeling agree for both gross and net carbon erosion (Fig. 2-32) in the attached case, showing the near-surface transport and redeposition of the carbon is well understood. Here, physical sputtering (with enhancement from self-sputtering and oblique incidence) is dominant and the carbon's effective sputtering yield

(Y_{eff}) for all ions incident at the divertor plate is greater than 10%. For the detached divertor cases, the cold incident plasma eliminates physical sputtering. Attempts to measure chemically eroded hydrocarbon molecules spectroscopically indicate an upper limit of $Y_{eff} \leq 0.1\%$ for the chemical sputtering yield. Therefore, detachment reduces the effective sputtering yield about a factor of 100 compared to the attached cases. This suppresses net erosion at the outer strike point, which becomes a region of net redeposition (~4 cm/exposure-year). This promising result of reduced erosion in detached plasmas is being further investigated.

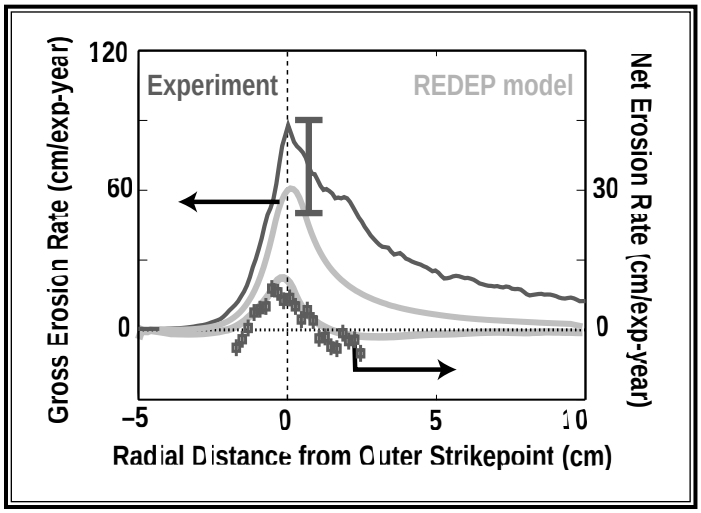

Fig. 2-32. Comparison of experiment and REDEP erosion modeling for carbon erosion near the outer strike point of a low power (q ~ 0.7 MW/m^2) attached divertor plasma. Gross erosion is measured using visible spectroscopy of singly ionized carbon. Net erosion is measured using the depth-marked DiMES graphite probe.

2.4. WAVE-PARTICLE INTERACTION

2.4.1. FAST WAVE CURRENT DRIVE SYSTEMS

There are three radio frequency (rf) systems on DIII–D used for fast wave current drive (FWCD) experiments in the ion cyclotron range of frequencies (ICRF). This year the transmission system for one of these FWCD systems was physically reconfigured to test a new type of robust operation based upon promising data from the year before. The test was successful.

Robust operation refers to the ability to keep an FWCD transmitter on-line, generating rf power, in spite of rapid changes in the load impedance presented by the plasma. A mismatched impedance generates reflected power. If only a relatively small level of reflected power returns to the transmitter, protection circuits are triggered which cut off the output power since reflected power could harm the transmitter components.

The test reconfiguration uses a so-called hybrid splitter to isolate the transmitter from the plasma load. Reflected power is diverted harmlessly to a dummy load if the antenna rf wave phasing is set for current drive operation. Additionally, this reconfigured method did away with some previously required large tuning elements which are often weak points in the system for high voltage breakdown.

Figure 2-33 shows the operation of this system into an H–mode discharge with edge localized modes (ELMs). The ELMs cause a rapid variation in the edge plasma density which causes a rapid variation in the plasma rf impedance. Figure 2-33(b) shows the rf impedance in ohms together with a trace of edge visible light measured with a photodiode. The photodiode light

varies with the edge density and the traces show that the loading varies with this edge density. The percentage of transmitter power coupled to the plasma is shown in Fig. 2-33(c). In spite of the rapid variations in loading, this percentage maintains a relatively high averaged value. Throughout, the transmitter is protected as evidenced by Fig. 2-33(d) which shows that only a very small safe level of power is reflected to the transmitter. Figure 2-33(a) gives the overall power accountability, showing power out of the transmitter, power to the plasma, and the difference power to the dummy load.

Without this robust system, the ELMs would cause sufficient transmitter power reflection to interrupt rf power. After a number of such trips, the transmitter circuitry shuts the transmitter down, thus removing any rf power from the rest of the discharge. This system allows the transmitter to ride safely through any loading conditions subject to the usual limits on transmission line and antenna voltage. The other two FWCD systems will be operated in this mode for the 1998 campaigns.

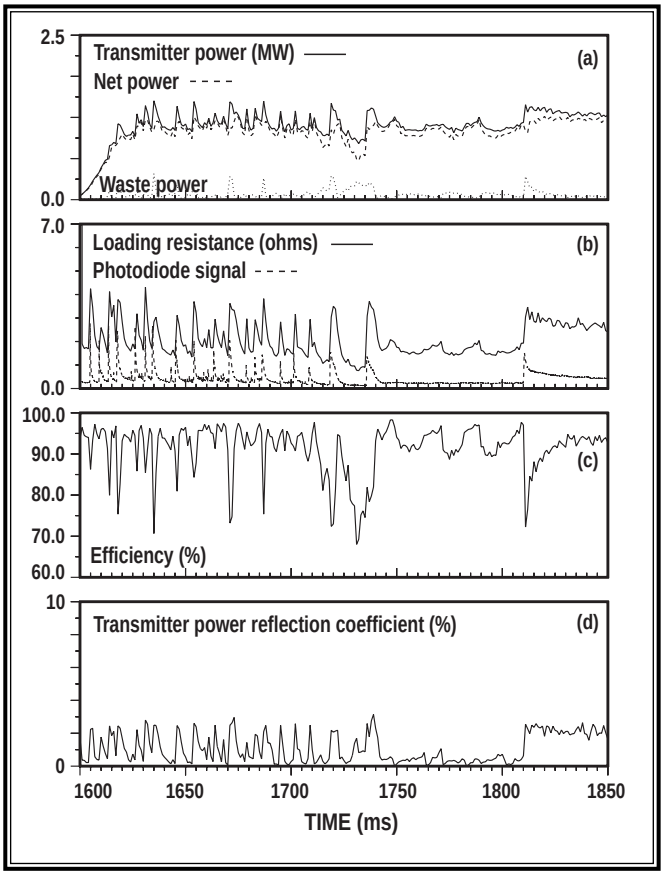

Fig. 2-33. Robust transmitter operation during ELMing H–mode. (a) Transmitter power stays on at the MW level during vigorous ELMs, with small "waste power" shunted to the dummy load. (b) Photodiode signal indicates ELM spikes, while plasma loading impedance follows. (c) Percentage of transmitter power coupled to the plasma. (d) The reflection of power to the transmitter remains low.

2.5. ADVANCED TOKAMAK

We have installed and operated a new upper divertor baffle and cryopump to control the core electron density in high-triangularity discharges. Density control is important in DIII–D experiments because the efficiency of the radio frequency sources used to drive noninductive currents is inversely proportional to the core plasma density. As shown in Fig. 2-34(a), the upper baffle is an inertially cooled support structure covered with graphite tiles similar to the construction of the rest of the DIII–D wall. The helium-cooled cryopump has a deuterium pumping speed of ~40 k ls^{-1}, and the exhaust rate can be decreased by moving the outer plasma strike point away from the pump entrance (i.e., inwards). Electromagnetic forces from "halo currents" induced by disruptions were an integral part of the design. The baffle was constructed with flexible gas seals so that the conductance into the main chamber was very small; this isolates the high pressure region in the pump from the core plasma. The baffles were aligned in situ with precision supports to the measured DIII–D toroidal field.

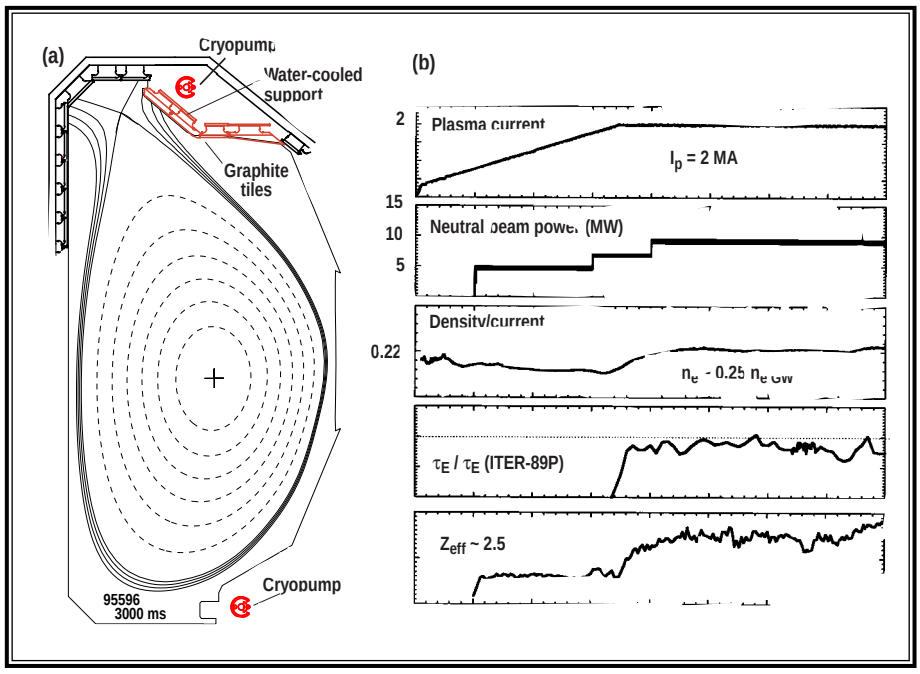

Fig. 2-34. Operation of the upper pump and baffle at I_p = 2 MA and 9 MW of neutral beam power. Plasma conditions included good H–mode confinement τ_E/τ_E (ITER–89P) ~ 1.8, fairly clean plasma core (Z_{eff} ~ 2.5), an ddensity control η_e/n_{eGW} ~ 0.25.

In ELMing H–mode plasmas, we have reduced the "natural" (no gas puffing) core density from n_e/n_{GW} ~ 0.5 – 0.6 to 0.3 with cryopumping, where n_{GW} is the Greenwald density. At a plasma current of I_p = 1.6 MA, the core plasma is "clean" with Z_{eff} ~ 2.0. Shown in Fig. 2-34(b) is an upper single-null high-triangularity discharge with I_p = 2.0 MA, the Z_{eff} increases to 2.5, n_e/n_{GW} ~ 0.25, and τ_E/τ_E which is the ratio of the energy confinement time to ITER89–P scaling is ~1.8, i.e., good H–mode confinement. The pump exhaust at these low densities was approximately equal to the beam fueling rate (~15 T ls^{-1}). This operation is similar to that obtained with the lower pump in low triangularity discharges.

Effective wall conditioning was important in obtaining these results. The normal DIII–D baking and boronization procedures were used after the upper baffle was installed. The plasma strike points were swept back and forth over the baffle plates for several discharges. Helium glow discharge cleaning was used between shots. When the walls were conditioned, cleanup from disruptions or impurity puffing was accomplished quickly; a "cleanup" shot was not always necessary. We also observed that cleanup was necessary when the direction of the ∇B drift (toroidal field) was changed; we operated with the ∇B towards the upper divertor plate for these experiments.

We have also compared single-null divertor operation with the upper baffled divertor and the lower open divertor. Fluid modeling of the plasma (UEDGE) and Monte Carlo modeling of the neutrals (DEGAS) was used to predict a reduction in the core ionization with the baffle by a factor of 3.75. We prepared two matched discharges: one with an upper single-null (baffled divertor) high-triangularity shape (Fig. 2-35), and the other a lower single-null (open divertor) high-triangularity shape. A measurement of the core ionization (from density and temperature profiles) indicated a reduction of 2.6 by the baffles in rough agreement with the code predictions. The energy confinement was similar in the two discharges. We also observed that the plasma "detached" (i.e., when the heat flux is reduced by deuterium gas puffing) at a lower core density with the baffled divertor.

Preliminary high-triangularity double-null operation has shown that the measured exhaust in DN (with the plasma only coupled to the single upper pump) is about half (10 T ls^{-1}) of the upper single-null rate (~17–20 T ls^{-1}). We have been able to vary the exhaust of the upper pump by varying the up/down magnetic balance of the plasma. As shown in Fig. 2-36, we have two additional planned divertor modifications: first, in 1999, an installation of an upper-outer pump followed by a full double-null installation with four cryopumps in 2001. The predicted reduction in the core ionization due to the baffling for the double-null case is nearly an order of magnitude.

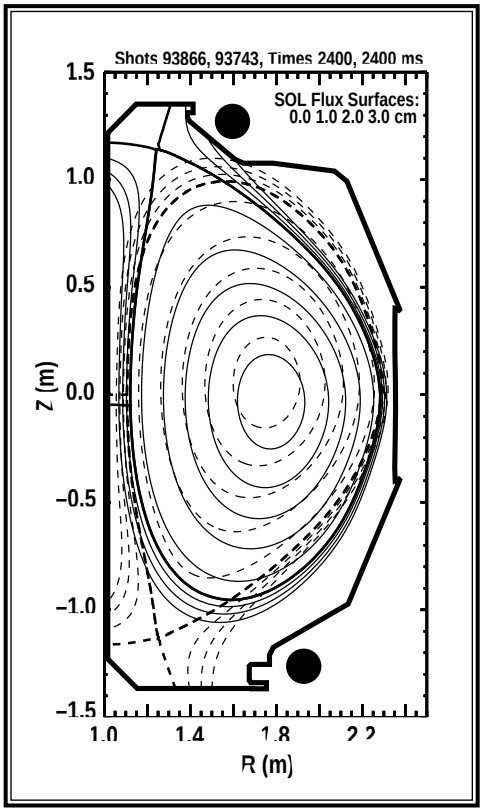

Fig. 2-35. The two SN plasmas used for the baffled (USN, solid) and open (LSN, dashed) divertor comparison.

2.5.1. RI–MODE

The goals of the RI–mode experiment in DIII–D are twofold: (1) to extend the enhanced confinement radiating mantle results to larger, diverted tokamak; and (2) to explore impurity injection in the AT scenario in particular synergism with high the ℓ_i scenario and edge pressure gradient and current control. The experiments in the first year were successful in contributing significantly in these goals. Enhanced confinement, radiating mantle discharges were obtained with inner wall limited as well as diverted L–mode configuration. The features are similar to RI–mode in TEXTOR. Increase in confinement (H_{89P}) up to 1.6 with P_{rad}/P_{in} ~ 0.7 and heat flux to the inner wall in the limited case was decrease factor 2 with neon injection. Neon puffing in an USN discharge (shown in Fig. 2-37) produced a quasi-stationary ELMing H–mode phase following a VH–mode phase and maintained $\beta_N \cdot H$ above 6 for more than 0.6 s only limited by the end of the high power phase. Mantle radiation is observed to increase internal inductance (ℓ_i) which allows higher performance AT operation ($\beta_N \sim 4 \times \ell_i$).

DIII–D discharges with neon injection which makes a transition from an improved low (IL) mode to an improved high (IH) mode were analyzed. The IH–mode is an ELM-free plasma with edge transport barrier but with energy confinement higher than normal H–modes. In order to understand what causes the improved confinement, comprehensive gyrokinetic stability analysis was carried out by taking into account the E×B shear suppression. In addition to the ion temperature gradient (ITG) and trapped electron mode (TEM) modes, high wave number electron temperature gradient modes (ETG) can contribute to transport, particularly electron transport. The result is shown in Fig. 2-38 in terms of growth rate and E×B shearing rate divided by wave number versus log k for inner and outer radii. (This plot gives a measure of the turbulence diffusivity including E×B shear.) At the inner radii, the ITG–TEM modes are separated from the ETG mode by a stable gap. In this region, Waltz's ITG quench rule is expected to work and does. At the outer radius,

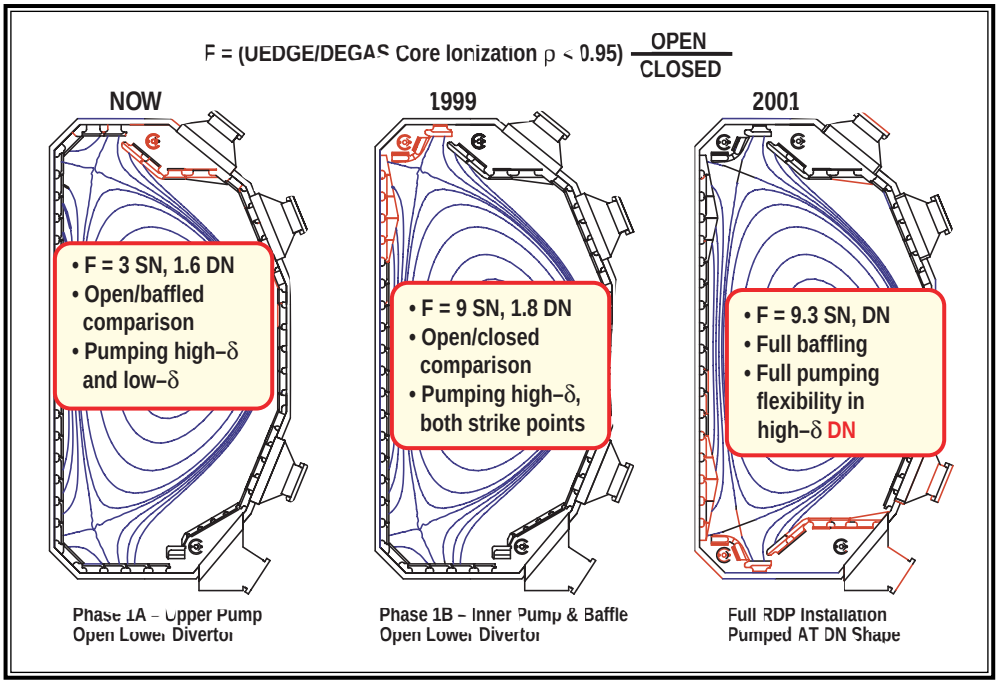

Fig. 2-36. Improvements in the modeled ionization of neutrals inside the separatrix are shown as the divertor becomes more highly baffled.

there is no stable gap in the drift wave spectrum. The E×B shear is expected to eliminate only the low k part of the spectrum. However, neon is directly stabilizing to the high k ETG modes. Indeed, transport with neon injection after E×B shear suppression is about half as large as in a hypothetical plasma. The neon stabilization of ETG modes is consistent with the inverse correlation between the electron thermal diffusivity and the neon concentration in IH–mode. The neon stabilization of the ETG modes is a mass dependent effect and should primarily effect the electron thermal transport. The future RI–mode experiment will be performed with fluctuation measurements, particularly with high-k FIR scattering.

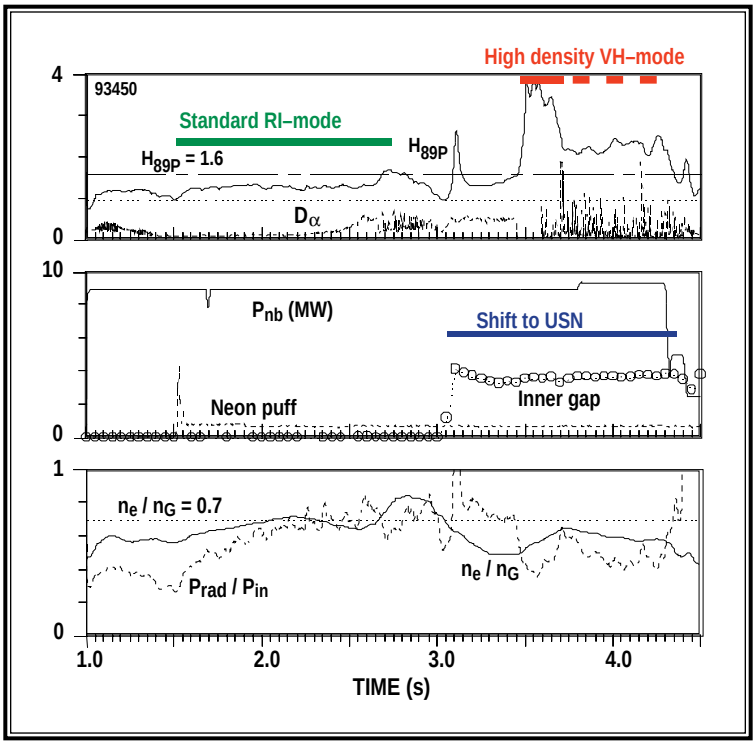

Fig. 2-37. Temporal evolution of a discharge with neon impurity gas puffing.

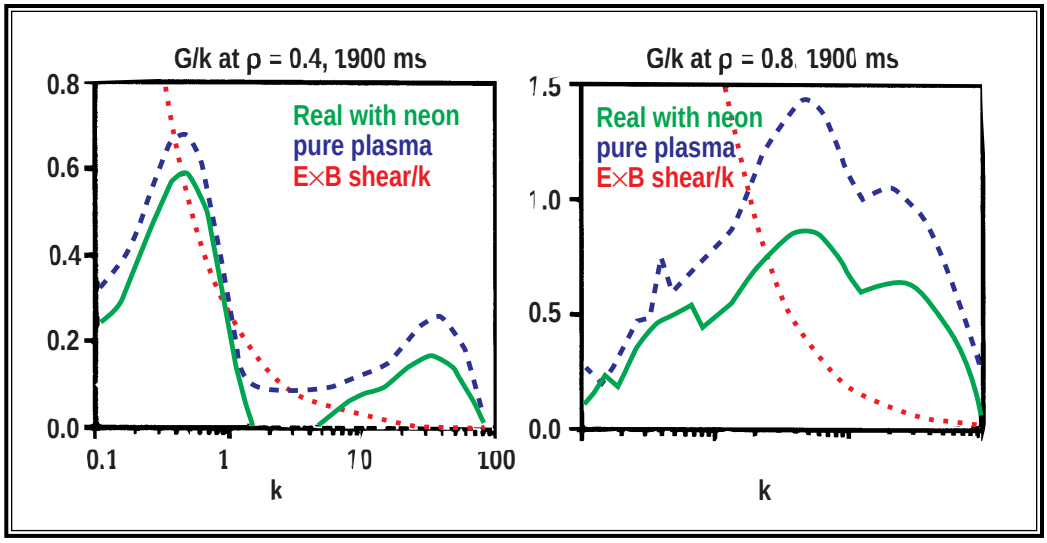

Fig. 2-38. Linear driftwave growth rate spectrum (growth rate/wave number k) of an RI–mode discharge at two radial locations. The spectrum of the real plasma with neon (solid) is compared with a hypothetical pure plasma (dashed). Also shown is the measured E×B velocity shear (dashed) at each location.

REFERENCES

Greenwald, M., et al., Nucl. Fusion **28**, 2199 (1988).

Hill, D.N., et al., Plasma Physics and Controlled Nuclear Fusion **3**, 487 (1991).

Lasnier, C.J., et al., "Survey of Target Plate Heat Flux in Diverted DIII–D Tokamak Discharges," to be published in Nucl. Fusion; General Atomics Report GA-A22231 (1998).

Mahdavi, M.A., et al., "Recent H–mode Density Limit Experiments on DIII–D," in Proc. 24th European Conf. on Controlled Fusion and Plasma Physics, June 9–14, 1997, Berchtesgaden, Germany (European Physical Society, to be published); General Atomics Report GA-A22636 (1997).

Maingi, R., et al., "Density Limit Experiments in DIII–D," presented at the Proc. 13th Int. Conf. on Plasma Surface Interactions in Controlled Fusion Devices, May 18–22, 1998, San Diego, California, to be published in J. Nucl. Mater.; General Atomics Report GA-A22873 (1998).

Maingi, R., et al., Phys. Plasmas **4**, 1752 (1997).

Petrie, T.W., et. al., J. Nucl. Mater. **241-243** (1997) 639.

3. OPERATIONS

3.1. OVERVIEW

This year was characterized by a number of important activities, most notably, two 110 GHz ECH gyrotrons were installed and commissioned, the upper RDP cryopump and baffle was installed, and the ohmic heating coil lead was successfully reinforced to allow return to the design coil configuration and an increase to 7.5 V-s next year. Real-time "Isoflux" plasma control was implemented to control the shape and position of the plasma. This system solves the MHD equilibrium equation in real time to accurately determine the location of the plasma boundary. At the same time, we were able to improve our safety record with three minor accidents and no lost time accidents. The staff available for operations tasks was substantially reduced owing to recent budget reductions and this impacted a number of activities.

The tokamak was operated for 127 days, including 61 days dedicated to the research program. The availability during research operations was 57%; historically, this number is low and this can be partially accounted for by one time events and the reduction in staff.

The neutral beams continued to be the workhorse heating system with up to 20 MW of power and an availability of 90%. During the year, two new high power 110 GHz gyrotrons, one from Gycom in Russia and one from CPI, were commissioned and operated into plasma. Both worked remarkably well for new one-of-a-kind systems. By the end of the year, they had injected a combined power of 1.2 MW into DIII–D for 1 s. The installation of a balanced loop configuration for the feed of one of the ICRF antennas demonstrated this to be a robust configuration with much less sensitivity to the details of the plasma configuration. Operation of two of the three ICRF power systems continued to be hampered by poor performance of the final amplifier tube while we awaited a replacement final output stage in 1998.

The computing systems continued to evolve in response to user needs. The largest stored data set of a plasma discharge increased 15% to 219 Mbytes. A new shot server was purchased to provide better access to the shot data, and a number of the major computers were upgraded in their capability. The computer systems used to operate both the tokamak and the neutral beam heating systems were upgraded to new operating systems and hardware because it had become essential to replace the obsolete operating systems.

The installation of the upper pumped divertor baffle and cryopump was a major six-month effort, taxing the available staff when combined with the other ongoing tasks. The rather large task along with its associated cryogenic and diagnostic tasks were completed in time for the start of operations in May. Successful operation was achieved and the pumping speed of the pump was shown to be comparable to that of the pump previously installed in the bottom of the vessel.

Much of the diagnostic work for this year focused on modifying or adding diagnostics in conjunction with the installation of the upper radiative divertor cryopump and baffle. The most noteworthy diagnostic improvement was the addition of the capability to routinely measure the radial electric field E_r in the plasma by making motional Stark effect (MSE) measurements along two different viewing chords allowing separation of the magnetic field pitch angle from E_r.

The work described here was completed within a relatively safe work environment. There were only three minor accidents — none of which resulted in lost time. The laboratory continued to benefit from a positive and proactive attitude toward both occupational and radiation safety. The facility was operated within its ALARA radiation goals with the long period of in-vessel work and associated large in-vessel tasks providing a particularly challenging scheduling task.

3.2. TOKAMAK OPERATIONS

In FY97, DIII–D was operated for 127 days. This included 61 days for physics experiments and 45 days for wall conditioning with plasma, diagnostic calibration, and power testing. An additional 21 days were used for high-temperature vessel bakeout and boronization (Fig. 3-1).

During experimental operations, the machine availability was 57% and a total of 1274 discharges were fired. The sources of downtime as a fraction of total scheduled time for experiments is shown in Fig. 3-2. There were a considerable number of operation problems in the third quarter. Two of the largest sources of downtime included five days lost due to an intermittent vacuum leak and five days lost due to mandated facility shutdowns by the power company due to high power loads on the electric grid. To locate the leak, a new leak-checking technique was developed that uses a palladium catalyst to significantly increase our leak sensitivity following deuterium plasma operation. This will improve our ability to rapidly locate vacuum leaks in the future. In response to the power outages, the typical DIII–D vent schedule has been changed so that we will no longer operate during the hot months of August and September. This should help to avoid these shutdowns in future years.

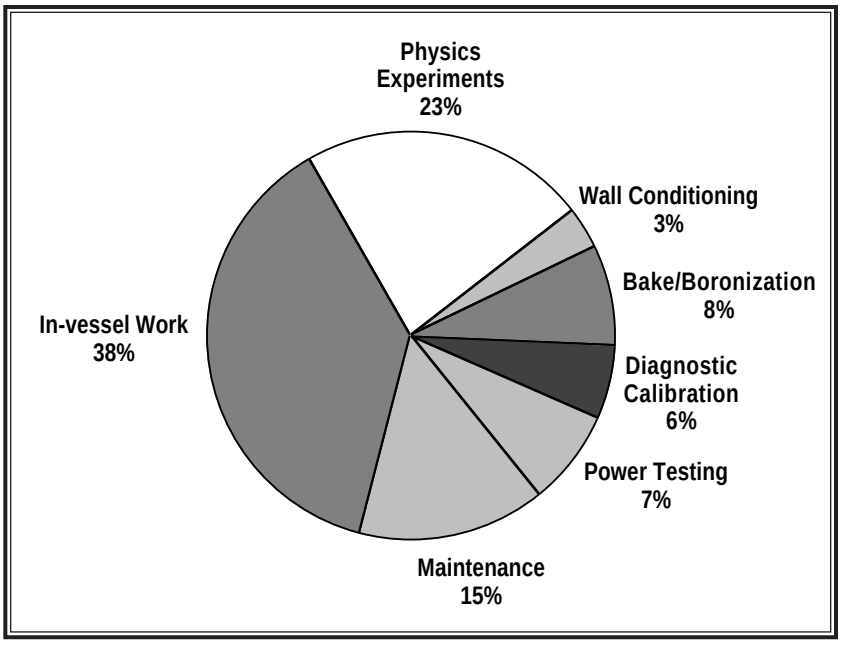

Fig. 3-1. Use of DIII–D facility in FY97.

The chronology of events and highlights for FY97 is shown in Fig. 3-3. The machine was vented in August 1996 and remained

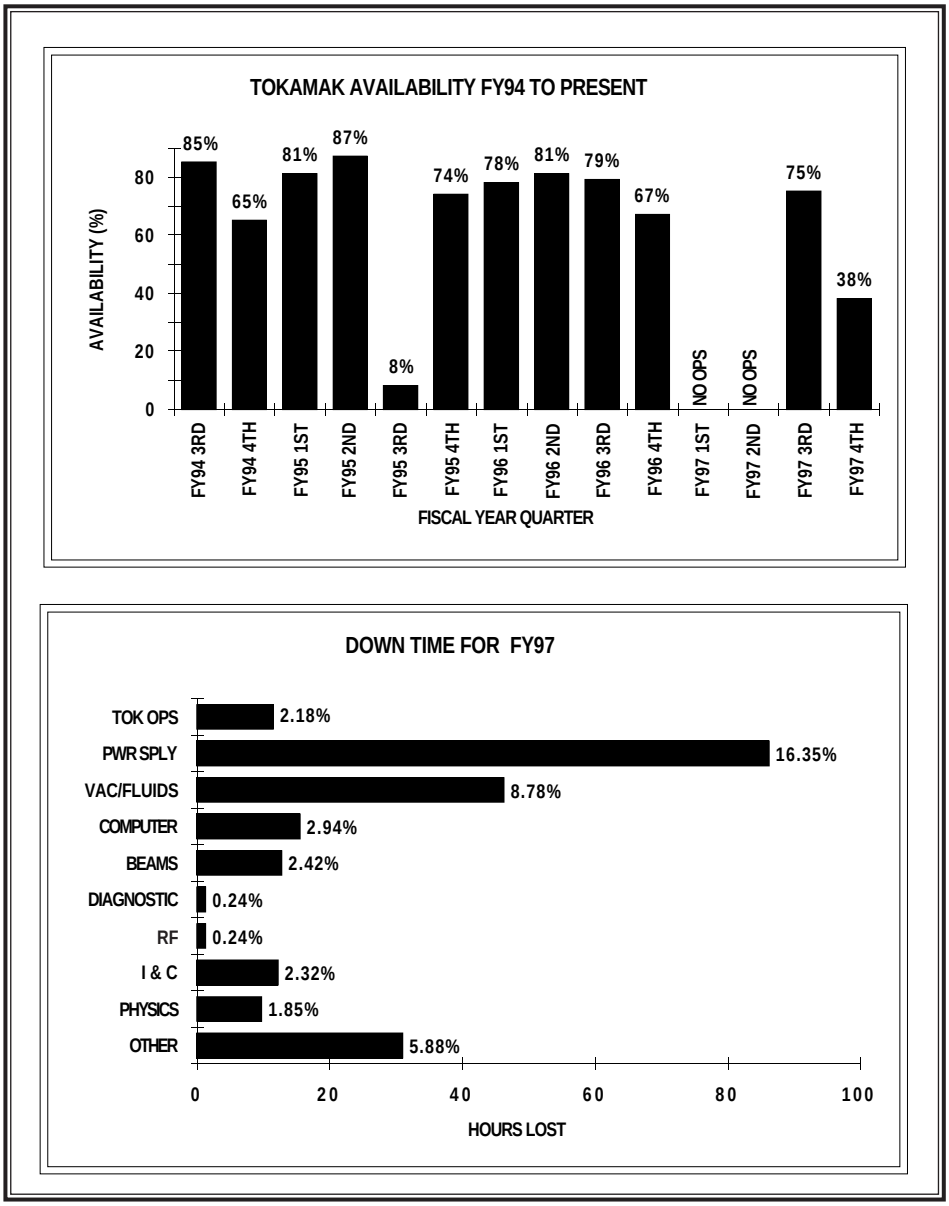

Fig. 3-2. Tokamak availability and causes of down time.

vented until March 1997. The major tasks during this vent were the installation of the upper radiative divertor project (RDP), installation of new diagnostics, and repair of the ohmic heating coil lead.

The new RDP installation includes an in-vessel cryopump and an upper divertor baffle that is optimized for high triangularity, advanced tokamak plasmas. The pumping speed without plasma is ~40,000 l/s, similar to the lower pump. The pump has been operated routinely throughout the year and in conjunction with the lower pump has allowed us to pump both upper and lower single-null divertors and triangular double-null divertors. In order to provide more precise control of the plasma shape during the divertor pumping experiments, an improved control

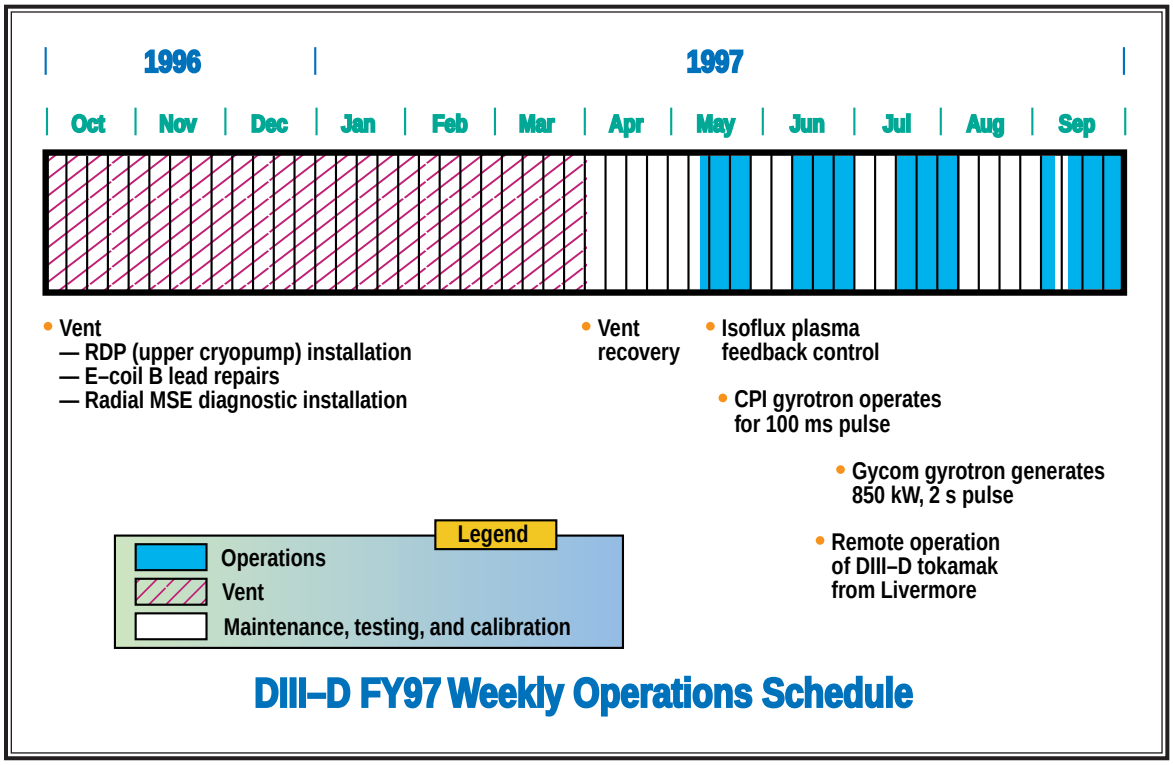

Fig. 3-3. Chronology of events for FY97.

system was required. The new "ISOFLUX" control was implemented this year that performs a real-time solution to the EFIT magnetic equilibrium code to locate the plasma boundary.

Considerable diagnostic work was done during the vent including modification of eight diagnostics to accommodate the new RDP installation and eight new diagnostics. The largest addition is a new array of motional Stark effect (MSE) channels whose principle mission is to determine the electric field contribution to the MSE measurement. The new channels have a significantly different viewing geometry than the existing systems and this has permitted routine measurements of the radial profile of both the plasma current and the radial electric field. Other diagnostic additions include several new Langmuir probes in the divertor throats, a flow measurement in the divertor region, a fast pressure measurement under the RDP baffle and a new reflectometry system that will measure the ion mass and, thus, may provide an innovative technique for determining the n_D/n_T profile on ITER.

During the vent, the damaged lead of the unused half of the ohmic heating coil solenoid was repaired. Although the repair was initially thought impossible because of restricted access to the lead, the use of remote manipulator tools in combination with limited access through a hole cut in the vessel permitted the lead to be repaired successfully. The repair involved building and installing a bracket that provides adequate preload to the cracked lead so it will not flex if the current in the OH–coil is kept below the level that provides 7.5 V-s of flux. This is a 50% increase over what was available before the repair and should be adequate for all our discharge needs. One

of the three water leaks in the coil was also repaired in FY97 and the remaining leaks were repaired or plugged in early FY98. The full coil was successfully operated in January 1998.

In anticipation of the need to remotely operate large fusion facilities in the future, a test of this capability was performed on DIII–D this year. The tokamak was remotely controlled from Lawrence Livermore National Laboratory (LLNL). Multiple audio and video communication links were established between key people at the two sites and all plasma parameters were controlled from LLNL and all the plasma data were available for analysis. The experiment was successful and should provide useful input to future implementation of this control concept.

3.3. NEUTRAL BEAM OPERATIONS

Nine weeks of plasma heating experiments were supported by neutral beams in FY97. Additional weeks of beam system operation in late March and April were required to condition ion sources, perform beam power calibrations, solve problems of the new neutral beam AEG computers, and support DIII–D vessel cleaning and diagnostic calibrations after a six-month shutdown. The 150 and 210 deg ion sources were operated in helium beams to support two days helium plasma experiments in the third quarter. Beam systems were operated in hydrogen for one day in September to inject hydrogen beams into hydrogen plasmas to help reduce deuterium level inside the tokamak for vessel leak checking purposes.

A simple method for catalytically reducing high deuterium background in the sample stream of helium leak detector to leak check beamline was implemented. This method was successfully used to find a small leak on the bellows of the 30 deg beamline source isolation valve actuator. It was also successfully applied to the DIII–D vessel in September resulting in restoring maximum sensitivity to the leak detector, enabling personnel to quickly find the major leak which had been impacting tokamak operations for weeks, and had defied all prior attempts to locate it.

The computers which control neutral beam shot cycle sequences, while also performing data acquisition and display functions, have been upgraded to modern hardware running a variant of the Unix operating system. After the first two months (April and May) of operation in 1997, high reliability has been achieved. The current focus for this project is to provide additional capabilities, automating startup and conditioning of beam system daily operation, and to provide enhanced system protection and performance reliability. Modifications of the neutral beam control consoles were also performed and completed.

Availability of the neutral beam system by month is shown in Fig. 3-4. The “Available” category is based on the beam system requirement requested by the physics experiments. The difference between the “Available” and “Injecting” categories represents beam systems which were available but were not used for injection during physics experiments. The various causes for downtime are shown in Fig. 3-5.

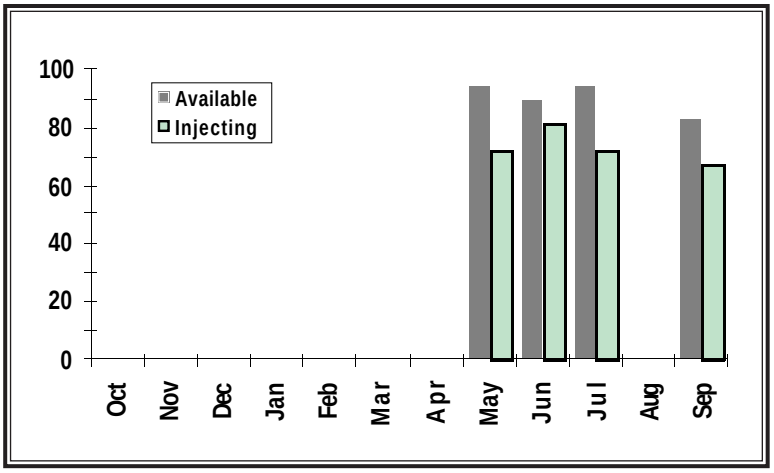

Fig. 3-4. Neutral beam availability by month.

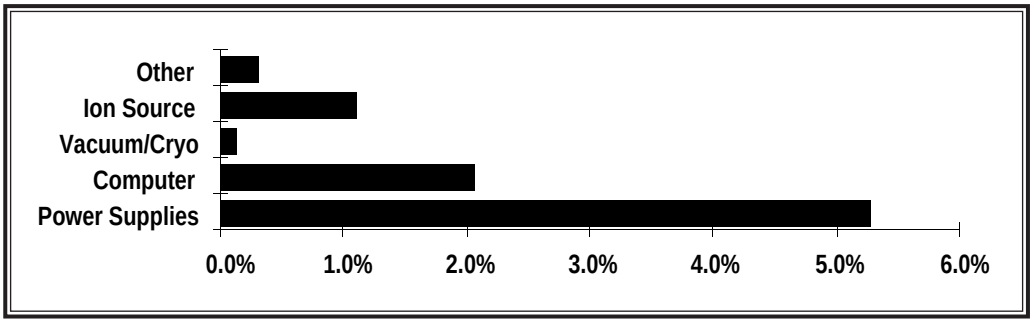

Fig. 3-5. Causes of downtime by category (percent of total operating time).

3.4. ICRF

A decision has been made to convert the 285 deg antenna/matching system into a balanced feed configuration. Work on the transmission line reconfiguration was begun early February. The transmission line preliminary layout of the balanced feed configuration system for the 285 deg antenna was completed and a design review was held. Based on this review, parts were placed on order with an expected delivery in early April. Fabrication of the hybrid loop for the 285 deg antenna was completed and extensive low-level measurements were conducted to assure proper operation before installation. To date, power levels of up to 1 MW both into vacuum and plasmas have been demonstrated. Extensive testing and refining of the 285 deg transmission and vswr/voltage balance networks was carried after the transmission line modifications. The system is now much more robust in its ability to handle limited load changes. The new configuration now gives us the ability to vacuum condition between shots and be ready for plasma injection with only a slight change in the decoupler stub position. A new feedback and monitoring circuit has given us the ability to regulate the output power based on antenna voltage which may be beneficial during H–mode transitions.

Talks with both ORNL and PPPL were undertaken to determine the level of effort and areas in which each can contribute to the rf program at GA. These talks have focused on areas of responsibility and number of people involved for this year and future years. The rf group from PPPL arrived and presented their plan for DIII–D rf support. There will be a full-time engineer and support person here for most of the remainder of this year and all of FY98. Specific areas of responsibility for PPPL, ORNL, and GA were identified and agreed upon. PPPL will be looking into the possibility of retrofitting the ABB transmitters with Eimac tubes. This retrofit could result in a significant increase in performance over the now derated tubes. An engineer from PPPL was here for almost two months as part of the collaboration agreement. He returned to PPPL in September but is due to return in early October for a one-year tour of duty. A senior support person is also scheduled to arrive in October for the same one-year stay.

ABB Nos. 1 and 2 were both fitted with the new high-voltage regulator system. Dummy load testing has verified the improved voltage regulation. The need for the new regulator became pressing as we tried to reach higher power levels. The poor response time of the supply caused excessive screen grid current which would initiate the automatic power reduction circuits internal to the ABB systems. A new and improved stripline section was also installed in the driver output stage on both ABB transmitters. This was done to improve the contact force which had been a troublesome area when trying to tune for operation at some frequencies. Testing of the modification showed improvement at the nominal 82 MHz operating frequencies but there is still some arcing problem when trying to operate at 56 MHz. This problem is looking as if it is not related to the stripline and will need to be investigated further.

Franz Braun from ASDEX was here for almost a month. The purpose of his visit was to discuss with us and show his results of his low frequency arc detection. Implementation of a similar system on DIII–D is currently being worked on by our collaborators from PPPL.

3.5. ECRF

The reporting period began with the Gycom gyrotron installed on DIII–D and producing over 800 kW pulses 500 ms in duration. It ended with two gyrotrons in routine operation together injecting over 1.2 MW into DIII–D for 1-s-long pulses and with the Gycom gyrotron reliably producing 2-s-long pulses at full power.

Initial high power injection into DIII–D demonstrated that the copper-coated graphite mirrors on the in-vessel launcher assembly would have to be replaced due to arcing. These mirrors were successfully replaced with copper mirrors which remain in pristine condition after a year of operation. The thermal performance of the new mirrors has been better than predicted. Early in the fiscal year, Gycom and GA collaborated to increase the maximum pulse length for our first 1 MW gyrotron, Katya, to 2.0 s. Generated power levels in excess of 800 kW for these pulse lengths were routinely obtained during DIII–D experiments and modulation at frequencies up to 50 kHz was tested. Using Katya, transport experiments with modulated application of the ECH power were performed, the power deposition profile was measured as a function of deposition location and, for low density plasmas, record central T_e values in excess of 10 keV were achieved.

In January, the first CPI (formerly Varian) gyrotron, christened Dorothy, was received and fitted into its magnet. About six weeks later, both gyrotrons were operated simultaneously for beam profile tests into the vented DIII–D vacuum vessel. The launchers were found to be working as designed and the beam spots were about 10 cm in diameter and 10 cm apart at the center of the tokamak. In conjunction with CPI, Dorothy's performance was carefully increased, and operations with 750 kW generated rf power and 1 s pulses were regularly available for DIII–D experiments. The power/pulse length limit for Dorothy, as with the Gycom gyrotron, is determined by microwave heating of the output window.

Losses in the Matching Optics Unit (MOU), the chamber connected directly to the gyrotron in which mirrors focus the beam and couple it to the waveguide, initially were higher than expected both for Katya and Dorothy. Free space beam profile measurements were made to enable the beam phase and spatial structure to be retrieved. Using these data fully describing the output beam, new MOU mirrors were built by Gycom for Katya and by CPI for Dorothy and the MOU losses were reduced to less than 20% of the generated power for both systems. With these mirrors in place, 75% of the power passing through the gyrotron windows was transported to DIII–D and injected into the plasma.

The project to design and build new MOU mirrors for Dorothy represented a strong collaboration among MIT, the University of Wisconsin, CPI and GA. A second CPI gyrotron was damaged in final testing at CPI and the decision was made to take advantage of new technology for production of large samples of artificial diamond and to rebuild the damaged gyrotron with a diamond output window. A sample of the diamond material was tested at Gycom and found to have extremely low absorption of the 110 GHz microwave beam and thermal conductivity more than five times better than copper. Redesign of the internal mirrors for this gyrotron to produce a Gaussian output beam has begun by the same collaborators, using the phase retrieval techniques which had been used in the project to design the MOU mirrors for Dorothy. This work is continuing with the goal of delivering a 1 MW gyrotron equipped with a diamond output window to DIII–D and operating it during the summer of 1998.

In parallel with installation and testing of the gyrotron systems and DIII–D experiments, development continued on the network based system for control of multiple gyrotrons and on enhancements to our testing and measurement capability. The system can display interactive screens for control, status annunciation and diagnostics on any networked terminal device and is expandable to handle more than the 10 gyrotron installations envisioned in the long range plan. Specialized modulation requirements for the individual gyrotrons can be programmed and the tubes can be managed individually or in groups as desired. The testing and diagnostic capability was improved by the acquisition of additional infrared and millimeter wave hardware which permit beam profile, window heating and mode purity measurements to be made.

The ECH installation has demonstrated reliable operation at high power from two gyrotrons with a third under development. The evacuated transmission line, waveguide switches and dummy loads have performed according to design specifications and injected power levels in excess of 1.0 MW are routinely available for DIII–D experiments. The results from the first group of physics experiments on current drive, heating, transport and ECH physics are described in other sections of this report.

3.6. COMPUTER SYSTEMS

During FY97, there were 2730 tokamak shots containing 278 Gbytes of data. These numbers were smaller than FY96 due to fewer operating weeks; however, the largest shot was 219.1 Mbytes — an increase of 15% over the previous year. Work this year has focused on improving data availability, completing the modernization of computer systems, improving data analysis usage, and enhancing the computer staff.

In order to greatly improve data availability, a new shot server system was purchased, installed, and implemented. This system is based on a Sparc processor running Solaris and has a 100 Mbit network interface and 100 Gbytes of usable RAID storage for data (2.5 times as much space as before). The system is being filled with data as new shot restores are requested and will allow about 2000 shots to be on magnetic disk. As a second phase for improving data availability, plans are being made to purchase a robotic tape library and optical jukebox to handle all DIII–D data. In addition to hardware improvements, a new shot restore program was put into place with considerable enhancements and efficiency improvements over the old program.

Usage of the hydra CPU server continued to increase with more users analyzing data. To better handle this usage, the swap space was expanded, and the memory was doubled to 1 Gbyte. Plans are in progress to increase the CPU power of hydra as well. All of the HP systems including hydra are beginning to be upgraded to HP–UX 10.20, the latest version of the HP operating system. Most of the office building workstation network connections have been moved to single ports on an Alantec powerhub switch. These network changes are part of the plan to improve the network availability in the office buildings. The ESnet Coordinating Committee meeting held in San Diego, and the August data analysis workshop were broadcast over the internet.

During this year, the upgrade to use of the new Neutral Beam computers was completed, the final phase of upgrading the old MODCOMP computers. This upgrade included a plotting package for NB waveforms, inclusion of data acquisition software and sequencing, programming of the beam timing CAMAC modules, creation of new mechanisms for the NB historical archive, and the creation of screens and the database for the Accessware control software. A second CAMAC software driver was programmed so that each of the two CAMAC highways has its own driver.

On the tokamak control computer, software was implemented for saving and plotting the San Diego Gas & Electric power monitoring values. This will enable examining long-term trends in power usage. New routines were developed for handling thermocouple data. Accessware problems that occurred on the neutral beam systems also occurred on the control system and workarounds were implemented.

A second CAMAC highway was added to the data acquisition system resulting in a 40% decrease in the overall data acquisition time since the highways were now running in parallel. Additional memory was added to this system to alleviate problems resulting from heavy data access.

The Plasma Control System (PCS) work has focused on the completion of the new parameter data routines which are essential to extending the control capabilities of the PCS

including isoflux control using the real-time EFIT code. A number of existing control algorithms were modified to make use of this new method for handling nontime-dependent data. The isoflux single-null divertor algorithm and isoflux low double delta null algorithm were modified to call the basis shape editor, segment editor, and reference editor. Work is also continuing on the development of a parameter data restore capability.

Initial computer software support of the Thomson scattering system began as part of the effort to improve and modernize that diagnostic system. The basic Rayleigh analysis code for reviewing Thomson scattering data was converted to IDL and used to analyze shots. Work has begun on the main Thomson analysis code to convert it from FORTRAN/DISPLA to C/IDL. The Thomson workstation has been set up for handling shot data, both for remote data access, and for creation, compression, and archiving. Work was completed on functions to read the data points and return the expected information to the user.

Many modifications have been made to the 4–D code in response to user requests. In addition, much of the code has been made more generic and ported from HP–UX to DEC UNIX. The operational version now runs from compiled IDL code rather than interpretive code. The TRANSP code was updated on the GA Alpha workstations. Changes were made to array sizes in the REVIEW code, and data combination problems were fixed. Several improvements were made to the TIMCON timing code, in particular for neutral beam purposes. The neutron counter code (NCTR) was converted to run under UNIX. All pending changes and updates have been incorporated into the ONETWO code. Work began on a Time Series Analysis code (Fourier analysis). A DEC UNIX workstation was developed for use as a new Web server. Various software was downloaded and installed on the system, and a web search service web page was created. Many bugs in the web site have been fixed. The web site has been reorganized in order to make it easier to maintain and administer.

Various database vendors were contacted in order to gather information relevant to deciding on a new database for physics. Other laboratories were also contacted in order to find out their database experiences. In-house technical presentations were made by several vendors. The MDSplus data system is being investigated for organization of DIII–D data. MDSplus was installed on local computers and demonstrations were made.

All old shot data that was on 6250 bpi tape has now been copied to 8 mm tape. All old tapes have been eliminated.

Five new people joined the computer staff this year including a scientific programmer to work on data analysis programming issues, a programmer to work primarily on requests for website material, a real-time programmer dedicated initially to the Thomson scattering diagnostic, a real-time programmer for various DIII–D systems, and a UNIX systems administrator.

A five-year plan for computer systems was written to define what needs to be done over the next five years to handle the increasing collaborators, quantities of data, and data analysis needs.

3.7. OHMIC HEATING COIL REPAIR

Half of the DIII–D solenoid ("B" windings) were disconnected in June 1995 due to a cooling water leak that had developed in the lead area located at 345 deg on the machine. Continuing tokamak operations used only the "A" windings of the solenoid with constrained performance parameters. The leaking water was traced to a crack in the hollow lead conductor located about 2 m from the end of the conductor. Inspection indicates that the original fabrication of the lead in 1978 had inadequate epoxy impregnation probably due to the difficult-to-seal geometry of the lead. This weakness had caused the lead overwrap to tear as it was subjected to repetitive I×B forces acting on individual conductors. Direct access to areas needing repair was prevented by the existing hardware precluding the use of conventional repair techniques such as replacing fiberglass overwrap or cutting and replacing of tubes. Full disassembly for direct access was not considered because of significant cost and schedule impacts.

The in situ repair approach was developed over nine months starting in October 1995. The concept was evolved and refined from about 12 ideas that were considered. The necessary actions were to stabilize the lead mechanically to prevent additional crack growth and to restore coolant flow using seals, plugs, or replacement cooling tubes. These five repair tasks were:

1. Restrain the conductor pack in the lead area using a clamp to produce 5200 lb downward preload against the conductors in the lead. This loading will eliminate cyclic stresses in the conductors which would result in continued crack growth. Install three band clamps around the lead between the F8B and F9B coils to maintain the conductors in their proper position since the overwrap has failed between the solenoid and the F9B coil.
2. Plug, seal, or divert cooling water past the crack in the conductor to prevent further leakage while cooling the cracked lead.
3. Restore adequate cooling flow in the leaky cooling return tubes at the top of the tokamak.
4. Monitor preload clamp performance and coolant flow repairs to assure proper operation. Develop interlocks to prevent operation with inadequate clamp load or coolant flow conditions.
5. Reconfigure the E-bus to the original DIII–D configuration and operate the A and B circuits of the solenoid with balanced current.

Only Task 1 of the five tasks required access into the vacuum vessel. This task was completed in March 1997. The other four tasks were completed later in CY97.

3.7.1. CONDITION BEFORE REPAIR

Figure 3-6 shows a vertical cross section through DIII–D at the 345 deg location of the solenoid lead. The failed lead conductor is 1 of 8 square copper conductors which comprise the B solenoid lead located at 345 deg at the base of the tokamak. The leaking conductor appeared somewhat displaced, upward from its normal condition, and is visible by bore scope through cracks in the overwrap of the lead. The structural damage to the overwrap of the lead appeared to extend over a length of about 80 cm and existed from the solenoid to below the F9B coil. The lead was reasonably well supported for downward loads but unrestrained against upward loads.

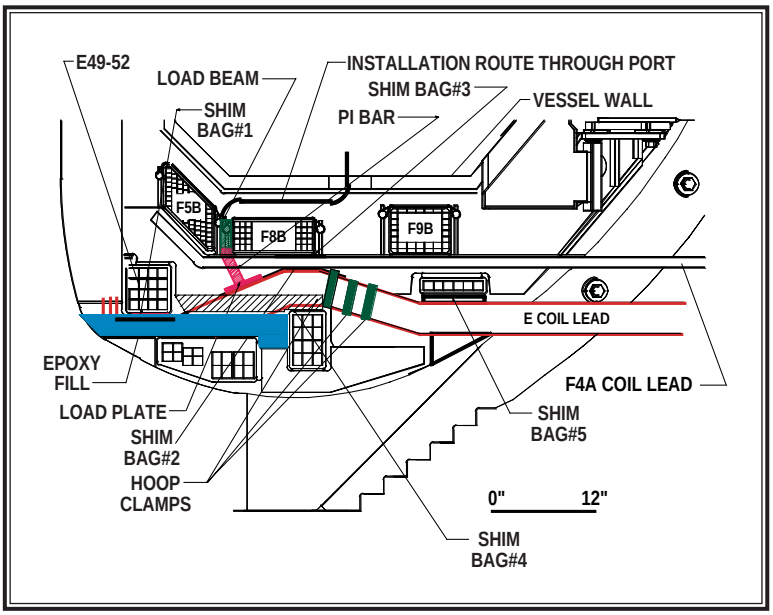

Fig. 3-6. DIII–D solenoid repair area.

Both up and down loading conditions existed on individual conductors during operation.

Removal of the 0 deg V-1 port was required (it is designed to be removable) to allow for a technician's right arm to directly access this area from inside the vessel. The selected repair was to install a local clamping device which applies about 5200 lb of downward preload against the conductors to exceed the calculated I×B upward load developed in the conductors. This produces only compressive stresses in the copper near the crack thereby preventing crack growth. This clamp is shown in Fig. 3-7. The clamp designed uses Belleville washers to maintain the preload force and is comprised of three major elements each sized to allow sequential installation within the restricted space. Five epoxy-filled shim bags were installed in the lead area in order to further constrain the solenoid B lead and the F4A coil lead and for reasons of conformal loading between the load plate and the solenoid lead.

3.7.2. SOLENOID LEAD CLAMP

The basic mechanical clamp design (Figs. 3-6 and 3-7) was developed in 1996 based on drawing dimensions. Space and access ruled out machining or welding on existing components. The clamp applies downward force to a load plate which in turn applies pressure to the inclined solenoid lead through shimbag No. 2. Shimbag No. 2 functions to distribute the load evenly to the lead surface. Installation of the load plate was done along a horizontal path parallel to the solenoid lead. A 5-m long concentric tubular handle is used to position the plate past its final insertion position at which time the plate is

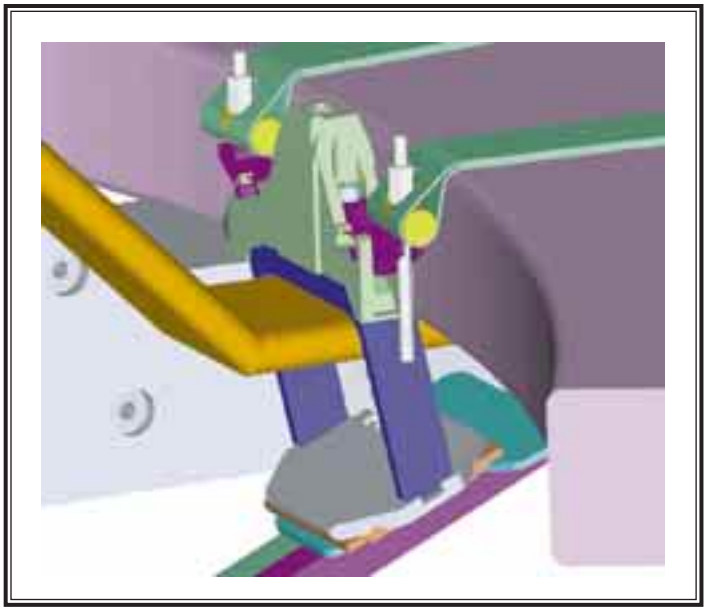

Fig. 3-7. Solenoid lead clamp system.

rotated 90 deg about two perpendicular axes and then tilted 25 deg about the third axis in order to align with the surface of the lead. This key installation step was demonstrated prior to the task decision to proceed. The pi bar (a structural bridge that looks like Π) was brought into position through the vertical port opening and rotated into place straddling the F4A coil lead and engaging mechanical keys into the load plate to prevent slippage between the pi bar and load plate. The load beam is then brought in through the vertical port with the load arms retracted to allow the beam to be positioned over the pi bar and between the F8B coil attachment studs. Once the arms were deployed under the studs and tightened into place, the clamp load is applied by rotating the jacking screw located at the top of the load beam.

The 0 deg V-1 port was removed in August 1996 which allowed for measurements of the as-built condition. Throughout the course of this inspection and repair activity, technicians developed about a dozen specialized long reach (about 10 ft) tools that saw repeated use. There were push tools, hook tools, gripper tools and several prebent, 0.5-in. diam copper tubes semi-permanently installed for the purpose of forming guide sleeves to rapidly relocate the bore scopes to the specific areas of interest.

The removal of failed shrink tube overwrap revealed that the tear in the fiberglass structural overwrap extended outward. This extensive failure of the overwrap resulted in the requirement to install three metal strap bands, as shown in Fig. 3-6, to replace the function of the failed overwrap. Remote cleaning of crumbled epoxy debris from the lead area revealed significant gaps between the eight square conductors as they occur in a single layer under the E49-52 coil near the solenoid. It was decided to fill these gaps by epoxy flooding prior to installation of shimbag No. 1.

An intensive installation period started on January 13, 1996, for installation of the production clamp system. Final installation of the clamp components produced many challenges. These included tangled positioning and retrieval strings, tangles with existing I&C wiring, broken retrieval strings, special tool requirements, etc. The installation took 20 days and required daily in-vessel technician and ex-vessel video operator activities for each of the 20 days. Installation of the remote tightening system was completed and this system was first used to restore load two days after the initial loading of the clamp.

3.7.3. REPAIR TO CRACKED AND LEAKING COPPER CONDUCTOR AT THE BOTTOM OF DIII–D

The cracked conductor in the solenoid coil lead appeared to have a vertical crack through about 33% of the top of the 2.5 cm square section caused by cyclic vertical deflections which should be greatly reduced by the preloaded clamp. The crack is at the top of a 11-mm diam coolant passage which has three 30-deg bends between the leak and the accessible end. Direct repair by welding or soldering were considered not feasible. The adopted method was to install a dual elastomer, expandable plug as shown in Fig. 3-8. The dual plug design provides sealing on both sides of the crack to isolate the crack from the coolant. The elastomers are expanded 15% in diameter by axial compression developed using a wire cable/copper tube push-pull system operated from outside the end of the coil lead. A second copper tube is connected to the interspace between the seals to supply high-pressure nitrogen buffer.

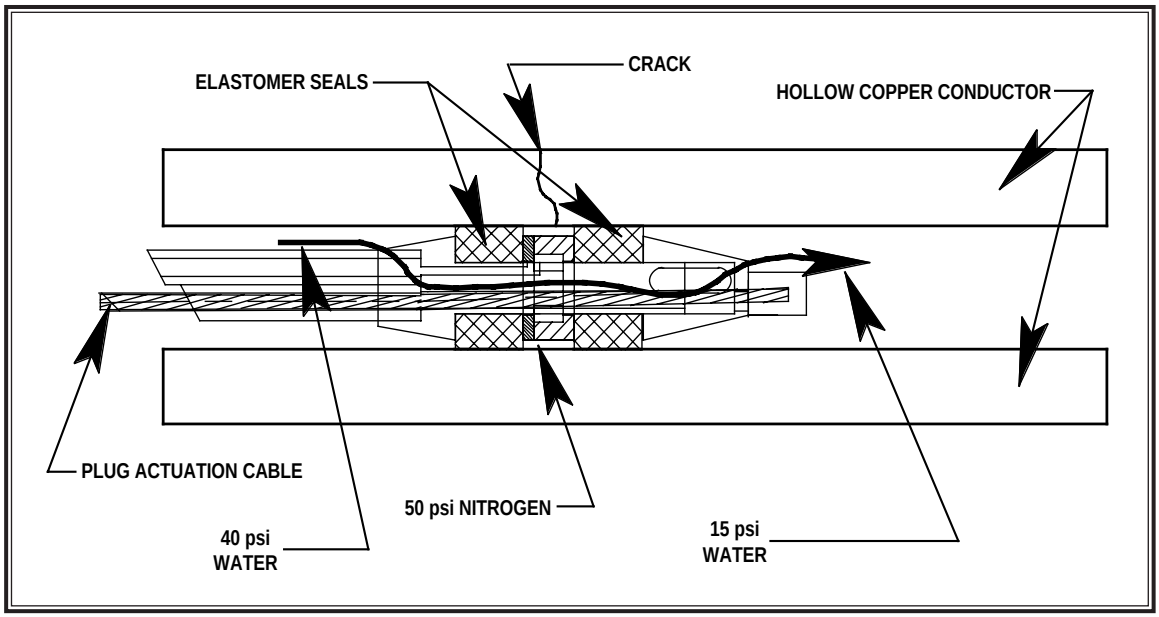

Fig. 3-8. Dual expandable plug.

3.7.4. REPAIR TO LEAKING COOLING TUBES AT THE TOP OF DIII–D

Two of the four 0.50 o.d. soft copper coolant outlet tubes at the top of DIII–D developed leaks during grit blasting to remove scale inside the tubes. The electrical insulation on the outside of the tube was viewed using bore scopes but the leak areas were not visible through the insulation.

The repair plan was to remotely cut the copper tubes beyond the leaks and remotely solder replacement tube sections. The leaks had been located in the radially oriented tubes approximately 10 and 40 cm from the outside of the solenoid. Due to the differences in tube configurations and access limitations, this approach required the development of both external and internal cutting and joining systems.

One tube was cut using a rotary saw on the outside of the tube. This tube was successfully replaced using a remote outside diameter solder joint in August 1997. This repaired tube provides full coolant flow in these conductors. The second, more challenging tube was cut using a whirring inside tube cutter in November and December 1997. The inside diameter solder joint was installed and remotely soldered but the joint leaked. After several attempts to resolder, the decision was made to install the backup system which was to install two dual seal plugs similar to that installed in the cracked conductor. These plugs seal the passages 2 m inside the lead conductors. A re-entrant tube supplies water near the plug which then flows out providing proper cooling for the leads. The lead plugs were installed early January 1998. The plugs allow for continued effort, if justified, to develop serial or parallel flow in the currently plugged conductors without disturbing the plugs.

3.7.5. INSTRUMENTATION AND INTERLOCKS

Three diverse sensors were installed with the lead clamp to monitor preload. This provided redundancy and the hope of attaining at least one sensor that could monitor load while operating in the high magnetic field during a shot. All three have been in operation since clamp loading in March 1997.

The clamp was preloaded to 5400 lb (load cell) in March 1997 which relaxed to 4850 lb over nine months (80% in the first two months) due to indicated lead settlement and shimbag creep of about 0.7 mm (0.029 in.). The clamp was tightened remotely to restore the 5400 lb preload in January 1998 prior to tokamak operation. The load cell and strain gage outputs are monitored to prevent the start of a shot with clamp load below 4660 lb. Analysis indicates that clamp preloads below 4200 lb may allow crack growth in the lead conductors.

The dual expandable plugs installed in the cooled leads and across the crack use a nitrogen buffer supply between seals. The nitrogen buffer, although interlocked, is a precautionary system to provide acceptable conditions should the elastomers develop a leak. The nitrogen flow will be monitored to evaluate seal integrity and/or crack growth. The nitrogen flow meter output was 0.60 std l/min. prior to I×B forces being applied. This leak is equivalent to deflating a fat bicycle tire over a 20-minute period. After two days of operational checkout with combined E and B coil systems, the leak rate decreased to 0.36 std l/min., probably due to clamp-developed compressive stresses tending to close the crack. Water flow through the crack seal and in the cooled leads are individually monitored by flow switches which are set to prevent the next shot if the flow rate is below 0.54 liter/minute (0.15 gpm). A delta P switch compares nitrogen and water pressured to assure gas pressure greater than water pressure.

A schematic of the B solenoid coolant flow and sensors is shown in Fig. 3-9. Thermocouples and thermal switches have been added to the four coolant outlets. The thermocouples are for evaluation and confirmation of solenoid thermal performance while the thermal switches are monitored to assure temperatures below 30°C prior to beginning a shot.

3.7.6. THERMAL PERFORMANCE OF THE REPAIRED SOLENOID

A code was developed to determine the expected thermal behavior of the B portion of the solenoid when operated with the modified cooling circuit. The code handled specified flows for a combination of normally cooled, serially cooled, and plugged, nonactively cooled conductors and models both the thermally isolated leads and the solenoid area where heat transfer between conductors can be significant. Heat conduction between adjacent conductors was based on solenoid testing results. Analysis of the repaired solenoid indicated identical temperature rise for both solenoid halves but the repaired solenoid does not return fully to the initial starting temperature after the 10-minute period between shots. For 25°C inlet water, 6.7 10^{10} A^2-s per shot , and 10-minute rep rate, the nonmodified system operates between 25° and 42°C while the repaired circuit operates between 37° and 54°C as compared to the 70°C limit. The repaired solenoid does not limit high performance operation but may require longer periods between high performance shots to cool down fully before the next shot. Correlation to the thermal model was done

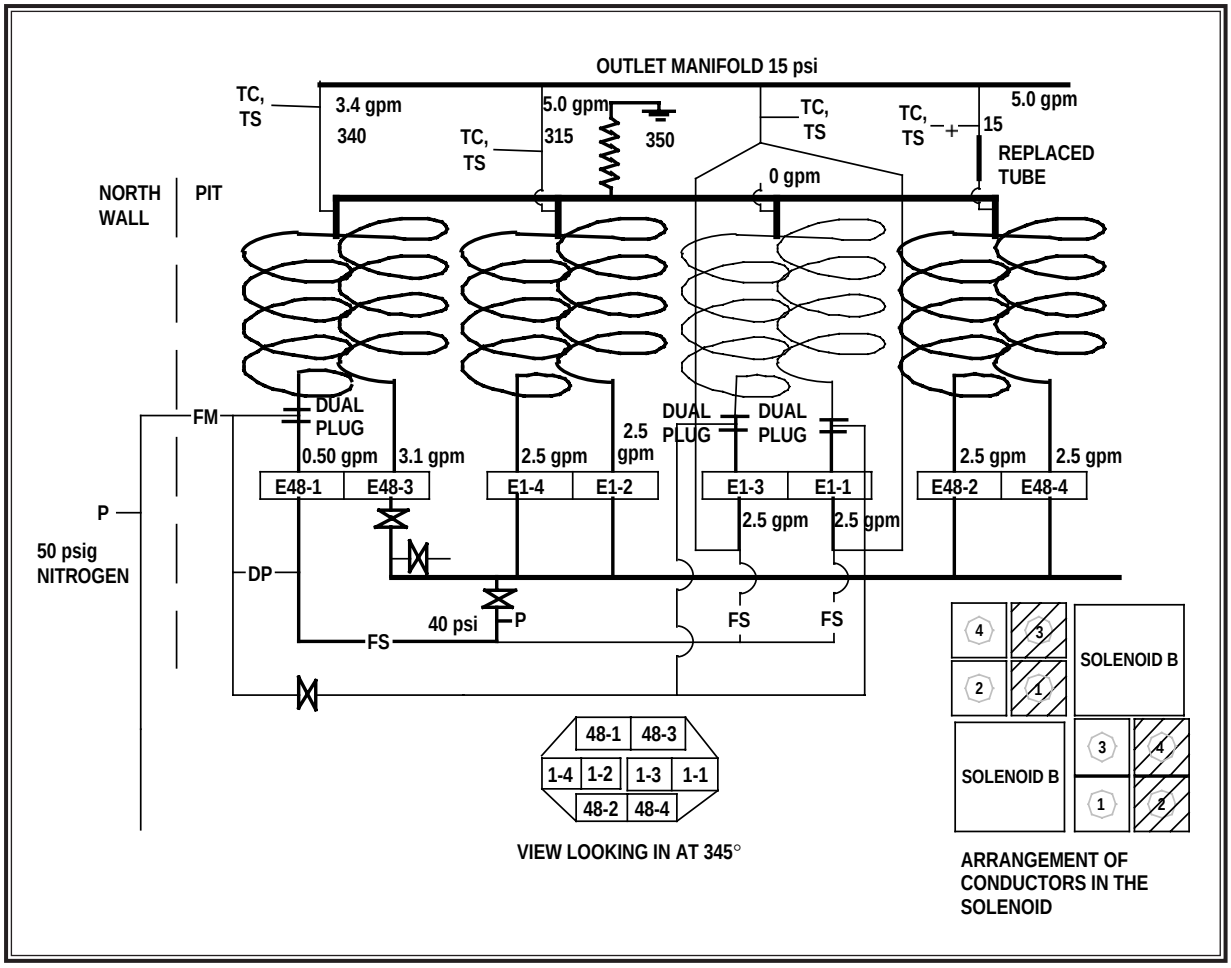

Fig. 3-9. Schematic of repaired DIII–D solenoid cooling system.

using the measurements from the four outlet thermocouples and indicates reasonable agreement although the testing to date did not duplicate the 10 full power shots on a 10-minute interval.

3.8. DIAGNOSTICS

The DIII–D diagnostic effort in FY97 focused completing the considerable changes required to the diagnostic set with the installation of the high-triangularity advanced tokamak RDP divertor pump (RDP 1A) and the addition of a radial MSE diagnostic for measurement of the radial electric field the corrected current profile.

The engineering design and preparation for the divertor diagnostic changes required for the installation of the RDP 1A was largely completed in FY96 and the fabrication and installation was started in late FY96 and completed in early FY97. A list of the diagnostic systems affected by the RDP 1A installation and the additions or improvements to diagnostics that were completed in FY97 is presented in Table 3-1.

TABLE 3-1
DIAGNOSTIC CHANGES DURING THE 96-97 WINTER VENT

RDP Moves/Modifications	New Capability
Bolometer	Radial MSE
Soft x-ray imaging arrays	Tile current arrays
RF probes	Runaway electron IR camera
Neutron detectors	Magnetic probes
ECE	Upper divertor fast pressure gauges
ICH antenna camera	Tangential divertor visible SPRED
	Upper divertor throat L.P.
	Lower divertor throat L.P.
	Tangential interferometer
	Fast wave reflectometer
	Midplane fast pressure gauge
	Radial particle analyzer
	Central CER channel
Future activity	

The radial electric field (E_r) has proven to play a very important role in transport in high confinement regimes in tokamaks, principally due to the stabilizing effect on turbulence due to shear in E_r. A first direct measure of E_r in a tokamak has been made using the MSE in DIII–D. MSE has been used for a number of years to measure the magnetic pitch angle (and thus the plasma current profile); but in high performance plasmas with transport barriers, the E_r term in the MSE is large. By employing two separate views of the neutral beam, both the E_r and magnetic pitch angle can be determined. A new MSE system was installed on DIII–D in FY97 that included a separate viewing geometry and has been able to make routine measurements of E_r for all types of DIII–D plasmas. These measurements cover the entire profile and have been used to study E_r effects in the core of NCS plasmas and the edge of H–mode plasmas. The E_r fitting is done self-consistently using the equilibrium code EFIT between shots and real-time feedback control signals of $q(0)$ or E_r are available for plasma control. The total number of MSE spatial channels was increased from 16 to 35.

There has been a critical need for a central electron density and temperature measurement on DIII–D for a number of years and it has been recognized that a Thomson scattering diagnostic would be the most appropriate diagnostic to fill that need. Because of the unique geometry of DIII–D, it is technically very challenging to build a Thomson scattering diagnostic with the appropriate view to make a central measurement. This has prevented us from pursuing such a system. In FY97, a new concept for a central Thomson measurement was explored and a conceptual

design developed. Based on this work, we are planning to build a central Thomson scattering diagnostic in FY98/FY99 with operation to begin sometime in late FY99.

The edge CER system upgrade was largely completed in FY97, all 16 edge channels now have CCD detectors. The high-speed CCD detectors replace the image intensified reticon arrays which was necessitated by the aging of the obsolete intensifiers. The central 16 channels of the CER system will be refurbished over the next two years.

Table 3-2 lists the major diagnostic systems operating on DIII–D at the end of FY97 along with the quantities measured. In addition to the development of new diagnostic systems, we continue to refurbish diagnostics that are known to be operating with critical components near or beyond their life expectancies.

In FY98, our plan in the diagnostic area will be to complete the design and to start the fabrication of the central Thomson scattering diagnostic. We also intend to start the design effort on the RDP 1B inner/upper diagnostics. This work will include building and testing a prototype fast pressure gauge that can be mounted on the vacuum vessel wall and testing a new concept for a partial pressure measurement. We also plan to install a VUV two-dimensional imaging system in the lower divertor. This, in conjunction with other existing diagnostics, will allow 2–D mapping of carbon concentrations in the divertor.

3.9. ENVIRONMENT SAFETY AND HEALTH

3.9.1. OCCUPATIONAL SAFETY

The fusion safety program provides for the safe operation of the DIII–D facility and for a safe working environment for employees and visitors. Special programs address high voltage and high current, high vacuum systems, ionizing radiation, microwave radiation, cryogenics and the use of power equipment and machine tools. DIII–D is provided support by GA's Licensing, Safety and Nuclear Compliance organization and GA's Human Resources Safety organization in areas such as health physics, industrial hygiene, environmental permitting, hazard communication, hazardous waste, and industrial safety.

The Fusion Safety Committee focuses on addressing both immediate and longer range safety needs and goals. The Safety Committee meets twice a month and solicits specialized help from any of the five fusion safety subcommittees during reviews of lasers, electrical systems, vacuum systems, the use of cryogens or chemicals. In addition, two individuals are dedicated full time to on-site "preventive" safety involvement. Their activities include writing and reviewing procedures, developing and conducting special training classes, conducting inspections and follow-up, and providing continuous oversight to assure compliance with established safety policies, procedures, and regulations.

The DIII–D Emergency Response Team consists of individuals involved directly with maintenance and operation of the DIII–D equipment. They are trained in cardiopulmonary resuscitation (CPR), first aid, use of self-contained breathing apparatus (SCBA), and the use of fire extinguishers, evacuation and crowd control, and facility familiarization. The team can respond within seconds to provide immediate assistance until outside emergency assistance arrive.

TABLE 3-2
DIAGNOSTIC SYSTEMS INSTALLED ON DIII–D

Electron Temperature and Density	
Multipulse Thomson scattering	8 lasers, 40 radial points
ECE Fourier transform spectrometer	Horizontal midplane profiles
ECE radiometer	Horizontal midplane
Multichannel vibration compensated (infrared) interferometer	3 vertical chords, 1 radial chord
Microwave reflectometer	Midplane edge profiles
Ion Temperature and Velocity	
Charge exchange recombination spectroscopy	16 vertical channels; 16 horizontal channels; 3 mm edge resolution
Core Impurity Concentration	
VUV survey spectrometer (SPRED dual range)	Radial midplane view
Visible Bremsstrahlung array	Radial profile at midplane, 16 channels
Radiated Power	
Bolometer arrays	2 poloidal arrays, 48 channels each
Divertor Diagnostics	
Visible spectrometer	7 channels
VUV survey spectrometer (SPRED)	Vertical view along outer divertor leg
Tangential TV (visible)	2–D image of lower divertor
Tangential TV (VUV)	2–D image of lower divertor
Infrared cameras	5 cameras
Graphite foil bolometers	12 locations
Fast neutral pressure gauges	4 locations in divertors
Penning gauges	Under divertor baffle
Baratron gauge	Under divertor baffle
Langmuir probes	18 radially across lower floor, 2 upper divertor throat
Moveable Langmuir probe	Scannable through lower divertor outer leg
Tile current monitors	Radial and toroidal arrays
Reflectometer	Vertical view through X-point
Magnetic Properties	
Rogowski loops	3 toroidal locations
Voltage loops	41 poloidal locations and 30 saddle loops
B_θ loops	2×29 in poloidal arrays
Diamagnetic loops	9 toroidal locations
Plasma Edge/Wall	
Plasma TV	4 cameras, radial view, rf antennae
IR camera	Inside wall and coiling views
Visible filter scopes	16 locations
Moveable Langmuir probe	Scannable across outer midplane

TABLE 3-2 (CONTINUED)

Fluctuations/Wave Activities	
Microwave reflectometers	2 radial systems
Far infrared scattering	Radial view
Infrared scattering	Vertical view
Mirnov coils	Toroidal, poloidal, and radial arrays
Li beam injector	Radial beam with 16 channel tangential viewing channels
X-ray imaging system	100 channels, 5 arrays
RF probes	10 probes in poloidal array, 10 probes in toroidal array, 1 launch antenna
Fast Ion Diagnostics	
Neutral particle analyzer	Scannable horizontal view, 3 vertical views
Fast neutron scintillation counters	2 radial channels
Fusion products probe	1 new midplane probe
Plasma Current Profiles	
Motional Stark polarimeter	35 channels, 2 radial arrays
Nonthermal Electron Distribution	
Soft x-ray pulse height spectrometer	1 scannable radial view
ECE Michelson spectrometer	1 vertical view
Miscellaneous	
Neutron detectors	3 toroidal locations
Hard x-ray monitors	2 toroidal locations
Synchrotron (IR) radiation detector	2 tangential chords on midplane
Torus pressure gauges	
Residual gas analyzer	

All new employees and collaborators must go through a thorough and comprehensive safety indoctrination by the Senior Fusion Safety Officer and the Pit Coordinator. They are informed of the specific potential hazards that are present daily at DIII–D and the special safety precautions and rules that apply, with specific emphasis on the areas where they will be working. Subcontractors also receive a similar indoctrination.

Training is all-important to the safety of both personnel and equipment. Due to the complexity of the DIII–D site and its potential hazards, numerous safety training classes are conducted. Subjects of the classes include: confined space entry, CPR, back injury prevention, radiological safety, laser safety, electrical and high voltage safety, hazard communication and hazardous waste disposal, cryogenic safety, crane and forklift operation, lockout/tagout, machine shop tool usage and basic industrial safety requirements.

Safety inspections are conducted throughout the year to promote an active hazard prevention program. The inspections are conducted by a combination of Fusion, GA Licensing Safety and Nuclear Compliance personnel and outside consultants.

Four internal safety inspections of the DIII–D site were conducted by representatives from GA Safety, Fusion Safety, Fusion Management, and Fusion Facilities Engineering with a total of 114 findings noted. At the close of FY97, there were three items remaining on the findings list.

The San Diego Fire Department's Combustible, Explosive and Dangerous Materials (CEDMAT) team inspected the DIII–D facility.

DOE–OAK conducted a safety review of the DIII–D site in April and identified 13 items that needed attention or correction. At close of FY97, there is still active progress on four remaining items. DOE inspectors gave DIII–D an overall excellent rating.

The Fusion Safety Committee met 24 times this fiscal year to discuss various safety issues. The committee reviewed and approved eight Hazardous Work Authorizations (HWA) after appropriate recommendations and changes by the Safety Committee and select safety subcommittees, a special review of the boronization HWA, and reviewed two incidents that involved no injury and three accidents that required minor off-site medical treatment. There were no lost time accidents. The committee also reviewed one DIII–D safety procedure.

3.9.2. RADIATION MANAGEMENT

Radiation management tasks include monitoring the site boundary radiation; monitoring the dose exposures of individuals from pit runs and vessel entries; ensuring compliance with legal limits, DOE guidelines and DIII–D procedures; monitoring material for activation, maintenance and operation of the radiation monitoring detectors (neutron and gamma); and maintaining a database of radiation measurements of personnel dose exposures.

The total neutron radiation at the site boundary for FY97 was 4.5 millirem, the total gamma radiation was 1.2 millirem, giving a total site dose for the year of 5.7 millirem (Fig. 3–10). This is below the SAN–DOE annual guideline limit of 40 millirem and the California annual limit of 100 millirem. Operations during the third quarter produced the highest amount of radiation (4.1 millirem) since the completion of the neutron shield in 1989 (Fig. 3–11).

The total dose exposure of personnel was kept below the DIII–D procedural limits of 30 millirem per day, 100 millirem per week, and 400 millirem per quarter (1600 millirem per year). The highest personnel dose for the year measured on the radiation monitoring film badges was 170 millirem of gamma radiation. A total of nine individuals had measurable film badge doses with a total person-rem for the year of 950 millirem. The highest dose accumulated and measured on the personnel digital dosimeters by an individual from pit runs and vessel entries (but not operations) for FY97 was 333 millirem. A total of 126 individuals received doses with 80% of the doses being below 25 millirem. All doses were logged in the database of personnel radiation doses.

The vessel was vented twice in FY96 for a total of 175 days. The usual radiation monitoring was performed: alpha, beta airborne samples; alpha, beta, and tritium wipe samples; dose rate and activity levels. The initial dose rate was typically 4 to 6 millirem per hour.

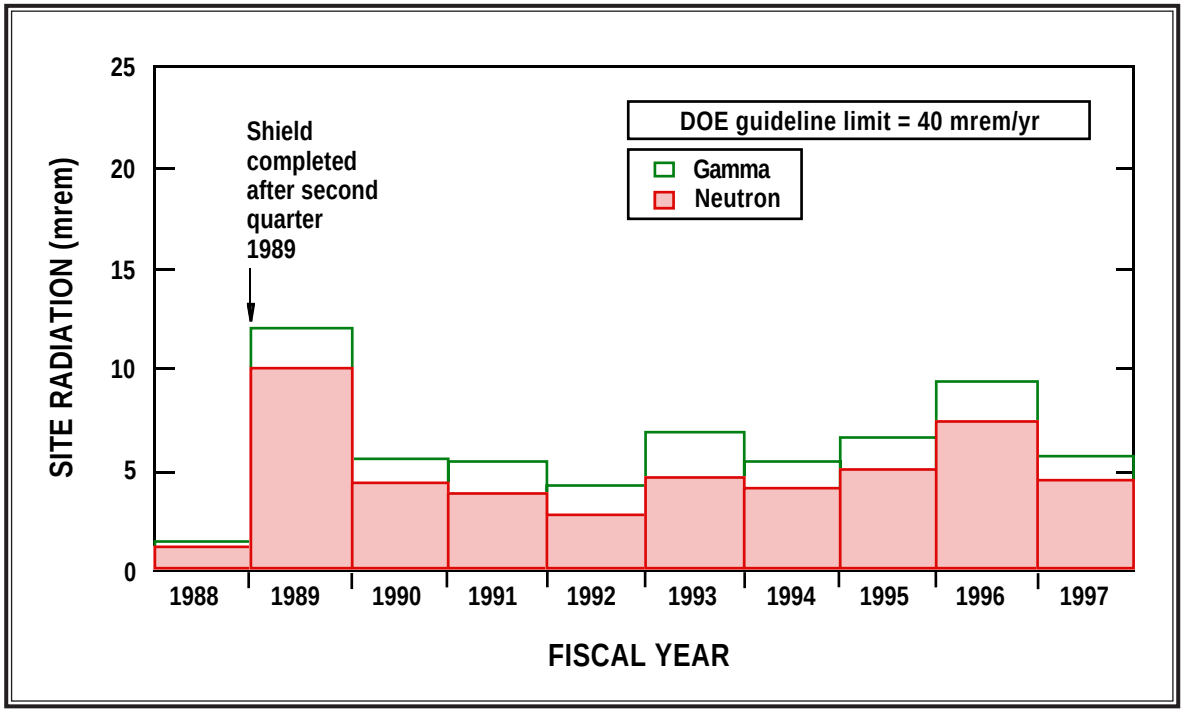

Fig. 3-10. Total radiation at the site boundary by year due to DIII–D operations.

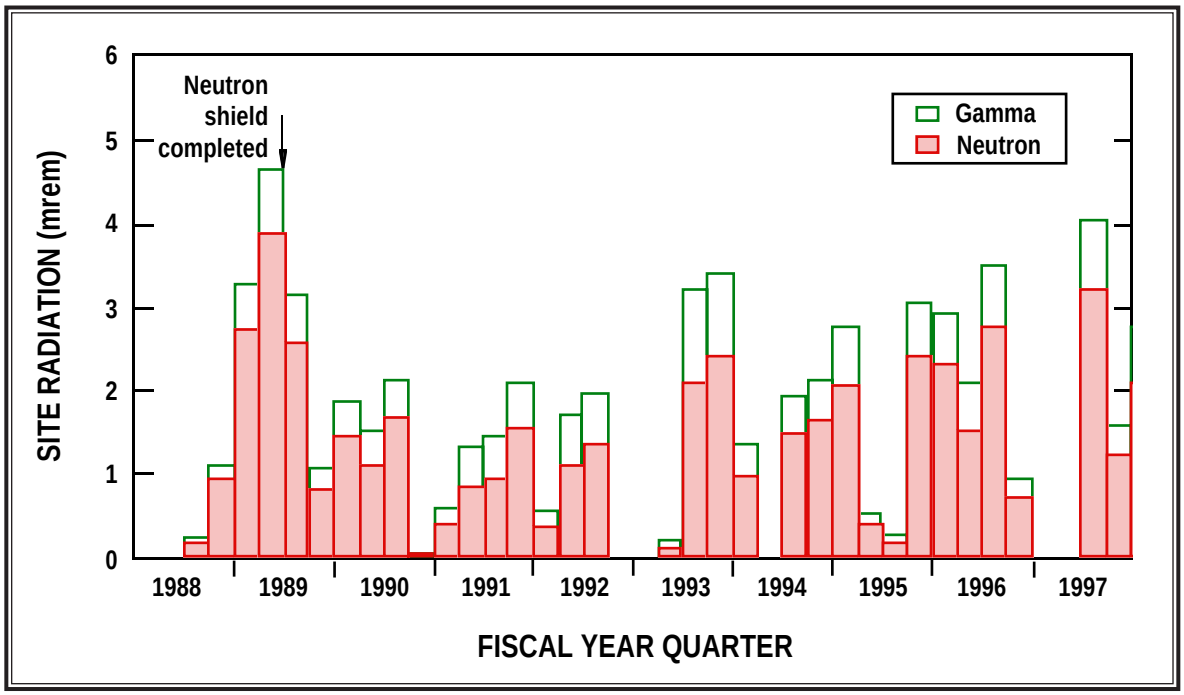

Fig. 3-11. Total radiation at the site boundary by quarter due to DIII–D operations.

Three DIII–D radiation training classes were given as part of the radiation training for new personnel and for refresher training. A total of 163 people received training.

The ALARA goal of limiting the maximum individual dose from vents and RWP work for calendar year 1996 to 500 millirem was met by careful planning of work activities; the highest accumulated dose for the calendar year was 461 millirem. The ALARA goal for the total collective dose was slightly exceeded (by 20%). The total collective dose goal, however, has not been very useful as a measure of improvement nor as a motivation for improvement; and after consideration of other possible goals, it was decided by the ALARA committee to eliminate the total collective dose goal. The maximum individual dose goal chosen for the year was lowered from last year's 500 millirem to 300 millirem based on the expectation that there will be no major work inside the vessel during the coming year.

GA Health Physics and the Criticality and Radiation Safety Committee (CRSC) conducted their annual audits; no action items were generated. The annual renewal of the DIII–D work authorization was completed with only minor modifications.

Two site boundary radiation badges from the North-East boundary of the site showed neutron doses of 50 and 80 millirem but no gamma doses for the third quarter of operation. The readings, which for these badges were based on the albedo portion of the badge (the TLD chips) instead of the normally used track etch film portion that was damaged, are believed to be erroneous. Track etch results are more reliable and normally reported when both track etch and albedo detectors are used in the same badge. All other factors indicate that the readings are erroneous: there was no gamma dose at these locations; the ratio of the site dose to the control room dose and to the number of neutrons produced were typical; other site badges, facility location badges, and personnel badges were typical.

Progress was made on clearing the high bay area storage area of possibly activated items that were removed from the machine pit during the vent. Many items were checked for activation and released; more than 400 tiles were checked for tritium contamination and released.

3.10. CONTINUOUS IMPROVEMENT

The Continuous Improvement process is a means by which every member of the Fusion Group continually examines all of the processes, procedures, methods and activities by which work is accomplished, and implements or suggests constructive changes. The process involves submitting a suggestion on a Continuous Improvement Opportunity form to a member of the Continuous Improvement Committee (CIC).

The CIC reports to the Fusion Group Senior Vice President. The CIC is chartered to provide an overview of and administer the Continuous Improvement Program. Each Fusion Director appoints at least one representative to serve on the CIC. The CIC receives, investigates, and makes recommendations associated with all suggestions.

Fourteen Continuous Improvement Opportunity forms were received and acted upon in 1997. The following are a few of the improvements that resulted from the suggestions submitted:

- The different forms used by the Fusion Group were put on the Fusion Server to make it quicker for users to access the most current version of a form.
- A standard set of guidelines were established for developing viewgraphs. The guidelines were put on the Fusion Server for easy access.
- A survey of electrical instruments on the calibration recall list was performed to determine if the instruments required calibration. The survey resulted in a significant number of instruments being removed from the recall list because they were not being used or their use did not require them to be calibrated.

3.11. VISITOR AND PUBLIC INFORMATION

Tours of the DIII–D facilities are open to organizations and institutions interested in fusion development (colleges, schools, government agencies, manufacturers, and miscellaneous organizations). These tours are conducted on a noninterference basis and are arranged through the DIII–D tour coordinator whose responsibilities include security, arranging tour guides, and scheduling tours. During 1997, 2,041 people toured DIII–D for a total of 18,515 during the last 11 years. Included in the 1997 count were 42 DIII–D educational tours which consisted of 1,174 teachers and students. A focused workshop detailing the fusion education program was held at DIII–D for local educators.

DIII–D personnel have also taken a more active role in supporting science education within the community. Four workshops covering topics in plasma science, the electromagnetic spectrum, fusion, and radiation were presented at national, state, and local conferences. School visits by staff members and exhibition of plasma and fusion science-related activities at off-site student science expositions has increased. The fusion education team's videotape "Fusion: Nature's Fundamental Energy Source" has become a regular program on the San Diego County Office of Education's Instructional TV channel. The education web site, http://fusioned.gat.com, continues to be a source for the general public to gain information about fusion or to contact the education group.

4. PROGRAM DEVELOPMENT

4.1. ECH UPGRADE PROJECT

4.1.1. 2 MW, 110 GHz, ECH SYSTEM

Introduction. To support the AT regimes in the DIII–D tokamak, methods need to be developed to control the current and pressure profiles across the plasma discharge. In particular, AT plasmas require substantial off-axis current in contrast to normal tokamak discharges where the current peaks on-axis. At present, AT plasmas can only be produced transiently because there is no means of driving off-axis currents. To correct this, an effort is under way to use electron cyclotron current drive (ECCD) as a method of sustaining AT plasmas. The first step in this campaign is the installation of three megawatts of electron cyclotron heating power. This involves the installation of three rf systems operating at 110 GHz, the second harmonic resonance frequency on DIII–D, with each system generating nominally 1 MW for 2 s or longer. The three systems will use one GYCOM (Russian) gyrotron and two CPI (formerly Varian) gyrotrons, all with windowless evacuated corrugated low loss transmission lines.

RF System Overview. Two gyrotrons have been installed and operated on the DIII–D tokamak. One, a GYCOM gyrotron has been in operation for over a year, and the second a Communications and Power Industries (CPI) gyrotron model VGT-8011A has been in service since May 1997. Both gyrotrons are nominally 1 MW at a central frequency of 110 GHz. Although each gyrotron is designed for long pulse capability (>10 s), their present pulse capability is limited to 2 and 0.8 s, respectively, owing to the output windows currently installed upon the tubes. The GYCOM gyrotron uses a BN edge-cooled window, and CPI uses a double-disk sapphire window design with an inert Chloro-fluorocarbon (FC-75) coolant flowing between the two disks. The gyrotron performance parameters are shown in Table 4-1.

The transmission line is 31.75 mm diameter aluminum corrugated waveguide carrying the HE_{11} mode. The waveguide diameter represents a compromise between power handling capability and the desirability that the transmission line be insensitive to misalignment, thermal growth, and motion. The rf beam exiting the side of the gyrotron is a modified Gaussian beam with a flattened profile to minimize the peak temperature of the window so as to produce the minimum thermal stress within the window. The window and rf beam are made as large as practical, ≈100 mm, to reduce the thermal load on the window; therefore, direct coupling from the gyrotron into the waveguide is impractical and an interface device is required. The rf beam exiting the gyrotron is phase corrected to restore it to a free-space Gaussian and is also focused to properly couple to the 31.75 mm waveguide diameter. The mirrors are housed in a Mirror Optics Unit (MOU), as shown in Fig. 4-1, which also contains a water-cooled resistive load which absorbs any stray rf power that exits the gyrotron at an angle that it cannot be focused into the waveguide.

TABLE 4-1
GYROTRON PERFORMANCE PARAMETERS

	GYCOM	CPI
Frequency, GHz	109.8–110.15	110
RF Output Power, kW	926.0	105–905.0
RF Pulse Duration, (kW)/s	960/2.0	(105)/cw, (350)/10, (400)/6, (530)/2, (1000)/0.8
Efficiency, %	38.0	32.0
Beam Voltage, kV	72.0	80.0
Peak Cavity Ohmic Loss, kW/cm^2	≤2.0	≤2.0
Beam Current, A	33.8	35

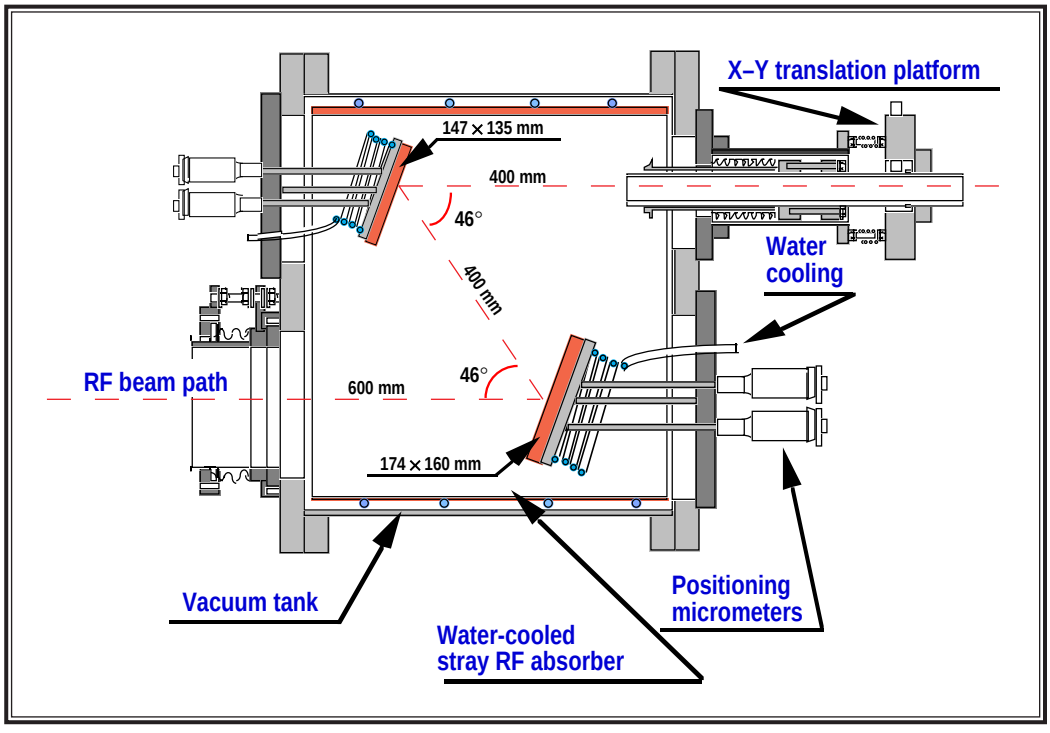

Fig. 4-1. Diagram of the Mirror Optical Unit for interfacing the gyrotron to the 1.25 in. corrugated waveguide.

The entire transmission line system (Fig. 4-2) consists of six miter bends and is ≈40-m long with estimated 2% loss in the waveguide and 0.6% loss per miter bend. The miter bend losses are from mode conversion 0.5% and ohmic losses 0.1%. The waveguide is evacuated to a pressure of $\approx 1 \times 10^{-5}$ torr by a turbomolecular pump at the MOU and a similar pump on a special section of waveguide near the tokamak where the waveguide has been slotted to allow pumping between the corrugations. This waveguide pumping section is placed as close as is practical to the DIII–D vacuum vessel so that any impurities evolving from the waveguide upstream of the tokamak can be pumped out before they reach the plasma and possibly contaminate it. However in the case of a catastrophic vacuum failure, there is a fast shutter located just upstream of the pumping section. This shutter can close faster than the pressure wave can travel down the waveguide and, in conjunction with the pumping section, maintains the vacuum pressure at the tokamak entrance waveguide long enough for the torus isolation valve to close ≈ 0.8 to 1.0 s.

To aide in gyrotron optimization, a dummy load is connected to the system via a waveguide switch located near the gyrotron. Polarization control is achieved by a set of grooved polarizing mirrors mounted in two of the miter bends. By appropriate rotation of these two mirrors, any elliptical polarization desired can be obtained.

Inside the tokamak are two mirrors, a focusing mirror and a flat turning mirror, permanently angled at 19 deg off normal to provide the appropriate current drive injection. The tilting mirror rotates vertically so the injected beam can be steered poloidally from slightly below the midplane of the plasma to the outermost top edge of the plasma.

Initial Operation into DIII–D. An important issue for the usefulness of the ECH system is the validation of the spot size that interacts with the plasma. The launcher was designed to inject the rf beam 19 deg off normal to drive current. Analysis of the launcher optics predicts that 98% of the rf

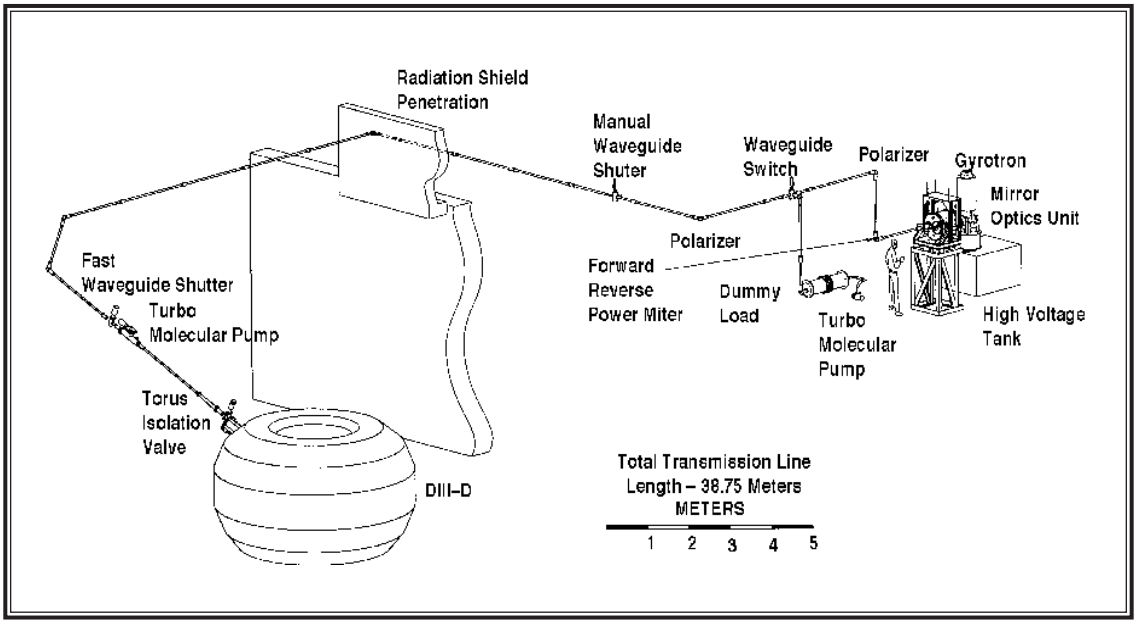

Fig. 4-2. ECH System layout showing the routing of the transmission line and the location of the major transmission line components.

power will be in an area with a diameter of 19.7 cm at the plasma center. The full-width half maximum (FWHM) value for a Gaussian beam with a 19.7 cm 98% power spot size is 8.3 cm. The actual power deposition profile was measured from IR images of the rf beam impinging on a paper target placed inside the DIII–D vacuum vessel at the plasma center location. These measurements are summarized in Fig. 4-3 where the power deposition profile is seen to match the expected Gaussian profile except for a low level wing, which may indicate the presence of some higher order modes.

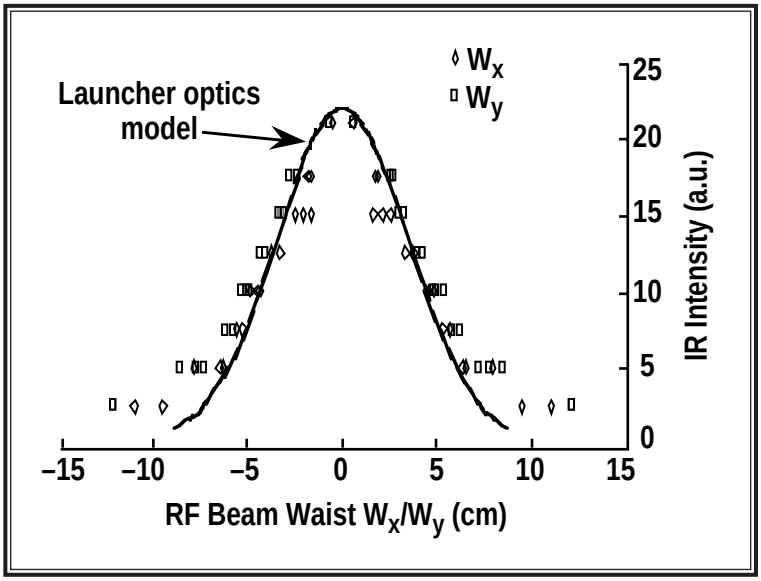

Fig. 4-3. Power deposition profile measured from IR camera images of the rf beam striking a paper target placed at the center of the DIII–D vacuum vessel. The Gaussian profile developed from the launcher optics is also shown.

One of the other useful applications of ECH is the determination of the localized thermal transport coefficient. To perform this task, the rf power is modulated at a relatively high repetition rate. This is simply achieved by modulating the gyrotron voltage by only 16% for the GYCOM gyrotron and by turning on and off the mod-anode on the CPI gyrotron. Modulation frequencies as high as 1 kHz have been tested. Figure 4-4 shows a typical response of the central electron temperature as measured by the ECE diagnostic.

Injection of approximately 500 kW into low density plasmas has resulted in central electron temperatures as high as 12 keV. Traces of a discharge with a peak electron temperature of 10 keV is shown in Fig. 4-5 along with the electron profile determined from the Michelson interferometer, the heterodyne radiometer, and Thomson scattering.

4.2. RADIATIVE DIVERTOR UPGRADE PROJECT

The goal of the Radiative Divertor Project (RDP) is to install a more closed baffle which will provide particle control for high-triangularity advanced tokamak operation. UEDGE-DEGAS modeling has suggested and experiments have subsequently shown that better isolation between the core and divertor plasmas improves plasma performance.

Due to funding limitations, a phased implementation plan has been developed for the divertor installation (Fig. 4-6). The final installation [Fig. 4-6(c)] will have baffles and pumping at all four strike points of a double-null, high-triangularity plasma. Either single- or double-null configurations can be run. The installation of Phase 1A [Fig. 4-6(a)] consisting of a cryopump and baffle structure in the upper-outer corner of DIII–D was completed in March 1997. This has been

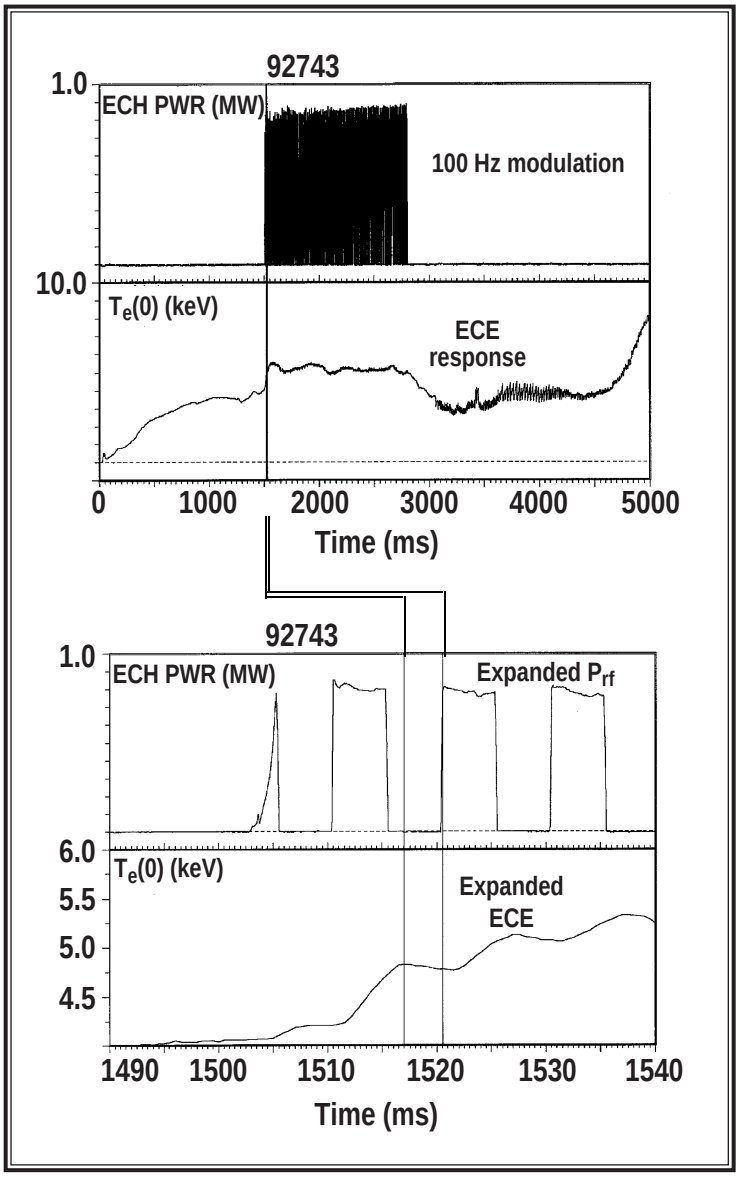

Fig. 4-4. Central electron temperatures measure by the ECE, diagnostic for a plasma heated with modulated ECH, modulation frequency ≈100 Hz. Gyrotron power was ≈850 kW.

successfully used for density control in high-triangularity single-null discharges, and the results are similar to those obtained with the lower pump in low-triangularity discharges. Comparisons of open and baffled operation have shown that the core ionization source is reduced by a factor of 2 to 3.

The design and analysis of Phase 1B [Fig. 4-6(b)] consisting of an additional cryopump and baffle structure to be located in the upper-inner corner of DIII–D continued in FY97. The design of the water-cooled structures and cryopump are similar to those installed during Phase 1A. The detail drawings for the panels are approximately 95% complete. Detailed drawings have been created for the water feed lines, supports, gas seals, and Thomson razor blade dumps. Approximately 80% of the private flux baffle tiles have been modeled. Analysis of the private flux structure shows the mechanical and thermal/hydraulic stresses to be well within design allowables. The installation of Phase 1B is presently scheduled for the 1999 summer vent.

4.3. VANADIUM DIVERTOR STRUCTURE

GA has been implementing a plan for the utilization of a low-activation vanadium alloy in the DIII–D tokamak. The goal of this plan was to demonstrate the design, fabrication, and operation of a water-cooled vanadium alloy structure in the Radiative Divertor upgrade.

Significant efforts were made during FY97 in the research and development of the methods needed to manufacture divertor structures from vanadium alloy (V-4Cr-4Ti) material. Chemical milling, required for the formation of the water channels, has been successfully demonstrated. Resistance spot and seam welding required to accommodate the electromagnetic forces applied

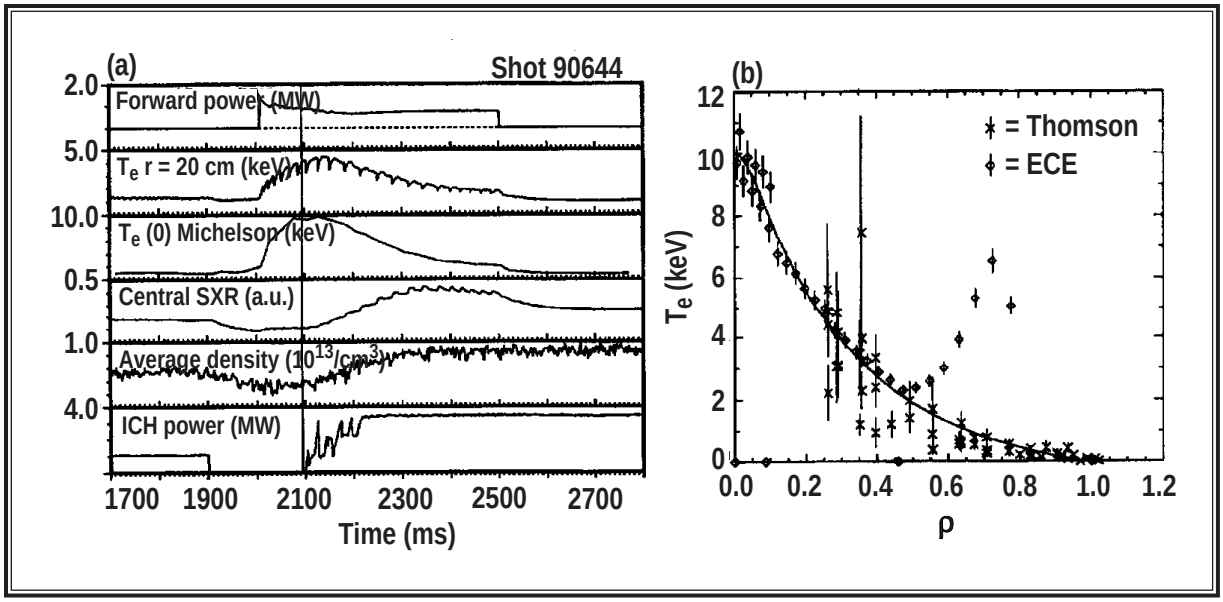

Fig. 4-5. Time dependence of the forward rf power and several diagnostic traces during ECH heated plasmas: (a) the electron temperature profile (b) from ECE and Thomson scattering is shown by the vertical line on the time plots.

to the structures show excellent strength and ductility. The vacuum-to-water helium leak tight seal weld is accomplished through an electron beam weld made around the perimeter of the water-cooled panel. This welding has also been successfully performed. The divertor design requires bimetallic tubing which has been created in a number of ways: friction welding and subsequent machining of Inconel rod to vanadium alloy rod, explosive bonding vanadium alloy to Inconel rod and performing secondary machining, and explosive bonding vanadium alloy sheet to Inconel sheet and performing a deep draw of the composite sheet. A helium leak tight electron beam weld of a tube-to-plate mockup was also made successfully. Friction welding to attach threaded vanadium alloy studs to the panels has been successfully demonstrated using electric/pneumatic, pneumatic, and hydraulic machines. The welds exhibit high strength and high ductility.

The design and analysis of the vanadium alloy structures began in FY97. At the end of FY97 nearly all of the engineering issues were resolved. Due to insufficient funding in FY98, we were unable to proceed to construction.

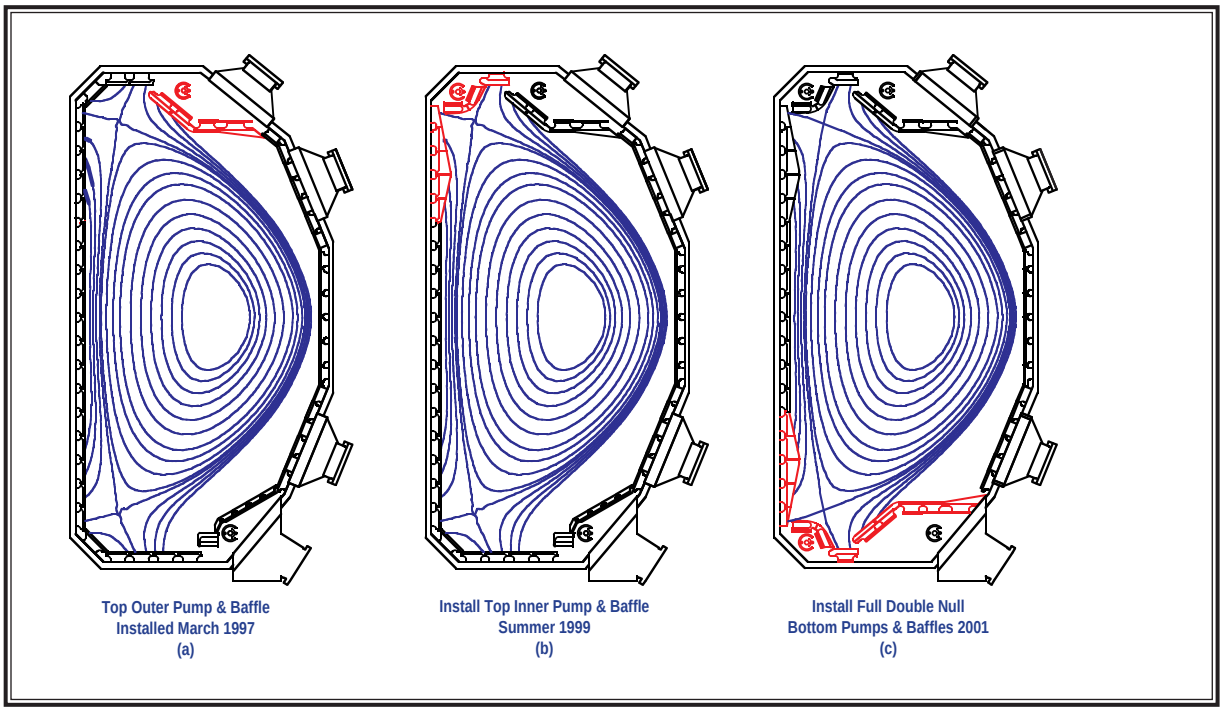

Fig. 4-6. DIII–D phased radiative divertor project.

5. SUPPORT SERVICES

5.1. QUALITY ASSURANCE

Fusion Quality Assurance (QA) engineers, inspectors, and support personnel maintained a high level of activity during 1997. Significant projects supported were the assembly and installation of the Radiative Divertor, installation of the CPI Gyrotron, and the E–coil repair.

The QA group performed the following:

1. Reviewed and approved all DIII–D design drawings, specifications, procedures, and procurement requisitions. Participated in design reviews and chaired the Material Review Board (MRB).

2. Developed an instruction to provide guidance for the assembly of a data package for each diagnostic installed on the DIII-D machine. The data package will serve as a reference document for any individual interested in a specific diagnostic and is made up of documents generated during the design, manufacturing, and installation of the diagnostic.

3. Completed the semi-annual building concrete footing and column settlement surveys; no unexpected subsidence was detected. An inspection of the cracks in the concrete walls adjacent to the machine was also performed with no noticeable changes.

4. Twelve Fusion Group Procedures were revised and released for use.

5. The Fusion Group training program continued to be developed and implemented. The development of the Group 2 training materials was completed. Group 2 training will address the needs of the directors and managers. It will provide them with an overview of the Fusion Procedures that affect them directly. Areas such as Management Assessments, Independent Assessments, Design Reviews, and How to Apply a Graded Quality Approach are addressed. A total of 55 Fusion Group employees and collaborators received Group 1 training. Group 1 training centers around an introduction to the Fusion Group procedures.

6. Chaired the Fusion Group Continuous Improvement Committee.

5.2. PLANNING

The Planning group supported operation and maintenance of the DIII–D facility. Planning and Control provided long-term program planning, as well as day-to-day scheduling (cost control,

preparation of Field Work Proposals, and Cost and Fee Proposals), processing of purchase requests, expediting and reporting of status. These support activities are essential to constraining the program within prescribed budgets and schedules. Our planning activities (budget, schedule, resource) enabled us to maximize the utilization of available resources for accomplishment of program goals and were important in planning and replanning of scope, budget, and schedule with fluctuating funding levels.

Major planning activities during FY97 included work on the 1 MW Russian and CPI ECH system, new AEG computer system, Radiative Divertor Project (RDP) diagnostic relocation, E–coil lead repair and numerous collaborator diagnostic modifications and upgrades and vent that started in August of 1996 and was completed in March of 1997 which centered around the installation of the radiative divertor, diagnostic modifications, and calibrations.

6. COLLABORATIVE PROGRAMS

6.1. DIII–D COLLABORATION PROGRAM OVERVIEW

The General Atomics DIII–D tokamak and its fusion research program has become a true national users facility. The total number of national and international collaborators on DIII–D in FY97 was over 200 including both full- and part-time collaborators. Through our national and international collaboration programs, DIII–D is playing a major role in the worldwide advancement of fusion research towards the goal of fusion science and energy. Our collaboration with universities and DOE national laboratories has brought new recognition to our program and broadened its scope. DIII–D international collaborations have helped the U.S. to maintain its international role as a strong contributor to ITER.

The DIII–D international collaboration program continues to provide a broad source of innovative ideas and opportunities which support the DIII–D research program. Collaborations were carried out with JET in England, ASDEX–Upgrade in Germany, Tore Supra in France and JT–60U and JFT–2M in Japan. In addition to the benefits gained from DIII–D staff assignments in these and other laboratories, foreign scientists visiting DIII–D have made significant contributions to DIII–D program goals. A summary of some of the recent major international collaborations by DIII–D staff members is given below.

In 1997, GA participated with the other major U.S. fusion laboratories in helping DOE Office of Fusion Energy Sciences develop a Strategic Plan for International Collaborations on Fusion Science and Technology Research.

The DIII–D collaborators have contributed to the results presented in the previous sections of this annual report and are discussed in specifics in the following.

6.2. LAWRENCE LIVERMORE NATIONAL LABORATORY (LLNL)

The LLNL Collaboration contributed significant progress to both the Divertor and Advanced Tokamak programs in FY97. Important new physics results were gained, partly as a result of the commissioning of several new or improved diagnostics. A professor from Dickinson College has joined our UEDGE modeling effort in this area.

An LLNL physicist was co-leader of a set of experiments to commission the new upper divertor pump and to examine the effects of the closed upper divertor versus the open lower divertor. We found that the closed divertor reduced the core ionization in rough agreement with our UEDGE calculations. We have not yet seen a dramatic increase in the energy confinement time τ_E. We also led an experiment with helium plasma and helium beams to investigate the effect of chemical sputtering during detached divertor operation. The different chemistry of helium compared to

D2 was predicted to strongly reduce chemical sputtering if such sputtering was present. When the detachment occurred, the carbon content in the plasma was dramatically reduced compared to D2 plasmas. The carbon reduction at the time of detachment confirms the importance of physical sputtering, and the comparison of the detached levels in He and D2 is consistent with production of carbon by chemical sputtering in the D2 plasma. Other signatures of chemical sputtering (e.g., spectroscopic) are not usually observed in the D2 case, so this requires further investigation.

The new divertor diagnostics include the VUV camera system developed in collaboration with Hampton University. This instrument has now provided the first 2–D images in carbon IV (C IV) light. The camera shows a tangential view of the tokamak plasma with light clearly delineating the separatrix. Analysis of this new data is now in progress.

Also new is a grating for the LLNL divertor SPRED provided courtesy of PPPL. After installing this grating and calibrating the instrument, we used it to measure C IV radiation at 1550 Å, which is a large fraction of the total radiation in the divertor. We also have obtained absolutely calibrated measurements of the Ly_α (1216 Å) and Ly_β (1025 Å) lines in detached plasmas which can be used to estimate the amount of recombination in these plasmas. Recombination was measured in 2–D using a new image splitting system for the LLNL Tangential TV. This allowed us to make simultaneous 2–D measurements of visible H_α and H_δ. From this the 2–D distribution of recombination and ionization as a function of time was derived and shown in a talk at the 1998 PSI meeting.

We have obtained a new camera for the LLNL IRTV system. This is a high-speed imaging and line-scanning focal plane array which will improve our capabilities for measuring disruption and ELM heat flux and improve the reliability of the routine heat flux measurements. We have begun testing this system on the tokamak with plasmas and recorded the first IR for this instrument. We are in the process of ordering three imaging-only solid-state cameras to replace outdated cameras at other viewing locations on DIII–D.

The LLNL divertor Thomson Scattering system was in regular use as a critical diagnostic in divertor experiments. The divertor temperature and density measurements are crucial in the interpretation of a variety of other measurements.

In the advanced tokamak area, we added new channels to the MSE system to allow simultaneous J(r) and E(r) measurements. These results compared well with the CER measurements of rotation which are then converted to E(r). A Physical Review Letter has been submitted on this result. We have now implemented the automatic between shot EFIT capability, so that both “normal” (e.g., JT EFIT snap file) and “MSE” EFITs can be calculated between shots using several off-site computers. We have also obtained an “MSE” HP workstation to calculate and archive the EFITs. The new computer will both take the load of computing EFIT off of the existing computers, and has a 9 GB disk to archive the EFITs. It will also provide the ability to do very detailed MSE analysis.

We are also planning to provide more emphasis on scenario development for DIII–D using simple spreadsheets, the CORSICA code, and simple physics models. Transport analysis continued this year, along with further development of the CORSICA code and comparisons with data. We have a graduate student working on comparing CORSICA runs with DIII–D data.

We have provided computation, engineering, and technical support for our Divertor and Advanced Tokamak efforts. We furnished help to GA in upgrading the UNIX operating systems of the DIII–D computers. The intershot automatic EFITs are supplied to DIII–D using LLNL programming support. We are collaborating with DIII–D and the theory group at LLNL on a general computing environment for CORSICA and, eventually, UEDGE.

6.3. OAK RIDGE NATIONAL LABORATORY (ORNL)

ORNL staff performed the steps necessary to compute the cryopump particle exhaust rate and deuterium particle balance in the upper single-null (USN) configuration. Analysis of the data from the campaign indicated that recycling was reduced during the course of each run day, and that the best density control was achieved only when wall outgassing was eliminated. Comparable density control has been achieved in USN and lower single-null (LSN) configurations.

A Neutrals Initiative was begun with the goal of better understanding the role of neutral particles in DIII–D. The filterscope was installed to detect D_α and D_β radiation from 16 chords intersecting the upper and lower divertor regions. Also included were C III and He II detectors along these chords. The C III light has proven to be a good indicator of MARFEs. An ASDEX pressure gauge was installed on the midplane of DIII–D to determine the neutral density during discharges.

ORNL led an experiment to determine the power and connection length scaling of divertor and core MARFE onset, as well as the back-transition from H–L mode at high density. Evaluation of the data indicates that the line density at the H–L transition decreases as the toroidal magnetic field is increased, as expected if MARFE formation on closed field lines causes this limit. An assessment of the H–mode pedestal parameters during high density discharges has shown that low q_{95} discharges are more robust to gas puffing than high q_{95} discharges, but that high q_{95} discharges start out with higher edge pressure gradient and energy confinement.

An experiment was carried out to the assess the impurity transport properties of helium, carbon, and neon in both VH–mode and negative central shear (NCS) discharges. A strong, *Z*-dependent accumulation of impurities is observed in NCS discharges with peaked electron density profiles and an internal transport barrier. Furthermore, a strong, *Z*-dependent outward convection (“pinch”) of impurities is observed in VH–mode discharges which have flat electron density profiles, consistent with the “temperature screening” prediction of neoclassical impurity transport theory.

Analysis of induced SOL experiments (so-called “puff and pump” experiments) has shown that the divertor enrichment of argon can be increased by a factor of 3 by inducing a strong main ion flow in the SOL through simultaneous deuterium gas injection at the midplane and divertor exhaust. In fact, the best enrichment values (~17) are of sufficient magnitude that a radiative divertor solution with the primary radiator being argon in the divertor plasma can now be considered possible. A paper entitled “Impurity Enrichment Studies Using Induced SOL Flow in DIII–D,” by M.R. Wade which includes the analysis results and interpretation of the results, has been submitted to Nuclear Fusion.

The efficacy of the new upper divertor in DIII–D was demonstrated with density control obtained in a high-triangularity plasma shape in an ELMing H–mode plasma. However, analysis of impurity data during USN operation indicates that core impurity levels vary considerably more with plasma condition than has been observed in LSN operation. The most concerning aspect of this data is that the core impurity concentration tends to increase when the plasma density is decreased.

ORNL divertor spectroscopy research was concentrated in two major areas this year: (1) investigations of recombination in low-temperature detached plasmas, and (2) measurements of parallel particle flows. In the DIII–D tokamak, it is observed that divertor detachment is accompanied by the formation of recombining regions where the electron temperature must be lower than 1.5 eV. It is found that a normal flow region of C II and C III is located several centimeters away from the separatrix whereas a reversed flow region lies adjacent to the outer separatrix. Such flow reversals have been predicted by 2–D fluid codes for certain conditions. In general, normal flows along the outer leg are in the Mach 0.3 to 0.7 range, and the reversed flows are close to Mach 1. So far, all flows detected along the inner leg are normal and tend to be close to Mach 1.

To study the effects of neutrals on the L–mode to H–mode transition power threshold in DIII–D, a broad range of plasma discharges have been analyzed with the B2.5 and DEGAS transport codes. The discharges were LSN with the grad-B drift toward the X–point. At constant magnetic field, the ratio of the transition power threshold to the density appears to be a function of a single parameter measuring the neutrals. Strong correlations of the power threshold with neutral density at the 95% normalized-flux surface, the radial scale length of the neutral density inside the separatrix, and the peak charge-exchange damping rate (near the X–point), were evident in the analysis results. A similar correlation exists between these neutral parameters and local plasma parameters such as electron and ion temperature. This indicates that a missing parameter linked to the neutrals exists in the power threshold scaling laws.

Several types of radio frequency (rf) waves have been compared in terms of their ability to drive electric field shear in tokamak plasmas. These include the fast magnetosonic wave, the mode-converted ion Bernstein wave (IBW), the kinetic shear Alfvén wave, the directly launched ion Bernstein wave, the lower hybrid wave, and the electron cyclotron wave. For each case, the average flow velocity is evaluated from a full-wave, numerical solution of Maxwell's equations in a finite temperature, perpendicularly stratified, one-dimensional plasma. Results show shear in both toroidal and poloidal velocities. Poloidal shear dominates for the low frequency electrostatic waves, while toroidal shear and pressure gradient terms are important for the electromagnetic and lower hybrid waves. The rf power required to suppress turbulence through E×B velocity shear is lowest for the directly launched ion Bernstein wave and the kinetic shear Alfvén wave. The mode-converted IBW requires somewhat more power, but gives added flexibility in the location of the shear layer which can be adjusted by varying the frequency and/or the minority ion fraction.

The reliability of all rf systems during ELMing H–modes was increased. The transmission line system for the antenna in the 285/300 deg ports was changed to a symmetric feed, tunerless configuration. The system was designed to achieve a perfect impedance match for a typical value

of plasma loading. Reflected power resulting from varying antenna loading conditions is diverted to the dummy load. The antenna has been operated at 1 MW into a plasma with an rf-induced H–mode transition without tripping. The arc protection for the antennas in the 0 deg and 180 deg ports was reconfigured to allow full advantage to be taken of the natural ELM-dump nature of the hybrid splitters. The new configuration relies on the voltage standing wave ratio on the transmitter output along with the ratio of the antenna voltage to the transmitter forward voltage for arc protection. Operation of all antennas without interruption during L–H transitions and during ELMs has now been demonstrated.

Publications:

Isler, R.C., R.D. Wood, C.C. Klepper, N.H. Brooks, M.E. Fenstermacher, and A.W. Leonard, "Spectroscopic characterization of the DIII–D divertor," Phys. Plasmas **4**, 355 (1997).

Isler, R.C., G.R. McKee, N.H. Brooks, W.P. West, M.E. Fenstermacher, and R.D. Wood, "Signatures of deuterium recombination in the DIII–D divertor," Phys. Plasmas **4**, 2989 (1997).

6.4. PRINCETON PLASMA PHYSICS LABORATORY (PPPL)

In mid-FY97 a new collaboration was established, with an expected higher level in FY98 as TFTR staff complete data analysis and other activities. During FY97, PPPL staff made significant contributions in physics and engineering and in support of data analysis and began design work for the first stage of MHD feedback studies.

PPPL physicists participated effectively in the DIII–D scientific program. These efforts included MHD studies, fast plasma shutdown modeling, rf heating and current drive, and transport analysis.

PPPL supported ICRF operation and maintenance on the FMIT source during the July-August run. After investigating the cause of power trips, changes were implemented which now allow the transmitter to operate with far fewer trips at output powers in excess of 2 MW. PPPL also participated in an evaluation of transmission line reconfigurations and in studies of improved arc detection methods. It was concluded that the present transmission line configuration will be very nearly optimum after improvements are made in the arc detection system.

A full-time on-site PPPL engineer now supports DIII–D operations. In addition to his very effective role as a "COE in training," he has proposed and is implementing a number of important facility modifications, including an improved patch panel system, a more quickly changed TF reversing switch, and upgrades in the gas injection system.

PPPL provided support for a number of DIII–D computer codes. Improvements and upgrades were made in the 4d data analysis code, the Shot Logger Program, and the Time Series Analysis code. The SPARROW code, for visualization and analysis of MHD data, was imported from Princeton, converted to run on the unix-based HP computers, and configured to access DIII–D raw data files. SPARROW was then used to analyze a variety of modulated ECH shots

for power deposition and heat transport coefficients and to begin cataloging beta limit disruption precursors.

PPPL initiated the physics and engineering design of a nonaxisymmetric feedback coil project. The purpose of this important project is to allow achievement of higher beta plasmas and to compensate for resistive wall modes. In support of the program, PPPL will provide feedback coil power supplies and saddle coil sensor loops.

FY97 provided a successful start to the PPPL/DIII–D Collaboration. It is anticipated that the collaboration will become a significant program element for both organizations.

6.5. UNIVERSITY OF CALIFORNIA, LOS ANGELES (UCLA)

In order to facilitate the correlation reflectometer data analysis, an automated IDL routine has been developed. Briefly, it calculates the radial correlation lengths from the correlation reflectometer data, finds the radial position of the cutoff from EFIT outputs and Thomson scattering. Two sets of data (one of the slow L–H transition days and the ELM-size scaling day) have been analyzed in detail using the interactive version of this code. The correlation lengths tend to increase towards the core of the discharge (approximately 0.6 cm at the edge to 1.5 cm near r/a = 0.5). The steep edge H–mode region (Ln ~ 1 cm) has the shortest correlation length, 0.1 to 0.2 cm. While these edge H–mode correlation lengths are short, so is the density scale length and on physics grounds one would not expect the correlation length to be larger than the density scale length. This data is for a limited tokamak parameter space and, therefore, may not be general. Other data is being analyzed to extend this database. In particular, there is great interest in scalings with magnetic field, plasma current, etc., which could be used to differentiate between different types of turbulence, its drive, and damping. The upgraded correlation radiometer system for measuring electron temperature fluctuations was installed on DIII–D and tested. Initial tests showed that the hardware was performing correctly.

The FIR scattering system has been adopted for initial tests of its ability to detect large wavenumber fluctuations, which may be characteristic of modes responsible for electron transport.

An existing high frequency (50 to 75 GHz) profile reflectometer system was modified to utilize O–mode propagation, as a test of whether O–mode reflectometry can be utilized to measure core density profiles in NCS plasmas with peaked profiles. Initial data show that adequate return signals can be obtained from inside r of 0.4.

6.6. UNIVERSITY OF CALIFORNIA, SAN DIEGO (UCSD)

6.6.1. ANALYSIS OF POWER SCALING OF DIVERTOR PARAMETERS

Detailed profiles of divertor density, temperature, particle flux, and heat flux from the floor Langmuir probes, divertor Thomson and the IR camera were used in a comparison to UEDGE predictions for a power scan in ELMing H–mode. Initial results indicate that the standard UEDGE solution which gives good agreement with the outer midplane profiles do not agree well

with the divertor profiles at the floor. Work is underway to improve the model in this respect. The experimentally observed profiles exhibit a double exponential character. The most dramatic parameter dependence with power is the density in the divertor SOL. The results were extended to the inner strikepoint. The dependence of divertor parameters with density is also under study.

Also completed was a detailed characterization of plasma profiles and fluctuations in the vicinity of the divertor X–point. These data are crucial for evaluating models of the H–mode power threshold, where the "grad-B" dependence may arise due to changes in neoclassical flows in the X–point vicinity, and for testing models of scrapeoff layer equilibrium.

6.6.2. NEW X PROBE PARTS ARRIVED AND INSTALLED

New parts for the X–point probe head were fabricated by Sandia and sent to San Diego. Some parts were also fabricated by UCSD and GA. These minor modifications to the X–point probe head will hopefully improve flow measurements, make collector replacement easier, and provide more accurately shaped collector tips. The newly assembled probe head was installed and calibrated in DIII–D and first measurements of main ion flows parallel to the magnetic field in the SOL were obtained.

6.6.3. DISRUPTION STUDIES

Investigation of "slideaway" and runaway electron production in disruption thermal quenches and in "killer pellet" disruptions. Runaway electron production in preemptive killer pellets increases exponentially with cooling rate of pellet. An estimate of the parallel electric field created during the thermal quench of a killer pellet was obtained from the time derivative of ℓ_i calculated by EFIT. The measured maximum value of 180 V/m closely matched the electric field obtained in the KPRAD impurity modeling of 223 V/m. Disruptions were identified as a significant source of erosion in the DIII–D graphite divertor. Using the DiMES measurement of 5 nm erosion/redeposition per VDE disruption and a typical disruption frequency of 20%, it is shown that this would contribute 1 to 2 microns of erosion of the 5 microns total measured during the long term (1400 discharges) exposure of floor tiles.

6.6.4. FUTURE DIAGNOSTICS

For the future, UCSD scientists are leading the implementation of three new diagnostics at DIII–D: an electron temperature fluctuation and turbulent heat flux upgrade to the existing midplane reciprocating probe, a two-color IR radiometer for detection of synchrotron radiation from runaway electrons, and "DISRAD," an X-UV radiometer for fast measurement of the radiated power during disruption thermal quenches. Each of these systems is expected to generate experimental data in CY97.

6.7. INTERNATIONAL COLLABORATIONS

During FY97, the integrated total of international scientific collaboration was at the level of 8 FTE — approximately 10% of the physics research effort. These collaborations consisted of

2 FTE of DIII–D scientists collaborating abroad for several week periods and 6 FTE of incoming collaborations of foreign scientists residing in San Diego.

JET

Dr. Howard Wilson visited GA for one month for a joint study on the theoretical limits to tokamak beta at low collisionality. Drs. X. Garbet and J. Connor from JET were here for a brief visit for transport discussions prior to their going to Madison for the Transport Task Force workshop. As part of our continuing collaborations with the JET high performance studies, Ted Strait, Chuck Greenfield, Brad Rice and Tim Luce participated in the JET Deuterium/Tritium hot ion H–mode and optimized shear, high power experiments. During these experiments, JET set new world records in the production of fusion power in a tokamak.

JAERI/Japan

The U.S./Japan Technical Planning Committee meeting and the JAERI/DIII–D Steering Committee meeting were held at GA in February.

Dr. Koide from JT–60U completed his long term exchange with the DIII–D CER group including participation in DIII–D experiments and the study of transport barriers and the effect of E×B shear on energy transport. Dr. Oshima is now at GA for a long term exchange on data acquisition and computer control systems. Also, Dr. Oshima concluded a several month exchange in the area of data acquisition and computerized plasma control systems.

Several other exchanges on NCS physics studies were completed.

TEXTOR

Drs. J. Ongena, A. Messiaen and B. Unterberg from the TEXTOR tokamak in Julich, Germany, are here to participate in the RI–mode experiments which were carried out on DIII–D during the month of September. Preliminary results showed some small increases in confinement with enhanced edge radiation. This collaboration is a complement to the GA participation in TEXTOR RI–mode experiments.

ASDEX Upgrade

Drs. O. Kardaun and F. Ryter from the Max-Planck Institute of Plasmaphysik visited DIII–D for confinement scaling and data analysis.

Netherlands/RTP Tokamak

Dr. G. Hogeweij from the small RTP Tokamak in the Netherlands had a short visit with DIII–D personnel for discussions on ECH and electron transport.

Italy

Dr. Zerbini of the Frascati Tokamak completed a very useful exchange with the ECH group. He helped set up a database for the ECH data and performed the power calibration for the ECH shots. He also developed an analysis routine for the analysis of modulated ECH experiments.

Korea

Dr. Hong-Young Chang, from KAIST, has returned to Korea after a year exchange with the ECH and rf division. He had two graduate students working with him.

Tore Supra

Dr. G. Giruzzi was at DIII–D for a few weeks for discussions on ECH and rf physics.

Russia

The DIII–D program has several active collaborations with Russian fusion research institutions. These include the Kurchatov Institute in Moscow, the TRINITI lab in Troitsk and the Ioffe Institute in St. Petersburg. The Kurchatov collaboration mainly involves experiments related to ECH and current drive using high power, high frequency gyrotrons. The TRINITI collaboration is concentrated in three areas: DINA code analysis of dynamic plasma events, first wall materials, and divertor spectroscopy. The Ioffe collaboration is in the area of H–mode physics in circular and noncircular tokamaks.

China

Drs. R. Stambaugh and V. Chan visited China for a week exchange. They visited both the Southwestern Institute of Physics and the Academica Sinica Institute of Plasma Physics. Discussions were held on plans for future exchanges.

DIII–D has an active exchange program which has Chinese scientist coming to work on DIII–D for 6 to 12 month periods. This year there were three Chinese scientists here on long term exchange, Daqinq Zhang from the Institute of Plasma Physics (Academica Sinica) working on ECH, Guang Diao working on CER, and Junyu Zhao working on the Thomson Scattering system.

7. PUBLICATIONS

Allen, S.L., C.M. Greenfield, J. Boedo, D. Colchin, M.E. Fenstermacher, D.N. Hill, C.J. Lasnier, R. Lehmer, A.W. Leonard, T.C. Luce, M.A. Mahdavi, R. Maingi, R.A. Moyer, T.W. Petrie, G.D. Porter, B.W. Rice, M.J. Schaffer, J.P. Smith, R.D. Stambaugh, T.S. Taylor M.R. Wade, J.G. Watkins, W.P. West, R.D. Wood, DIII–D Team, "Effects of Divertor Geometry and Pumping on Plasma Performance on DIII–D," in Proc. 24th European Conf. on Controlled Fusion and Plasma Physics, June 9–14, 1997, Berchtesgaden, Germany, Vol. 21A, Part III, p. 1129 (European Physical Society, 1997); General Atomics Report GA-A22646 (1997).

Allen, S.L., C.M. Greenfield, DIII–D Team, "Results from the New High-Triangularity Upper Pump and Baffle on DIII–D," Bull. Am. Phys. Soc. **42**, 1843 (1997).

Allen, S.L., D.N. Hill, T.N. Carlstrom, D.G. Nilson, R.E. Stockdale, C.-L. Hsieh, T.W. Petrie, A.W. Leonard, D. Ryutov, G.D. Porter, R. Maingi, M.R. Wade, R. Cohen, W. Nevins, M.E. Fenstermacher, R.D. Wood, C.J. Lasnier, W.P. West, M.D. Brown, "Measurements of Electron Temperature and Density With DTS in Radiative Divertor Discharges on DIII–D," in J. Nucl. Mater. **241-243**, 595 (1997); General Atomics Report GA-A22357 (1996).

Anderson, P.M., "Scientific Basis and Engineering Design to Accommodate Disruption and Halo Current Loads for the DIII–D Tokamak," in Proc. 19th Symp. on Fusion Technology, September 16–20, 1996, Lisbon, Portugal, Vol. 1, p. 759 (Elsevier Science B.V., Amsterdam, 1997); General Atomics Report GA-A22451 (1996).

Anderson, P.M., J.I. Robinson, E. Gonzales, G.W. Rolens, "Restoration of the DIII–D Solenoid," in Proc. 17th IEEE/NPS Symp. on Fusion Engineering, October 6–11, 1997, San Diego, California (Institute of Electrical and Electronics Engineers, Inc., Piscataway, New Jersey, to be published); General Atomics Report GA-A22686 (1997).

Austin, M.E., G. Cima, R.F. Ellis, T.C. Luce, "Using ECE to Improve EFIT Results for NCS Discharges in DIII–D," Bull. Am. Phys. Soc. **42**, 1974 (1997).

Austin, M.E., R.F. Ellis, J.L. Doane, R.A. James, "Improved Operation of the Michelson Interferometer ECE Diagnostic on DIII–D," presented at 11th Top. Conf. on High Temperature Plasma Diagnostics, May 12–16, 1996, Monterey, California, in Rev. Sci. Instrum. **68**, 480 (1997); General Atomics Report GA-A22330 (1996).

Austin, M.E., R.F. Ellis, T.C. Luce, "Determination of Wall Reflectivity for ECE Frequencies in DIII–D," in Proc. 10th Joint Workshop on Electron Cyclotron Emission and Electron Cyclotron Resonance Heating, April 6–11, 1997, Ameland, The Netherlands; General Atomics Report GA-A22581 (1997).

Baity, F.W., R.H. Goulding, D.J. Hoffman, P.M. Ryan, D.J. Taylor, R.W. Callis, R.I. Pinsker, J.E. Lindemuth, J.H. Rosenfeld, "Faraday Shield Development on DIII–D," Bull. Am. Phys. Soc. **42**, 1934 (1997).

Baker, D.R., "Density Profile Consistency Particle Pinch and Cold Pulse Propagation in DIII–D," Phys. Plasmas **4**, 2229 (1997); General Atomics Report GA-A22413 (1996)

Baker, D.R., "Modeling of the Recycling Particle Flux and Electron Particle Transport in the DIII–D Tokamak," in J. Nucl. Mater. **241-243**, 602 (1997); General Atomics Report GA-A22341 (1996).

Baker, D.R., M.N. Rosenbluth, "Derivation of Expression for Canonical Density Profiles and Comparison with DIII–D Measurements," Bull. Am. Phys. Soc. **42**, 1920 (1997).

Baker, D.R., M.R. Wade, G.L. Jackson, R. Maingi, R.E. Stockdale, J.S. deGrassie, R.J. Groebner, C.B. Forest, G.D. Porter, DIII–D Team, "Measurement of Electron Transport Coefficients in Different Operational Modes of DIII–D," to be published in Nucl. Fusion; General Atomics Report GA-A22553 (1997).

Baylor, L.R., T.C. Jernigan, S.K. Combs, C.R. Foust, P. Gohil, "Plans for High Field Side Pellet Fueling in DIII–D," Bull. Am. Phys. Soc. **42**, 1920 (1997).

Baxi, C.B., "Thermal Analysis and Testing for DIII–D Ohmic Heating Coil Repair," in Proc. 17th IEEE/NPS Symp. on Fusion Engineering, October 6–11, 1997, San Diego, California (Institute of Electrical and Electronics Engineers, Inc., Piscataway, New Jersey, to be published); General Atomics Report GA-A22677 (1997).

Boedo, J.A., R. Lehmer, R.A. Moyer, J.G. Watkins, D.N. Hill, "Measurements of Flows in the DIII–D Divertor by Mach Probes," Bull. Am. Phys. Soc. **42**, 1917 (1997).

Bravenec, R.V., W.L. Rowan, D.M. Patterson, A.J. Wootton, R.J Fonck, G.R. McKee, M. Jakubowski, C.M. Greenfield, D.P. Schissel, M. Kotschenreuther, W. Dorland, "Density Fluctuations During Perturbative Experiments on DIII–D," Bull. Am. Phys. Soc. **42**, 1921 (1997).

Broesch, J.D., "Real Time Software for the Control and Monitoring of DIII–D System Interlocks," in Proc. 19th Symp. on Fusion Technology, September 16–20, 1996, Lisbon, Portugal, to be published (Elsevier Science B.V., Amsterdam, 1997); General Atomics Report GA-A22455 (1996).

Brooks, N.H., D. Fehling, D.L. Hillis, C.C. Klepper, N.N. Naumenko, N. Tugarinov, D.G. Whyte, "Visible Spectroscopy in the DIII–D Divertor," in Rev. Sci. Instrum. **68**, 978 (1997); General Atomics Report GA-A22352 (1996).

Brooks, N.H., R.C. Isler, G.R. McKee, S. Tugarinov, "Doppler Shift Measurements of Plasma Flow in the DIII–D Divertor," Bull. Am. Phys. Soc. **42**, 1918 (1997).

Burrell, K.H., DIII–D Core Transport Group, "Formation and Expansion of Core Transport Barriers in Negative Central Shear Discharges in DIII–D Tokamak," Bull. Am. Phys. Soc. **42**, 1921 (1997).

Burrell, K.H., "Effects of E×B and Velocity Shear on Turbulence and Transport in Magnetic Confinement Devices," in Phys. Plasmas **4**, 1499 (1997); General Atomics Report GA-A22516 (1996).

Burrell, K.H., M.E. Austin, C.M. Greenfield, L.L. Lao, B.W. Rice, G.M. Staebler, B.W. Stallard, "Effects of E×B Velocity Shear and Magnetic Shear in the Formation of Core Transport Barriers in the DIII–D Tokamak," presented at IAEA Tech. Committee Meeting on H–mode Physics, September 22–24, 1997, Kloster-Seeon, Germany, to be published in Plasma Physics and Controlled Fusion; General Atomics Report GA-A22715 (1997).

Callis, R.W., "Status of the DIII–D 110 GHz ECH System," in Proc. 12th Top. Mtg. on The Technology of Fusion Energy, June 16–20, 1996, Reno, Nevada, Vol. 30 (3), Part 2A, p. 825 (American Nuclear Society, La Grange Park, Illinois, 1996); General Atomics Report GA-A22378 (1996).

Callis, R.W., J. Lohr, R.C. O'Neil, D. Ponce, M.E. Austin, T.C. Luce, R. Prater, "Initial Results from the Multi-Megawatt 110 GHz ECH System for he DIII–D Tokamak," in Proc. 12th Top. Conf. on Radio Frequency Power in Plasmas, April 1–3, 1997, Savannah, Georgia, p. 191 (American Institute of Physics, Woodbury, 1997); General Atomics Report GA-A22576 (1997).

Callis, R.W., J. Lohr, R.C. O'Neill, D. Ponce, R. Prater, "Multi-Megawatt 110 GHz ECH System for the DIII–D Tokamak," in Proc. 17th IEEE/NPS Symp. on Fusion Engineering, October 6–11, 1997, San Diego, California (Institute of Electrical and Electronics Engineers, Inc., Piscataway, New Jersey, to be published); General Atomics Report GA-A22707 (1997).

Carlstrom, T.N. K.H. Burrell, R.J. Groebner, F.L. Hinton, G.M. Staebler, D.M. Thomas, "The Grade-B Drift Effect, Sawteeth, and the H–mode Power Threshold Scaling," Bull. Am. Phys. Soc. **42**, 1923 (1997).

Carlstrom, T.N., K.H. Burrell, R.J. Groebner, G.M. Staebler, "H–Mode Threshold Power Scaling and the Grad-B Drift Effect," in Proc. 24th European Conf. on Controlled Fusion and Plasma Physics, June 9–14, 1997, Berchtesgaden, Germany, Vol. 21A, Part III, p. 1089 (European Physical Society, 1997); General Atomics Report GA-A22630 (1997).

Carlstrom, T.N., C.-L. Hsieh, R.E. Stockdale, D.G. Nilson, and D.N. Hill, "Initial Operation of the Divertor Thomson Scattering Diagnostic on DIII–D," in Rev. Sci. Instrum. **68**, 1195 (1997); General Atomics Report GA-A22337 (1996).

Carolipio, E.M., W.W. Heidbrink, "Array of Neutral Particle Analyzers at DIII–D," in Rev. Sci. Instrum. **68**, 304 (1997); General Atomics Report GA-A22358 (1996). .

Carolipio, E.M., W.W. Heidbrink, C.B Forest, R.B. White, "Effect of Helical Field Perturbations on Fast-Ion Confinement in the DIII–D Tokamak," Bull. Am. Phys. Soc. **42**, 1975 (1997).

Cary, W.P., B.L. Burley, W.H. Grosnickle, "DIII–D ICRF High Voltage Power Supply Regulator Upgrade," in Proc. 17th IEEE/NPS Symp. on Fusion Engineering, October 6–11, 1997, San Diego, California (Institute of Electrical and Electronics Engineers, Inc., Piscataway, New Jersey, to be published); General Atomics Report GA-A22712 (1997).

Casper, T.A., D.N. Hill, W.H. Meyer, J.M. Moller, B.W. Stallard, R.D. Wood, J.T. Scoville, B.B. McHarg, Jr., Operations Group, "Remote Experimentation on DIII–D — Operations and Concepts," Bull. Am. Phys. Soc. **42**, 1977 (1997).

Chan, V.S., for the DIII–D Team, "DIII–D Tokamak Concept Improvement Research," in Proc. 16th Int. Conf. on Plasma Physics and Controlled Nuclear Fusion Research, October 7–11, 1996, Montreal, Canada, Vol. 1, p. 95 (International Atomic Energy Agency, Vienna, 1997); General Atomics Report GA-A22471 (1996).

Chiu, H.K., R.-M. Hong, "Comparison of Calculated Neutral Beam Shine Through with Measured Shine-Through in DIII–D," in Proc. 17th IEEE/NPS Symp. on Fusion Engineering, October 6–11, 1997, San Diego, California (Institute of Electrical and Electronics Engineers, Inc., Piscataway, New Jersey, to be published); General Atomics Report GA-A22735 (1997).

Colchin, R.J., R. Maingi, D.L. Hillis, C.C. Klepper, L.W. Owen, M.R. Wade, S.L. Allen, C.M. Greenfield, D.M. Thomas, G.R. McKee, "Neutrals Studies in the Modified Upper Divertor of DIII–D," Bull. Am. Phys. Soc. **42**, 1918 (1997).

DeBoo, J.C., D.P. Schissel, H.E. St. John, R.E. Waltz, K.H. Burrell, T.C. Luce, C.C. Petty, P.A. Politzer, J.E. Kinsey, E. Fredrickson, M. Kissick, "Temporal Response of Profiles to a Modulated Heat Source," Bull. Am. Phys. Soc. **42**, 1922 (1997).

deGrassie, J.S., D.R. Baker, K.H. Burrell, S.C. Chiu, H. Ikezi, J.M. Lohr, Y.R. Lin-Liu, C.C. Petty, R.I. Pinsker, R. Prater, B.W. Rice, "Toroidal Velocity and RF Power in DIII–D," Bull. Am. Phys. Soc. **42**, 1976 (1997).

deGrassie, J.S., D.R. Baker, K.H. Burrell, C.M. Greenfield, H. Ikezi, Y.R. Lin-Liu, C.C. Petty, R. Prater, "Reduction of Toroidal Rotation by Fast Wave Power on DIII–D," in Proc. 12th Top. Conf. on Radio Frequency Power in Plasmas, April 1–3, 1997, Savannah, Georgia, p. 93 (American Institute of Physics, Woodbury, 1997); General Atomics Report GA-A22571 (1997).

Doyle, E.J., K.H. Burrell, T.N. Carlstrom, S. Coda, J.C. DeBoo, R. Durst, R.J. Fonck, P. Gohil, C.M. Greenfield, R.J. Groebner, J. Kim, K.W. Kim, R.J. La Haye, L.L. Lao, E.A. Lazarus, R.A. Moyer, G.A. Navratil, T.H. Osborne, W.A. Peebles, C.L. Rettig, T.L. Rhodes, B.W. Rice, D.P. Schissel, G.M. Staebler, E.J. Strait, T.S. Taylor, D.M. Thomas, R.E. Waltz, "Physics of Turbulence Control and Transport Barrier Formation in DIII–D," in Proc. 16th Int. Conf. on Plasma Physics and Controlled Nuclear Fusion Research, October 7–11, 1996, Montreal, Canada, Vol. 1, p. 547 (International Atomic Energy Agency, Vienna, 1997); General Atomics Report GA-A22487 (1996).

Doyle, E.J., T.L. Rhodes, W.A. Peebles, "Core Reflectometer Density Profile Measurements on DIII–D," Bull. Am. Phys. Soc. **42**, 1920 (1997).

Evans, T.E., D.F. Finkenthal, Y.S. Loh, M.E. Fenstermacher, G.D. Porter, W.P. West, "Comparisons of Physical and Chemical Sputtering in High Density Divertor Plasmas with the Monte Carlo Impurity (MCI) Transport Model," presented at 6th Int. Workshop on Plasma Edge Theory in Fusion Devices, September 15–17, 1997, Oxford United Kingdom, to be published in Contribution to Plasma Physics; General Atomics Report GA-A22693 (1997).

Evans, T.E., A.G. Kellman, D.A. Humphreys, M.J. Schaffer, P.L. Taylor, D.G. Whyte, T.C. Jernigan, A.W. Hyatt, and R.L. Lee, "Measurements of Non-Axisymmetric Halo Currents With and Without 'Killer' Pellets During Disruptions in the DIII–D Tokamak," in J. Nucl. Mater. **241-243**, 606 (1997); General Atomics Report GA-A22344 (1996).

Evans, T.E., A.G. Kellman, P.L. Taylor, P.B. Parks, D.A. Humphreys, M.J. Schaffer, A.W. Hyatt, R.L. Lee, S.C. Chiu, D.G. Whyte, S. Luckhardt, T.C. Jernigan, L.R. Baylor, S. Jardin, G.L. Schmidt, R.W. Harvey, "Impurity Killer Pellet Plasma Termination and Disruption Mitigation Physics in the DIII–D Tokamak," Bull. Am. Phys. Soc. **42**, 1978 (1997).

Fenstermacher, M.E., R.D. Wood, S.L. Allen, N.H. Brooks, D.A. Buchenauer, T.N. Carlstrom, J.W. Cuthbertson, E.J. Doyle, T.E. Evans, P.-M. Garbet, R.W. Harvey, D.N. Hill, A.W. Hyatt, R.C. Isler, G. Jackson, R.A. James, R. Jong, C.C. Klepper, C.J. Lasnier, A.W. Leonard, M.A. Mahdavi, R. Maingi, W.H. Meyer, R.A. Moyer, D.G. Nilson, T.W. Petrie, G.D. Porter, T.L. Rhodes, M.J. Schaffer, R.D. Stambaugh, D.M. Thomas, S. Tugarinov, M.R. Wade, J.G. Watkins, W.P. West, and D.G. Whyte, "Comprehensive 2D Measurements of Radiative Divertor Plasmas in DIII–D," in J. Nucl. Mater. **241-243**, 666 (1997); General Atomics Report GA-A22347 (1997).

Fenstermacher, M.E., R.D. Wood, S.L. Allen, D.N. Hill, C.J. Lasnier, A.W. Leonard, R.C. Isler, "2–D Profiles of Radiating Constituents from Deuterium and Helium Radiative Divertor Plasmas in DIII–D," Bull. Am. Phys. Soc. **42**, 1919 (1997).

Ferron, J.R., C.M. Greenfield, E.J. Strait, R.J. La Haye, G.L. Jackson, T.H. Osborne, B.W. Rice, B.W. Stallard, "MHD Stability in Tokamak Discharges with High Squareness," Bull. Am. Phys. Soc. **42**, 1979 (1997).

Ferron, J.R., M.L. Walker, L.L. Lao, G.B. Penaflor, H.E. St. John, D.A. Humphreys, J.A. Leuer, "Real Time Equilibrium Reconstruction for Control of the Discharge in the DIII–D Tokamak," in Proc. 24th European Conf. on Controlled Fusion and Plasma Physics, June 9–14, 1997, Berchtesgaden, Germany, Vol. 21A, Part III, p. 1125 (European Physical Society, 1997); General Atomics Report GA-A22637 (1997).

Ferron, J.R., M.L. Walker, L.L. Lao, H.E. St. John, D.A. Humphreys, J.A. Leuer, "Real Time Equilibrium Reconstruction for Tokamak Discharge Control," to be published in Nucl. Fusion; General Atomics Report GA-A22586 (1997).

Garofalo, A.M., M.E. Mauel, G.A. Navratil, S.A. Sabbagh, E.J. Strait, R.J. La Haye, A.D. Turnbull, DIII–D Team, "Study of the Resistive Wall Mode in DIII–D," Bull. Am. Phys. Soc. **42**, 1979 (1997).

Gohil, P., K.H. Burrell, L.R. Baylor, T.C. Jernigan, "Effect of Pellet Injection on the Edge Radial Electric Field and the H–mode Power Threshold," Bull. Am. Phys. Soc. **42**, 1924 (1997).

Gohil, P., K.H. Burrell, T.N. Carlstrom, "The Parametric Dependence of the Edge Radial Electric Field in the DIII–D Tokamak," to be published in Nucl. Fusion; General Atomics Report GA-A22585 (1997).

Gohil, P., K.H. Burrell, T.H. Osborne, "Energy Transport During Off-Axis Neutral Beam Heating in the DIII–D Tokamak," to be published in Nucl. Fusion; General Atomics Report GA-A22554 (1997).

Gray, D.S., S. Luckhard, D.G. Whyte, J. Zhang, D.A. Humphreys, A.W. Hyatt, A.G. Kellman, R.L. Lee, J.A. Leuer, P.L. Taylor, T.C. Jernigan, "A Wide-Bandwidth Multichannel Radiometer Diagnostic for Disruptions and Other Transient Phenomena on DIII–D," Bull. Am. Phys. Soc. **42**, 1977 (1997).

Greene, K.L., B.B. McHarg, Jr., "Development of Improved Methods for Remote Access of DIII–D Data and Data Analysis," in Proc. 17th IEEE/NPS Symp. on Fusion Engineering, October 6–11, 1997, San Diego, California (Institute of Electrical and Electronics Engineers, Inc., Piscataway, New Jersey, to be published); General Atomics Report GA-A22730 (1997).

Greenfield, C.M., D.P. Schissel, B.W. Stallard, E.A. Lazarus, G.A. Navratil, K.H. Burrell, T.A. Casper, J.C. DeBoo, E.J. Doyle, R.J. Fonck, C.B. Forest, P. Gohil, R.J. Groebner, M. Jakubowski, L.L. Lao, M. Murakami, C.C. Petty, C.L. Rettig, T.L. Rhodes, B.W. Rice, H.E. St. John, B.M. Staebler, E.J. Strait, T.S. Taylor, A.D. Turnbull, K.L. Tritz, R.E. Waltz, and the DIII–D Team, "Transport and Performance in DIII–D Discharges with Weak or Negative Central Magnetic Shear," in Phys. Plasmas **4**, 1596 (1997); General Atomics Report GA-A22517 (1996).

Greenfield, C.M., J.C. DeBoo, T.H. Osborne, F.W. Perkins, M.N. Rosenbluth, D. Boucher, "Enhanced Fusion Performance Due to Plasma Shape Modification of Simulated ITER Discharges in DIII–D," in Nucl. Fusion **37**, 1215 (1997); General Atomics Report GA-A21842 (1997).

Greenfield, C.M., J.R. Ferron, A.W. Hyatt, M.J. Schaffer D.P. Schissel, S.L. Allen, T.A. Casper, B.W. Rice, B.W. Stallard, E.A. Lazarus, R. Maingi, M.R. Wade, DIII–D Team, "High Performance Plasmas with a Pumped and Baffled Divertor in DIII–D," Bull. Am. Phys. Soc. **42**, 1980 (1997).

Groebner, R.J., T.N. Carlstrom, "Critical Edge Parameters for H–mode Transition in DIII–D," presented at IAEA Tech. Committee Meeting on H–mode Physics, September 22–24, 1997, Kloster-Seeon, Germany, to be published in Plasma Physics and Controlled Fusion; General Atomics Report GA-A22723 (1997).

Groebner, R.J., T.N. Carlstrom, K.H. Burrell, S. Coda, E.J. Doyle, P. Gohil, K.W. Kim, Q. Peng, R. Maingi, R.A. Moyer, C.L. Rettig, T.L. Rhodes, D.P. Schissel, G.M. Staebler, R.D. Stambaugh, D.M. Thomas, J.G. Watkins, "Study of H–Mode Threshold Conditions in DIII–D," in Proc. 16th Int. Conf. on Plasma Physics and Controlled Nuclear Fusion Research, October 7–11, 1996, Montreal, Canada, Vol. 1, p. 867 (International Atomic Energy Agency, Vienna, 1997); General Atomics Report GA-A22443 (1996).

Harvey, R.W., V.S. Chan, S.C. Chiu, T.E. Evans, D.G. Whyte, M.N. Rosenbluth, "Comparisons of Runaway Electron Production in DIII–D with the CQL3D Model," Bull. Am. Phys. Soc. **42**, 1975 (1997).

Heidbrink, W.W., P.L. Taylor, J.A. Phillips, "Measurements of the Neutron Source Strength at DIII–D," Rev. Sci. Instrum. **68** (1), 536 (1997); General Atomics Report GA-A22325 (1996).

Heidbrink, W.W., E.M. Carolipio, T. Tran, K.H. Burrell, "Neutral particle Measurements of the Pitch-angle Scattering Rate, Beam-Ion Transport, and Radial Electric Field," Bull. Am. Phys. Soc. **42**, 1975 (1997).

Hicks, N.K., R.I. Pinsker, H. Ikezi, "Fast Alfvén Wave Interferometry and Reflectometry on the DIII–D Tokamak," Bull. Am. Phys. Soc. **42**, 1927 (1997).

Hill, D.N., DIII–D Divertor Physics Team, "Divertor Detachment in Helium Plasmas," Bull. Am. Phys. Soc. **42**, 1844 (1997).

Holland, C., R. Maingi, R. Owen, R.I. Pinsker, "Development of a Graphical User Interface to Assess Solutions of 2–D Plasma Transport Equations," Bull. Am. Phys. Soc. **42**, 1927 (1997).

Hollerbach, M.A., J.P. Smith, "Fabrication and Installation of the DIII–D Radiative Divertor Structures," in Proc. 17th IEEE/NPS Symp. on Fusion Engineering, October 6–11, 1997, San Diego, California (Institute of Electrical and Electronics Engineers, Inc., Piscataway, New Jersey, to be published); General Atomics Report GA-A22724 (1997).

Holtrop, K.L., G.L. Jackson, A.G. Kellman R.L. Lee, W.P. West, R.D. Wood, D.G. Whyte, "Characterization of Wall Conditions in DIII–D," J. Vac. Sci. Technol. A **15 (3)**, 678 (1997); General Atomics Report GA-A22474 (1996).

Humphreys, D.A., A.G. Kellman, R.R. Khayrutdinov, V.E. Lukash, "Scoping Studies of ITER Disruption Halo Currents Using the DINA Code," Bull. Am. Phys. Soc. **42**, 1832 (1997).

Hyatt, A.W., P.L. Taylor, A.G. Kellman, "Database Analysis of Disruption Frequency in DIII–D," Bull. Am. Phys. Soc. **42**, 1978 (1997).

Ikezi, H., J.S. deGrassie, R.I. Pinsker, R.T. Snider, "Plasma Mass Density, Species Mix and Fluctuation Diagnostics Using Fast Alfven Wave," in Rev. Sci. Instrum. **478**, 68 (1997); General Atomics Report GA-A22340 (1996).

Ikezi, H., D.A. Phelps, "Traveling Wave Antenna for Fast Wave Heating and Current Drive in Tokamaks," in Fusion Tech. **106**, 31 (1997); General Atomics Report GA-A21993 (1995).

Isler, R.C., N.H. Brooks, W.P. West, G.R. McKee, M.E. Fenstermacher, "Deuterium Recombination in the DIII–D Divertor," Bull. Am. Phys. Soc. **42**, 1919 (1997).

Jackson, G.L., E.A. Lazarus, G.A. Navratil, R.J. Bastasz, N.H. Brooks, D.T. Garnier, K.L. Holtrop, J.C. Phillips, E.S. Marmar, T.S. Taylor, D.M. Thomas, W.R. Wampler, D.G. Whyte, W.P. West, "Enhanced Performance in the DIII–D Tokamak with Lithium Wall Conditioning," in J. Nucl. Mater. **241-243**, 655 (1997); General Atomics Report GA-A22361 (1996).

Jackson, G.L., G.M. Staebler, S.L. Allen, N.H. Brooks, T.E. Evans, J.R. Ferron, A.W. Leonard, R. Maingi, T.W. Petrie, M.J. Schaffer, R.D. Wood, W.P. West, D.G. Whyte, "Impurity Feedback Control for Enhanced Divertor and Edge Radiation in DIII–D Discharges," in J. Nucl. Mater. **241-243**, 618 (1997); General Atomics Report GA-A22345 (1996).

Jackson, G.L., G.M. Staebler, A.W. Hyatt, A.W. Leonard, W.P. West,. C.J. Lasnier, R.A. Moyer, M. Murakami, J. Ongena, "Radiating Mangle Discharges in DIII–D with Enhanced Confinement," Bull. Am. Phys. Soc. **42**, 1923 (1997).

Jakubowski, M., R.J. Fonck, G.R. McKee, C.M. Greenfield, R.V. Bravenec, "Density Fluctuations in Microturbulence and High Beta MHD in DIII–D Plasmas," Bull. Am. Phys. Soc. **42**, 1921 (1997).

Jernigan, T.C., L.R. Baylor, S.K. Combs, S.L. Milora, T.E. Evans, P.B. Parks, "Hardware Advanced in Disruption Mitigation by Pellet Injection on DIII–D," Bull. Am. Phys. Soc. **42**, 1980 (1997).

Johnson, W.R., J.P. Smith, "Production and Fabrication of Vanadium Alloys for the Radiative Divertor Program of DIII–D — Semiannual Report Input for 1997" General Atomics Report GA-A22662 (1997).

Kadota, K., C.C. Petty, T.C. Luce, "Dimensionless Size Scaling of the H–mode Power Threshold," Bull. Am. Phys. Soc. **42**, 1928 (1997).

Kellman, A.G., J.W. Cuthbertson, T.E. Evans, D.A. Humphreys, A.W. Hyatt, G.L. Jahns, T.C. Jernigan, C.J. Lasnier, R.L. Lee, J.A. Leuer, S. Luckhardt, M.J. Schaffer, P.L Taylor, D.G. Whyte, D. Wroblewski, J. Zhang, "Disruption Studies in DIII–D," in Proc. 16th Int. Conf. on Plasma Physics and Controlled Nuclear Fusion Research, October 7–11, 1996, Montreal, Canada, Vol. 1, p. 739 (International Atomic Energy Agency, Vienna, 1997); General Atomics Report GA-A22476 (1996).

Kellman, D.H., R.-M. Hong, "Recent Improvements to the DIII–D Neutral Beam Instrumentation and Control System," in Proc. 17th IEEE/NPS Symp. on Fusion Engineering, October 6–11, 1997, San Diego, California (Institute of Electrical and Electronics Engineers, Inc., Piscataway, New Jersey, to be published); General Atomics Report GA-A22718 (1997).

La Haye, R.J., "Physics of Locked Modes in ITER — Error Field Limits, Rotation for Obviation, and Measurement of Field Errors," General Atomics Report GA-A22468 (1997).

La Haye, R.J., J.D. Callen, M.S. Chu, S. Deshpande, T.A. Gianakon, C.C. Hegna, S. Jardin, L.L. Lao, J. Manickam, D.A. Monticello, A. Pletzer, A.J. Reiman, O. Sauter, E.J. Strait, T.S. Taylor, A.D. Turnbull, H.R. Wilson, "Practical Beta Limit in ITER-Shaped Discharges in DIII–D and Its Increase by Higher Collisionality," in Proc. 16th Int. Conf. on Plasma Physics and Controlled Nuclear Fusion Research, October 7–11, 1996, Montreal, Canada Vol. 1, p. 747 (International Atomic Energy Agency, Vienna, 1997); General Atomics Report GA-A22427 (1996).

La Haye, R.J., J.D. Callen, T.A. Gianakon, C.c. Hegna, L.L. Lao, C. Ren, O. Sauter, E.J. Strait, T.S. Taylor, H.R. Wilson, "Metastable Beta Limit in DIII–D," in Proc. 24th European Conf. on Controlled Fusion and Plasma Physics, June 9–14, 1997, Berchtesgaden, Germany, Vol. 21A, Part III, p. 1121 (European Physical Society, 1997); General Atomics Report GA-A22616 (1997).

La Haye, R.J., L.L. Lao, E.J. Strait, T.S. Taylor, "High Beta Tokamak Operation in DIII–D Limited at Low Density/Collisionality by Resistive Tearing Modes," in Nucl. Fusion **37**, 397 (1997); General Atomics Report GA-A22229 (1997).

La Haye, R.J., O. Sauter, "Threshold for Neoclassical Tearing Modes in DIII–D," Bull. Am. Phys. Soc. **42**, 1844 (1997).

Lao, L.L., V.S. Chan, M.S. Chu, J.R. Ferron, R.L. Miller, T.H. Osborne, E.J. Strait, T.S. Taylor, A.D. Turnbull, S.A. Sabbagh, "Edge Instabilities and Termination of DIII–D High Performance Discharges with an H–mode Edge," Bull. Am. Phys. Soc. **42**, 1980 (1997).

Lao, L.L., J.R. Ferron, E.J. Strait, V.S. Chan, M.S. Chu, E.A. Lazarus, T.C. Luce, R.L. Miller, G.A. Navratil, T.H. Osborne, P.A. Politzer, B.W. Rice, T.S. Taylor, A.D. Turnbull, "Impact of Edge Current Density and Pressure Gradient on the Stability of DIII–D High Performance Discharges," in Proc. 24th European Conf. on Controlled Fusion and Plasma Physics, June 9–14, 1997, Berchtesgaden, Germany, Vol. 21A, Part III, p. 1117 (European Physical Society, 1997); General Atomics Report GA-A22640 (1997).

Lao, L.L., R.J. La Haye, K.H. Burrell, V.S. Chan, J.R. Ferron, C.L. Rettig, G.W. Rewoldt, J.T. Scoville, G.M. Staebler, E.J. Strait, W.M. Tang, T.S. Taylor, D. Wroblewski, "Role of E×B Flow Shear on Confinement Enhancement in DIII–D High Internal Inductance Discharges with High-Confinement Edge," to be published in Phys. Plasmas; General Atomics Report GA-A22675 (1997).

Lasnier, C.J., M.E. Fenstermacher, D.N. Hill, W.P. West, A.W. Leonard, T.W. Petrie, J.G. Watkins, "Comparison of Divertor Heat Flux Profiles and Power Balance for Attached and Detached Helium and Deuterium Plasmas," Bull. Am. Phys. Soc. **42**, 1919 (1997).

Lasnier, C.J., R. Maingi, A.W. Leonard, S.L. Allen, D.A. Buchenauer, K.H. Burrell, T.A. Casper, J.W. Cuthbertson, M.E. Fenstermacher, D.N. Hill, R.A. Jong, L.L. Lao, E.A. Lazarus, R.A. Moyer, T.W. Petrie, G.D. Porter, B.W. Rice, B.W. Stallard, T.S. Taylor, J.G. Watkins, "Characteristics of the Scrape-Off Layer in DIII–D High-Performance Negative Central Magnetic Shear Discharges," in J. Nucl. Mater. **241-243**, 623 (1997); General Atomics Report GA-A22353 (1996).

Lazarus, E.A., A.W. Hyatt, G.L. Jackson, D.A. Humphreys, "Using a Multipole Expansion for Startup in the DIII–D Tokamak," to be published in Nucl. Fusion; General Atomics Report GA-A22590 (1997).

Lazarus, E.A., G.A. Navratil, C.M. Greenfield, E.J. Strait. M.E. Austin, K.H. Burrell, T.A. Casper, D.R. Baker, J.C. DeBoo, E.J. Doyle, R. Durst, J.R. Ferron, C.B. Forest, P. Gohil, R.J. Groebner, W.W. Heidbrink, R.-M. Hong, A.W. Howald, C.-L. Hsieh, A.W. Hyatt, G.L. Jackson, J. Kim, L.L. Lao, C.J. Lasnier, A.W. Leonard, J. Lohr, R.J. La Haye, R. Maingi, R.L. Miller, M. Murakami, T.H. Osborne, L.J. Perkins, C.C. Petty, C.L. Rettig, T.L. Rhodes, B.W. Rice, S.A. Sabbagh, D.P. Schissel, J.T. Scoville, R.T. Snider, B.W. Stallard, R.D. Stambaugh, H.E. St. John, R.E. Stockdale, P.L. Taylor, T.S. Taylor, D.M. Thomas, A.D. Turnbull, M.R. Wade, R.D. Wood, D.G. Whyte, "Higher Fusion Power Gain With Profile Control in DIII–D Tokamak Plasmas," in Nucl. Fusion **37**, 7 (1997); General Atomics Report GA-A22416 (1996).

Lazarus, E.A., G.A. Navratil, E.J. Strait, B.W. Rice, J.R. Ferron, C.M. Greenfield, M.E. Austin, D.R. Baker, K.H. Burrell, T.A. Casper, V.S. Chan, J.C. DeBoo, E.J. Doyle, R. Durst, C.B. Forest, P. Gohil, R.J. Groebner, W.W. Heidbrink, R.-M. Hong, W.A. Houlberg, A.W. Howald, C.-L. Hsieh, A.W. Hyatt, G.L. Jackson, J. Kim, R.J. La Haye, L.L. Lao, C.J. Lasnier, A.W. Leonard, J. Lohr, R. Maingi, R.L. Miller, M. Murakami, T.H. Osborne, L.J. Perkins, C.C. Petty, C.L. Rettig, R.L. Rhodes, S.A. Sabbagh, D.P. Schissel, J.T. Scoville, A.C.C. Sips, R.T. Snider, F.X. Sölder, G.M. Staebler, B.W. Stallard, R.D. Stambaugh, H.E. St John, R.E. Stockdale, T.S. Taylor, D.M. Thomas, A.D. Turnbull, M.R. Wade, R.D. Wood, D.G. Whyte, "Stability in High Gain Plasmas in DIII–D," in Proc. 16th Int. Conf. on Plasma Physics and Controlled Nuclear Fusion Research, October 7–11, 1996, Montreal, Canada, Vol. 1, p. 199 (International Atomic Energy Agency, Vienna, 1997); General Atomics Report GA-A22489 (1996).

Lehmer, R., R.A. Moyer, J.A. Boedo, J.G. Watkins, K.H. Burrell, "Edge Electron Temperature Fluctuation Measurements in DIII–D," Bull. Am. Phys. Soc. **42**, 1923 (1997).

Leonard, A.W., S.L. Allen, N.H. Brooks, T.E. Evans, M.E. Fenstermacher, D.N. Hill, R.C. Isler, C.J. Lasnier, M.A. Mahdavi, R. Maingi, R.A. Moyer, T.W. Petrie, G.D. Porter, M.J. Schaffer, M.R. Wade, J.G. Watkins, W.P. West, D.G. Whyte, R.D. Wood, "Energy and Particle Transport in the Radiative Divertor Plasmas of DIII–D," in Proc. 24th European Conf. on Controlled Fusion and Plasma Physics, June 9–14, 1997, Berchtesgaden, Germany, Vol. 21A, Part III, p. 1109 (European Physical Society, 1997); General Atomics Report GA-A22634 (1997).

Leonard, A.W., M.A. Mahdavi, S.L. Allen, N.H. Brooks, M.E. Fenstermacher, D.N. Hill, C.J. Lasnier, R. Maingi, G.D. Porter, T.W. Petrie, J.G. Watkins, W.P. West, "Distributed Divertor Radiation through Convection in DIII–D," in Phys. Rev. Lett. **78**, 4769 (1997); General Atomics Report GA-A22488 (1997).

Leonard, A.W., W. Suttrop, T.H. Osborne, T.E. Evans, D.N. Hill, A. Hermann, C.J. Lasnier, D.M. Thomas, J.G. Watkins, W.P. West, M. Weinlich, H. Zohm, "Divertor Heat and Particle Flux D to ELMs in DIII–D and ASDEX–U," in J. Nucl. Mater. **241-243**, 628 (1997); General Atomics Report GA-A22346 (1996).

Lin-Liu, Y.R., F.L. Hinton, "Trapped Electron Correction to Beam Driven Current in General Tokamak Equilibria," Phys. Plasmas **4**, 4179 (1997); General Atomics Report GA-A22620 (1997).

Lin-Liu, Y.R., F.L. Hinton, "Trapped Electron Corrections to Ohkawa Current in General Tokamak Equilibria," Bull. Am. Phys. Soc. **42**, 1977 (1997).

Lin-Liu, Y.R., T.C. Luce, S.C. Chiu, R.L. Miller, R. Prater, "Modeling of 110 GHz Electron Cyclotron Wave Propagation and Absorption on DIII–D," in Proc. 12th Top. Conf. on Radio Frequency Power in Plasmas, April 1–3, 1997, Savannah, Georgia, p. 195 (American Institute of Physics, Woodbury, 1997); General Atomics Report GA-A22598 (1997).

Loh, Y.S., T.E. Evans, W.P. West, D.F. Finkenthal, M.E. Fenstermacher, G.D. Porter, "Development and Testing of a Chemical Sputtering Model for the Monte Carlo Impurity Code," Bull. Am. Phys. Soc. **42**, 1927 (1997).

Lohr, J., "Summary of the Experimental Session EC–10 Workshop," in Proc. 10th Joint Workshop on Electron Cyclotron Emission and Electron Cyclotron Resonance Heating, April 6–11, 1997, Ameland, The Netherlands; General Atomics Report GA-A22618 (1997).

Lohr, J., R.W. Callis, R.C. O'Neil, D. Ponce, T.C. Luce, M.E. Austin, M. Murakami, D. Zhang, "The 110 GHz ECH Installation on DIII–D — Status and Initial Experimental Results," in Proc. 10th Joint Workshop on Electron Cyclotron Emission and Electron Cyclotron Resonance Heating, April 6–11, 1997, Ameland, The Netherlands; General Atomics Report GA-A22584 (1997).

Lohr, J., D. Ponce, R.W. Callis, I. Popov, M. Zerbini, P. Cahalan, "The 110 GHz Gyrotron Installation on DIII–D — Status and Experimental Results," Bull. Am. Phys. Soc. **42**, 1976 (1997).

Lohr, J., D. Ponce, L. Popov, J.F. Tooker, D. Zhang, "Initial Tests and Operation of a 110 GHz, 1 MW Gyrotron with Evacuated Waveguide System on the DIII–D Tokamak," ed. A.G. Litvak, in Proc. 3rd Int. Wkshp. on Strong Microwaves in Plasmas, August 7–14, 1996, St. Petersburg, Russia, Vol. 2, p. 694 (Institute for Applied Physics, Nizhny Novgorod, Russia, 1996); General Atomics Report GA-A22420 (1996).

Luce, T.C., B. Alper, C.B. challis, G.A. Cottrell, C. Gormezano, C.M. Greenfield, J.C.M. deHaas, G.T.A. Huysmans, E.A. Lazarus, D.P.J. O'Brien, B.W. Rice, A.C.C. Sips, F.X. Söldner, G.M. Staebler, E.J. Strait, T.S. Taylor, B.J.D. Tubbing, A.D. Turnbull, M.R. Wade, D.J. Ward, W.P. Zwingmann, "Comparison of Discharges with Core Transport Barriers on DIII–D and JET," in Proc. 24th European Conf. on Controlled Fusion and Plasma Physics, June 9–14, 1997, Berchtesgaden, Germany, Vol. 21A, Part III, p. 1105 (European Physical Society, 1997); General Atomics Report GA-A22645 (1997).

Luce, T.C., J.S. deGrassie, C.C. Petty, R. Prater, J.M. Lohr, R.I. Pinsker, M.E. Austin, S. Bernabei, "Electron Cyclotron Heating and Current Drive Experiments in the DIII–D Tokamak," Bull. Am. Phys. Soc. **42**, 1976 (1997).

Luce, T.C., C.C. Petty, B. Balet, J.G. Cordey, "Implications from Dimensionless Parameter Scaling Experiments," in Proc. 16th Int. Conf. on Plasma Physics and Controlled Nuclear Fusion Research, October 7–11, 1996, Montreal, Canada, Vol. 1, p. 611 (International Atomic Energy Agency, Vienna, 1997); General Atomics Report GA-A22467 (1996).

Luxon, J.L., "DIII–D Team, An Overview of the DIII–D Program," in Proc. 19th Symp. on Fusion Technology, September 16–20, 1996, Lisbon, Portugal, Vol. 1, p. 221 (Elsevier Science B.V., Amsterdam, 1997); General Atomics Report GA-A22458 (1996).

Mahdavi, M.A., S.L. Allen, N.H. Brooks, R.J. Bastasz, L.R. Baylor, J.N. Brooks, D.A. Buchenauer, J.W. Cuthbertson, T.E. Evans, M.E. Fenstermacher, D.N. Hill, D.L. Hillis, J.T. Hogan, A.W. Hyatt, R.C. Isler, G.L. Jackson, T.C. Jernigan, R.A. Jong, C.C. Klepper, R.J. La Haye, C.J. Lasnier, A.W. Leonard, R. Maingi, P.K. Mioduszewski, R.A. Moyer, M. Murakami, L.W. Owen, T.W. Petrie, G.D. Porter, M.E. Rensink, T. Rognlien, M.J. Schaffer, G.M. Staebler, R.D. Stambaugh, D.M. Thomas, M.R. Wade, W.R. Wampler, J.G. Watkins, W.P. West, D.G. Whyte, C.P.C. Wong, R.D. Wood, DIII–D Physics and Operations Teams, "Divertor Plasma Physics Experiments on the DIII–D Tokamak," in Proc. 16th Int. Conf. on Plasma Physics and Controlled Nuclear Fusion Research, October 7–11, 1996, Montreal, Canada, Vol. 1, p. 397 (International Atomic Energy Agency, Vienna, 1997); General Atomics Report GA-A22478 (1996).

Mahdavi, M.A., R. Maingi, R.J. La Haye, T.C. Jernigan, T.W. Petrie, L.R. Baylor, A.W. Hyatt, A.W. Leonard, M. Murakami, L.W. Owens R.T. Snider, R.D. Stambaugh, M.R. Wade, J.G. Watkins, W.P. West, D.G. Whyte, R.D. Wood, DIII–D Team, "Recent H–mode Density Limit Experiments on DIII–D," in Proc. 24th European Conf. on Controlled Fusion and Plasma Physics, June 9–14, 1997, Berchtesgaden, Germany, Vol. 21A, Part III, p. 1113 (European Physical Society, 1997); General Atomics Report GA-A22636 (1997).

Mahdavi, M.A., G.M. Staebler, R.D. Wood, D.G. Whyte, W.P. West, "Stability of a Radiative Mantle in ITER," in J. Nucl. Mater. **241-243**, 305 (1997); General Atomics Report GA-A22348 (1996).

Maingi, R., "Investigation of Physical Processes Limiting Plasma Density in DIII–D," in Phys. Plasmas **4**, 1752 (1997); General Atomics Report GA-A22521 (1996).

Maingi, R., L.R. Baylor, T.C. Jernigan, M.R. Wade, M.A. Mahdavi, A.W. Hyatt, R.J. La Haye, T.H. Osborne, T.W. Petrie, DIII–D Team, "Overview of Density Limit Experiments on DIII–D," Bull. Am. Phys. Soc. **42**, 1844 (1997).

Maingi, R., B. Terreault, G. Haas, H.S. Bosch, S.C. Chiu, G.L. Jackson, P.K. Mioduszewski, M.A. Mahdavi, M.J. Schaffer, M.R. Wade, W. Zuzak, "Comparison of Wall/Divertor Deuterium Retention and Plasma Fueling Requirements on the DIII–D, TdeV, and ASDEX–Upgrade Tokamaks," in J. Nucl. Mater. **241-243**, 672 (1997); General Atomics Report GA-A22359 (1996).

McHarg, Jr., B.B., "Overview of the DIII–D Program Computer Systems," in Proc. 17th IEEE/NPS Symp. on Fusion Engineering, October 6–11, 1997, San Diego, California (Institute of Electrical and Electronics Engineers, Inc., Piscataway, New Jersey, to be published); General Atomics Report GA-A22717 (1997).

McKee, G.R., R.J. Fonck, M. Jakubowski, K.H. Burrell, C.M. Greenfield, "Turbulence Suppression Dynamics During Internal Transport Barrier Formation on DIII–D," Bull. Am. Phys. Soc. **42**, 1921 (1997).

Miller, R.L., Y.R. Lin-Liu, T.H. Osborne, T.S. Taylor, "Ballooning Mode Stability for Self-Consistent Pressure and Current Profiles at the H–mode Edge," presented at IAEA Tech. Committee Meeting on H–mode Physics, September 22–24, 1997, Kloster-Seeon, Germany, to be published in Plasma Physics and Controlled Fusion; General Atomics Report GA-A22711 (1997).

Miller, R.L., Y.R. Lin-Liu, T.H. Osborne, T.S. Taylor, "Ballooning Mode Stability for Self-Consistent Pressure and Current Profiles at the H–mode Edge of Tokamaks," Bull. Am. Phys. Soc. **42**, 1980 (1997).

Miller, R.L., Y.-R. Lin-Liu, A.D. Turnbull, V.S. Chan, L.D. Pearlstein, O. Sauter, L. Villard, "Stable Bootstrap-Current Driven Equilibria for Low Aspect Ratio Tokamaks," eds. J.W. Connor, E. Sindoni and J. Vaclavik, in Theory of Fusion Plasmas, p. 11 (Editrice Compositori, Bologna, 1997); General Atomics Report GA-A22433 (1996).

Moyer, R.A., R. Lehmer, J.A. Boedo, T.L. Rhodes, C.L. Rettig, E.J. Doyle, J.G. Watkins, R.J. Groebner, K.H. Burrell, "Coherent Modes in the Edge of DIII–D H–modes," Bull. Am. Phys. Soc. **42**, 1923 (1997).

Moyer, R.A., T.L. Rhodes, C.L. Rettig, E.J. Doyle, K.H. Burrell, J.W. Cuthbertson, R.J. Groebner, K.W. Kim, A.W. Leonard, R. Maingi, G.D. Porter, J.G. Watkins, "Study of the Phase Transition Dynamics of the L-to-H Transition," presented at IAEA Tech. Committee Meeting on H–mode Physics, September 22–24, 1997, Kloster-Seeon, Germany, to be published in Plasma Physics and Controlled Fusion; General Atomics Report GA-A22726 (1997).

Murakami, M., "Overview of DIII–D 1997 Experiment Campaign," Bull. Am. Phys. Soc. **42**, 1917 (1997).

Nilson, D.G., B.W. Stallard, T.N. Carlstrom, C.L. Hsieh, R.E. Stockdale, "Central Thomson Scattering Upgrade on DIII–D," in Proc. 17th IEEE/NPS Symp. on Fusion Engineering, October 6–11, 1997, San Diego, California (Institute of Electrical and Electronics Engineers, Inc., Piscataway, New Jersey, to be published); General Atomics Report GA-A22722 (1997).

Osborne, T.H., R.J. Groebner, L.L. Lao, A.W. Leondard, R. Maingi, R.L. Miller, G.D. Porter, D.M. Thomas, R.E. Waltz, "H–mode Pedestal Characteristics, ELMs, and Energy Confinement in ITER Shape Discharge on DIII–D," presented at IAEA Tech. Committee Meeting on H–mode Physics, September 22–24, 1997, Kloster-Seeon, Germany, to be published in Plasma Physics and Controlled Fusion; General Atomics Report GA-A22733 (1997).

Osborne, T.H., R.J. Groebner, L.L. Lao, A.W. Leonard, R. Maingi, R.L. Miller, G.D. Porter, D.M. Thomas, R.E. Waltz, "Scaling of ELM and H–Mode Pedestal Characteristics in ITER Shape Discharges in the DIII–D Tokamak," in Proc. 24th European Conf. on Controlled Fusion and Plasma Physics, June 9–14, 1997, Berchtesgaden, Germany, Vol. 21A, Part III, P. 1101 (European Physical Society, 1997); General Atomics Report GA-A22638 (1997).

Olstad, R.A., J.L. Doane, C.P. Moeller, R.C. O'Neill, M. Di Martino, "High-Power Corrugated Waveguide Components for Millimeter Wave Fusion Heating Systems," in Proc. 19th Symp. on Fusion Technology, September 16–20, 1996, Lisbon, Portugal, Vol. 1, p. 573 (Elsevier Science B.V., Amsterdam, 1997); General Atomics Report GA-A22466 (1996).

Parks, P.B., M.N. Rosenbluth, "Equilibrium Pellet and Liquid Jet Shapes Under High Ablation Pressures," to be published in Phys. Plasmas; General Atomics Report GA-A22772 (1997).

Peebles, W.A., C.L. Rettig, X. Nguyen, K.H. Burrell, M.E. Austin, G. Cima, "Electron Temperature Fluctuation Measurements in DIII–D," Bull. Am. Phys. Soc. **42**, 1922 (1997).

Penaflor, B., J.R. Ferron, M.L. Walker, "A Structured Architecture for Advanced Plasma Control Experiments," in Proc. 19th Symp. on Fusion Technology, September 16–20, 1996, Lisbon, Portugal, Vol. 1, p. 965 (Elsevier Science B.V., Amsterdam, 1997); General Atomics Report GA-A22545 (1996).

Penaflor, B.G., B.B. McHarg, Jr., D. Piglowski, "Software Development on the DIII–D Control and Data Acquisition Computers," in Proc. 17th IEEE/NPS Symp. on Fusion Engineering, October 6–11, 1997, San Diego, California (Institute of Electrical and Electronics Engineers, Inc., Piscataway, New Jersey, to be published); General Atomics Report GA-A22713 (1997).

Petersen, P.I., DIII–D Team, "Recent Results from the DIII–D Tokamak," in Proc. 17th IEEE/NPS Symp. on Fusion Engineering, October 6–11, 1997, San Diego, California (Institute of Electrical and Electronics Engineers, Inc., Piscataway, New Jersey, to be published); General Atomics Report GA-A22748 (1998).

Petrie, T.W., S.L. Allen, T.N. Carlstrom, D.N. Hill, R. Maingi, D.G. Nilson, M.D. Brown, D.A. Buchenauer, T.E. Evans, M.E. Fenstermacher, R.A. Jong, C.J. Lasnier, A.W. Leonard, M.A. Mahdavi, G.D. Porter, M.R. Wade, W.P. West, "Investigation of Electron Parallel Pressure Balance in the Scrape-Off Layer of Deuterium-Based Radiative Divertor Discharges in DIII–D," in J. Nucl. Mater. **241-243**, 639 (1997); General Atomics Report GA-A22349 (1996).

Petrie, T.W., A.W. Leonard, M.A. Mahdavi, W.P. West, R. Maingi, S.L. Allen, M.E. Fenstermacher, D.N. Hill, C.J. Lasnier, G.D. Porter, "Behavior of Double-Null H–mode Discharges at High Density in DIII–D," Bull. Am. Phys. Soc. **42**, 1919 (1997).

Petrie, T.W., R. Maingi, S.L. Allen, D.A. Buchenauer, D.N. Hill, C.J. Lasnier, "Partially Detached Radiative Divertor with Active Divertor Pumping," in Nucl. Fusion **37**, 643 (1997); General Atomics Report GA-A22154 (1997).

Petty, C.C., C.B. Forest, R.I. Pinsker, J.S. deGrassie, F.W. Baity, R.W. Callis, W.P. Cary, S.C. Chiu, R.L. Freeman, P. Gohil, R.J. Groebner, H. Ikezi, E.F. Jaeger, Y.R. Lin-Liu, M. Murakami, M. Porkolab, R. Prater, B.W. Rice, "Fast Wave Current Drive in Neutral Beam Heated Plasmas on DIII–D," in Proc. 12th Top. Conf. on Radio Frequency Power in Plasmas, April 1–3, 1997, Savannah, Georgia, p. 225 (American Institute of Physics, Woodbury, 1997); General Atomics Report GA-A22575 (1997).

Petty, C.C., T.C. Luce, "Understanding Transport through Dimensionless Parameter Scaling Experiments," in Proc. 24th European Conf. on Controlled Fusion and Plasma Physics, June 9–14, 1997, Berchtesgaden, Germany, Vol. 21A, Part III, p. 1085 (European Physical Society, 1997); General Atomics Report GA-A22626 (1997).

Petty, C.C., T.C. Luce, J.C. DeBoo, R.E. Waltz, D.R. Baker, M.R. Wade, "Scaling of Heat Transport with Beta in the DIII–D Tokamak," to be published in Nucl. Fusion; General Atomics Report GA-A22572 (1772).

Phelps, D.A., "An ELM-Resilient RF Arc Detection System for DIII–D Based on Electromagnetic and Sound Emissions from the Arc," in Proc. 12th Top. Conf. on Radio Frequency Power in Plasmas, April 1–3, 1997, Savannah, Georgia, p. 401 (American Institute of Physics, Woodbury, 1997); General Atomics Report GA-A22577 (1997).

Phelps, D.A., F.W. Baity, R.W. Callis, J.S. deGrassie, C.P. Moeller, R.I. Pinsker, "Advantages of Traveling Wave Resonant Antennas for Fast Wave Heating Systems," in Proc. 12th Top. Conf. on Radio Frequency Power in Plasmas, April 1–3, 1997, Savannah, Georgia, p. 397 (American Institute of Physics, Woodbury, 1997); General Atomics Report GA-A22574 (1997).

Phillips, J.C., J.L. Busath, B.G. Penaflor, D. Piglowski, D.H. Kellman, H.K. Chiu, R.-M. Hong, "Advances in the Operation of the DIII–D Neutral Beam Computer Systems," in Proc. 17th IEEE/NPS Symp. on Fusion Engineering, October 6–11, 1997, San Diego, California (Institute of Electrical and Electronics Engineers, Inc., Piscataway, New Jersey, to be published); General Atomics Report GA-A22760 (1998).

Piglowski, D., B.G. Penaflor, J.C. Phillips, "Use of the Accessware Interface/Database Software in the Neutral Beam Control Systems Used by the DIII–D Tokamak," in Proc. 17th IEEE/NPS Symp. on Fusion Engineering, October 6–11, 1997, San Diego, California (Institute of Electrical and Electronics Engineers, Inc., Piscataway, New Jersey, to be published); General Atomics Report GA-A22745 (1997).

Pinsker, R.I., W.P. Cary, C.C. Petty, R.W. Callis, J.S. deGrassie, W.C. Martin, F.W. Baity, "System for Tunerless Operation of a Four-Element Phased Array Antenna for Fast Wave Current Drive," in Proc. 17th IEEE/NPS Symp. on Fusion Engineering, October 6–11, 1997, San Diego, California (Institute of Electrical and Electronics Engineers, Inc., Piscataway, New Jersey, to be published); General Atomics Report GA-A22752 (1997).

Pinsker, R.I., C.P. Moeller, C.C. Petty, D.A. Phelps, T. Ogawa, Y. Miura, H. Ikezi, J.S. deGrassie, R.W. Callis, R.H. Goulding, F.W. Baity, "Development of Fast Wave Systems Tolerant of Time-Varying Loading," in Proc. 19th Symp. on Fusion Technology, September 16–20, 1996, Lisbon, Portugal, Vol. 1, p. 629 (Elsevier Science B.V., Amsterdam, 1997); General Atomics Report GA-A22450 (1996).

Pinsker, R.I., C.P. Moeller, J.S. deGrassie, D.A. Phelps, C.C. Petty, R.W. Callis, F.W. Baity, "Fast Wave Antenna Array Feed Circuits Tolerant of Time-Varying Loading for DIII–D," in Proc. 12th Top. Conf. on Radio Frequency Power in Plasmas, April 1–3, 1997, Savannah, Georgia, p. 393 (American Institute of Physics, Woodbury, 1997); General Atomics Report GA-A22583 (1997).

Pinsker, R.I., D.A. Phelps, R.W. Callis, W.P. Cary, J.S. deGrassie, C.P. Moeller, R.C. O'Neill, C.C. Petty, F.W. Baity, "High Power Operation of Tunerless Fast Wave Current Drive Antenna Systems on DIII–D," Bull. Am. Phys. Soc. **42**, 1976 (1997).

Politzer, P.A., H.E. St. John, R.L. Miller, C.B. Forrest, W.M. Nevins, L.D. Pearlstein, "Plasma Current Rampu-up and Sustainment with Bootstrap Current," Bull. Am. Phys. Soc. **42**, 1980 (1997).

Ponce, D., J. Lohr, J.F. Tooker, W.P. Cary, T.E. Harris, "The DIII–D Multiple Gyrotron Control System," in Proc. 17th IEEE/NPS Symp. on Fusion Engineering, October 6–11, 1997, San Diego, California (Institute of Electrical and Electronics Engineers, Inc., Piscataway, New Jersey, to be published); General Atomics Report GA-A22720 (1997).

Prater, R., M.E. Austin, F.W. Baity, S.C. Chiu, R.W. Callis, W.P. Cary, J.S. deGrassie, R.L. Freeman, C.B. Forest, S.W. Ferguson, H. Ikezi, E.F. Jaeger, E. Joffrin, J.H. Lee, Y.-R. Lin-Liu, T.C. Luce, M. Murakami, C.C. Petty, R.I. Pinsker, D.A. Phelps, M. Porkolab, D.W. Swain, The DIII–D Team, "Fast Wave Heating and Current Drive in DIII–D in Discharges with Negative Central Shear," in Proc. 16th Int. Conf. on Plasma Physics and Controlled Nuclear Fusion Research, October 7–11, 1996, Montreal, Canada, Vol. 3, p. 243 (International Atomic Energy Agency, Vienna, 1997); General Atomics Report GA-A22449 (1996).

Prater, R., R.W. Callis, J.S. deGrassie, Y.R. Lin-Liu, J.M. Lohr, T.C. Luce, C.C. Petty, R.I. Pinsker, M.E. Austin, S. Bernabei, G. Giruzzi, R.W. Harvey, M. Murakami, M. Zerbini, "Initial Experiments on DIII–D Using Electron Cyclotron Heating at 110 GHz," Bull. Am. Phys. Soc. **42**, 1844 (1997).

Project Staff, "DIII–D Research Operations Annual Report, October 1, 1995 through September 30, 1996," General Atomics Report GA-A22550 (1997).

Project Staff, "DIII–D Tokamak Long Range Plan," General Atomics Report GA-C19596, Rev. 7 (1997).

Reis, E.E., P.M. Anderson, E. Chin, J.E. Robinson, "Analysis and Testing of the DIII–D Ohmic Heating Coil Lead Repair Clamp," in Proc. 17th IEEE/NPS Symp. on Fusion Engineering, October 6–11, 1997, San Diego, California (Institute of Electrical and Electronics Engineers, Inc., Piscataway, New Jersey, to be published); General Atomics Report GA-A22706 (1997).

Reis, E.E., J.P. Smith, C.B. Baxi, A.S. Bozek, E. Chin, M.A. Hollerbach, G.J. Laughon, D.L. Sevier, "Structural Design of the DIII–D Radiative Divertor," in Proc. 19th Symp. on Fusion Technology, September 16–20, 1996, Lisbon, Portugal, Vol. 1, p. 475 (Elsevier Science B.V., Amsterdam, 1997); General Atomics Report GA-A22445 (1996).

Reis, E.E., R.H. Ryder, "Creep-Fatigue Damage in OFHC Coolant Tubes for Plasma Facing Components," in Proc. 19th Symp. on Fusion Technology, September 16–20, 1996, Lisbon, Portugal, Vol. 1, p. 319 (Elsevier Science B.V., Amsterdam, 1997); General Atomics Report GA-A22436 (1996).

Rensink, M.E., Lodestro, L.L., G.D. Porter, T.D. Rognlien, C.P. Coster, "Comparison of Fluid and Monte Carlo Neutral Gas Models in Divertor Plasma Simulations," Bull. Am. Phys. Soc. **42**, 1918 (1997).

Rhodes, T.L., C.L. Rettig, W.A. Peebles, K.H. Burrell, F.L. Hinton, "Prompt Plasma Response to Neutral Beam Injection," Bull. Am. Phys. Soc. **42**, 1922 (1997).

Rice, B.W., "q-Profile Measurements with Motional Stark Effect in DIII–D," in Fusion Engineering and Design **34**, 135 (1997); General Atomics Report GA-A22269 (1996).

Rice, B.W., K.H. Burrell, L.L. Lao, "Effect of Plasma Radial Electric Field on Motional Stark Effect Measurements and Equilibrium Reconstruction," Nucl. Fusion **37**, 517 (1997); General Atomics Report GA-A22480 (1996).

Rice, B.W., T.A. Casper, B.W. Stallard, J.R. Ferron, C.M. Greenfield, G.L. Jackson, R.J. La Haye, T.C. Luce, E.J. Strait, R. Maingi, M.R. Wade, "Effect of the q and E×B Shear Profiles on Confinement and Stability of ELMing H–mode Discharges," Bull. Am. Phys. Soc. **42**, 1922 (1997).

Rice, B.W., L.L. Lao, K.H. Burrell, C.M. Greenfield, Y.R. Lin-Liu, "The Importance of the Radial Electric (E_r) on Interpretation of Motional Stark Effect Measurements of the q Profile in DIII–D High-Performance Plasmas," in Proc. 24th European Conf. on Controlled Fusion and Plasma Physics, June 9–14, 1997, Berchtesgaden, Germany, Vol. 21A, Part III, p. 1153 (European Physical Society, 1997); General Atomics Report GA-A22641 (1997).

Rice, B.W., K.H. Burrell, L.L. Lao, Y.R. Lin-Liu, "Direct Measurement of the Radial Electric Field in Tokamak Plasmas Using the Stark Effect," Phys. Rev. Lett. **79**, 2694 (1997); General Atomics Report GA-A22647 (1997).

Schaffer, M.J., "Helical–D Pinch" presented at IAEA Technical Committee Meeting on Innovative Approaches to Fusion Energy, October 20–23, 1997, Pleasanton, California; General Atomics Report GA-A22690 (1997).

Schaffer, M.J., "Poloidal Pressure Gradients, Divertor Detachment, and MARFEs," presented at 6th Int. Workshop on Plasma Edge Theory in Fusion Devices, September 15–17, 1997, Oxford United Kingdom, to be published in Contribution to Plasma Physics; General Atomics Report GA-A22703 (1997).

Schaffer, M.J., "Slow Linear Fusion" presented at IAEA Technical Committee Meeting on Innovative Approaches to Fusion Energy, October 20–23, 1997, Pleasanton, California; General Atomics Report GA-A22689 (1997).

Schaffer, M.J., N.H. Brooks, J.A. Boedo, R.A. Moyer, R.C. Isler, "Plasma Pressure and Flows Near the Divertor X–point," Bull. Am. Phys. Soc. **42**, 1918 (1997).

Schaffer, M.J., M.R. Wade, R. Maingi, P. Monier-Garbet, W.P. West, D.G. Whyte, R.D. Wood, M.A. Mahdavi, "Direct Measurement of Divertor Neon Enrichment in DIII–D," in J. Nucl. Mater. **241-243**, 585 (1997); General Atomics Report GA-A22343 (1996).

Schissel, D.P., C.M. Greenfield, J.C. DeBoo, L.L. Lao, E.A. Lazarus, G.A. Navratil, B.W. Rice, G.M. Staebler, B.W. Stallard, E.J. Strait, H.E. St. John, M.E. Austin, K.H. Burrell, T.A. Casper, D.R. Baker, V.S. Chan, E.J. Doyle, J.R. Ferron, C.B. Forest, P. Gohil, R.J. Groebner, W.W. Heidbrink, R.-M. Hong, A.W. Howald, C.-L. Hsieh, A.W. Hyatt, G.L. Jackson, J. Kim, C.J. Lasnier, A.W. Leonard, J. Lohr, R.J. La Haye, R. Maingi, R.L. Miller, M. Murakami, T.H. Osborne, C.C. Petty, C.L. Rettig, T.L. Rhodes, S.A. Sabbagh, J.T. Scoville, R.T. Snider, R.D. Stambaugh, R.E. Stockdale, P.L. Taylor, T.S. Taylor, D.M. Thomas, M.R. Wade, R.E. Waltz, R.D. Wood, D.G. Whyte, "Local Analysis of Confinement and Transport in Neutral Beam Heated DIII–D Discharges with Negative Magnetic Shear," in Proc. 16th Int. Conf. on Plasma Physics and Controlled Nuclear Fusion Research, October 7–11, 1996, Montreal, Canada, Vol. 1, p. 463 (International Atomic Energy Agency, Vienna, 1997); General Atomics Report GA-A22479 (1996).

Scoville, J.T., R.J. La Haye, "Coupled Resonant Error Field Mode Components and the Low Density Locked Mode Threshold," Bull. Am. Phys. Soc. **42**, 1979 (1997).

Sevier, D.L., C.B. Baxi, D.N. Hill, E.E. Reis, G.W. Silke, C.P.C. Wong, "Implications of Steady-State Operation on Divertor Design," in Proc. 12th Top. Mtg. on The Technology of Fusion Energy, June 16–20, 1996, Reno, Nevada, Vol. 30 (3), Part 2A, p. 720 (American Nuclear Society, La Grange Park, Illinois, 1996); General Atomics Report GA-A22388 (1996).

Simonen, T.C., "High Pressure Plasma Stability with Favorable Magnetic Field Line Curvature," to be published in Plasma Physics Reports; General Atomics Report GA-A22578 (1997).

Simonen, T.C., DIII–D National Team, "DIII–D National Program Progress and Plans," Bull. Am. Phys. Soc. **42**, 1843 (1997).

Simonen, T.C., D.M. Meade, "Recent Results of Engineering Experience from Operation of TFTR and DIII–D," presented at 4th Int. Symp. on Fusion Nuclear Technology, April 6–11, 1997, Tokyo, Japan, to be published in Fusion Engineering and Design; General Atomics Report GA-A22560 (1997).

Smith, J.P., C.B. Baxi, A.S. Bozek, E. Chin, M.A. Hollerbach, W.R. Johnson, G.J. Laughon, E.E. Reis, D.L. Sevier, D.G. Nilson, "The DIII–D Radiative Divertor Project, Status and Plans," in Proc. 12th Top. Mtg. on The Technology of Fusion Energy, June 16–20, 1996, Reno, Nevada, Vol. 30 (3), Part 2A, p. 706 (American Nuclear Society, La Grange Park, Illinois, 1996); General Atomics Report GA-A22389 (1996)

Smith, J.P., W.R. Johnson, C.B. Baxi, "Manufacturing Development of Low Activation Vanadium Alloys," in Proc. 12th Top. Mtg. on The Technology of Fusion Energy, June 16–20, 1996, Reno, Nevada, Vol. 30 (3), Part 2A, p. 982 (American Nuclear Society, La Grange Park, Illinois, 1996); General Atomics Report GA-A22382 (1996).

Smith, J.P., W.R. Johnson, E.E. Reis, "Fabrication Development and Usage of Vanadium Alloys in DIII–D," in Proc. 19th Symp. on Fusion Technology, September 16–20, 1996, Lisbon, Portugal, Vol. 1, p. 479 (Elsevier Science B.V., Amsterdam, 1997); General Atomics Report GA-A22452 (1996).

Snider, R.T., N.H. Brooks, N. Bogatu, "Argon K_α Measurement Technique on DIII–D," Bull. Am. Phys. Soc. **42**, 1977 (1997).

Snider, R.T., T.N. Carlstrom, T.R. Hodapp, F.C. Jobes, W.A. Peebles, "Application of Interferometry and Faraday Rotation Techniques for Density Measurements on the Next Generation of Tokamaks," in Rev. Sci. Instrum. **68**, 728 (1997); General Atomics Report GA-A22328 (1996).

St. John, H.E., Q. Peng, J. Freeman, J. Crotinger, "Development of a New System for Transport Simulation and Analysis at General Atomics," Bull. Am. Phys. Soc. **42**, 1977 (1997).

Staebler, G.M., "Theory of Internal and Edge Transport Barriers," presented at IAEA Tech. Committee Meeting on H–mode Physics, September 22–24, 1997, Kloster-Seeon, Germany, to be published in Plasma Physics and Controlled Fusion; General Atomics Report GA-A22694 (1997).

Staebler, G.M., C.M. Greenfield, D.P. Schissel, K.H. Burrell, T.A. Casper, J.C. DeBoo, E.J. Doyle, R.J. Fonck, L.L. Lao, E.A. Lazarus G.A. Navratil, C.L. Rettig, T.L. Rhodes, B.W. Rice, H.E. St. John, B.W. Stallard, E.J. Strait, R.E. Waltz, DIII–D Team, "Core Turbulence and Transport Reduction in DIII–D Discharges with Weak or Negative Magnetic Shear," in Proc. 24th European Conf. on Controlled Fusion and Plasma Physics, June 9–14, 1997, Berchtesgaden, Germany, Vol. 21A, Part III, p. 1097 (European Physical Society, 1997); General Atomics Report GA-A22617 (1997).

Staebler, G.M., G.L. Jackson, W.P. West, S.L. Allen, R.J. Groebner, M.J. Schaffer, D.G. Whyte, "Improved Energy Confinement with Neon Injection in the DIII–D Tokamak," in Proc. 24th European Conf. on Controlled Fusion and Plasma Physics, June 9–14, 1997, Berchtesgaden, Germany, Vol. 21A, Part III, p. 1093 (European Physical Society, 1997); General Atomics Report GA-A22643 (1997).

Staebler, G.M., G.L. Jackson, W.P. West, S.L. Allen, R.J. Groebner, M.J. Schaffer, D.G. Whyte, "Improved High-Mode with Neon Injection in the DIII–D Tokamak," to be published in Phys. Rev. Lett.; General Atomics Report GA-A22674 (1997).

Stallard, B.W., T.A. Casper, B.W. Rice, K.H. Burrell, C.M. Greenfield J.C. DeBoo, P. Gohil, C.C. Petty, D.P. Schissel, G.M. Staebler, E.J. Strait, C.L. Rettig, T.L. Rhodes, G.R. McKee, M.E. Austin, L.R. Baylor, "Electron Thermal Transport in L–mode Edge NCS Plasmas," Bull. Am. Phys. Soc. **42**, 1922 (1997).

Stambaugh, R.D., "Power and Particle Exhaust in Tokamaks," in Proc. 17th IEEE/NPS Symp. on Fusion Engineering, October 6–11, 1997, San Diego, California (Institute of Electrical and Electronics Engineers, Inc., Piscataway, New Jersey, to be published); General Atomics Report GA-A22794 (1997).

Stambaugh, R.D., V.S. Chan, P.M. Anderson, C.B. Baxi, R.W. Callis, H.K. Chiu, C.B. Forest, R.-M. Hong, T.H. Jensen, L.L. Lao, J.A. Leuer, M.A. Mahdavi, R.L. Miller, A. Nerem, R. Prater, P.A. Politzer, M.J. Schaffer, D.L. Sevier, T.S. Taylor, A.D. Turnbull, C.P.C. Wong, "The Spherical Torus Approach to Magnetic Fusion Development," in Proc. 12th Top. Mtg. on The Technology of Fusion Energy, June 16–20, 1996, Reno, Nevada, Vol. 30 (3), Part 2A, p. 1380 (American Nuclear Society, La Grange Park, Illinois, 1996); General Atomics Report GA-A22388 (1996).

Stambaugh, R.D., V.S. Chan, R.L. Miller, P.M. Anderson, C.B. Baxi, R.W. Callis, H.K. Chiu, S.C. Chiu, C.B. Forest, R. Hong, T.H. Jensen, L.L. Lao, J.A. Leuer, Y.R. Lin-Liu, M.A. Mahdavi, A. Nerem, R. Prater, P.A. Politzer, M.J. Schaffer, D.L. Sevier, T.S. Taylor, A.D. Turnbull, C.P.C. Wong, "The Spherical Torus Approach to Magnetic Fusion Development," in Proc. 16th Int. Conf. on Plasma Physics and Controlled Nuclear Fusion Research, October 7–11, 1996, Montreal, Canada, Vol. 3, p. 395 (International Atomic Energy Agency, Vienna, 1997); General Atomics Report GA-A22432 (1996).

Stambaugh, R.D., V.S. Chan, R.L. Miller, P.M. Anderson, H.K. Chiu, S.C. Chiu, C.B. Forest, C.M Greenfield, T.H. Jensen, R.J. La Haye, L.L. Lao, Y.R. Lin-Liu, A. Nerem, R. Prater, P.A. Politzer, H.E. St. John, M.J. Schaffer, G.M. Staebler, T.S. Taylor, A.D. Turnbull, C.P.C. Wong, "Development Path of Low Aspect Ratio Tokamak Power Plants," presented at 4th Int. Symp. on Fusion Nuclear Technology, April 6–11, 1997, Tokyo, Japan, to be published in Fusion Engineering and Design; General Atomics Report GA-A22565 (1997).

Stambaugh, R.D., V.S. Chan, R.L. Miller, M.J. Schaffer, "The Spherical Tokamak Path to Fusion Power," to be published in Fusion Technology; General Atomics Report GA-A22226 (1996).

Strait, E.J., T.A. Casper, M.S. Chu, J.R. Ferron, A. Garofalo, C.M. Greenfield, R.J. La Haye, L.L. Lao, E.A. Lazarus, R.L. Miller, G.A. Navratil, C. Ren, B.W. Rice, I. Semenov, A.C.C. Sips, F.X. Söldner, B.W. Stallard, T.S. Taylor, A.D. Turnbull, and the DIII–D Team, "Stability of Negative Central Magnetic Shear Discharges in the DIII–D Tokamak," in Phys. Plasmas **4**, 1783 (1997); General Atomics Report GA-A22522 (1996).

Strait, E.J., M.S. Chu, J.R. Ferron, R.J. La Haye, L.L. Lao, T.S. Taylor, A.D. Turnbull, DIII–D Team, J. Anderson, K. Commer, G. McKee, C. Ren, M.E. Austin, E.A. Lazarus, G.A. Navratil, B.W. Rice, "Stability Limits of DIII–D Discharges with Strongly Peaked Pressure Profiles," Bull. Am. Phys. Soc. **42** 1845 (1997).

Strait, E.J., J.D. Broesch, R.T. Snider, M.L. Walker, "A Hybrid Digital-Analog Long Pulse Integrator," in Rev. Sci. Instrum. **68**, 381 (1997); General Atomics Report GA-A22338 (1996).

Taylor, T.S., "Physics of Advanced Tokamaks," in Plasma Physics and Controlled Fusion **39**, B47 (1997); General Atomics Report GA-A22704 (1997).

Taylor, T.S., R.L. Lee, T.E. Evans, D.A. Humphreys, A.W. Hyatt, A.G. Kellman, M.J. Schaffer, D.S. Gray, S. Luckhardt, D.G. Whyte, J. Zhang, T.C. Jernigan, "Runaway Electron Diagnostic for Disruptions in DIII–D," Bull. Am. Phys. Soc. **42**, 1979 (1997).

Thomas, D.M., K.H. Burrell, R.J. Groebner, P. Gohil, D.H. Kaplan, C.C. Makariou, R.P. Seraydarian, " A Fast CCD Detector for Charge Exchange Recombination Spectroscopy on the DIII–D Tokamak," presented at 11th Top. Conf. on High Temperature Plasma Diagnostics, May 12–16, 1996, Monterey, California, in Rev. Sci. Instrum. **68**, 1233 (1997); General Atomics Report GA-A22329 (1996).

Thomas, D.M., R.J. Groebner, K.H. Burrell, T.H. Osborne, T.N. Carlstrom, "The Back Transition and Hysteresis Effects in DIII–D," presented at IAEA Tech. Committee Meeting on H–mode Physics, September 22–24, 1997, Kloster-Seeon, Germany, to be published in Plasma Physics and Controlled Fusion; General Atomics Report GA-A22697 (1997).

Thomas, D.M., R.J. Groebner, K.H. Burrell, T.H. Osborne, T.N. Carlstrom, "The Back Transition and Hysteresis Effects in DIII–D," Bull. Am. Phys. Soc. **42**, 1924 (1997).

Turnbull, A.D., T.S. Taylor, J.R. Ferron, R.J. La Haye, Y.R. Lin-Liu, R.L. Miller, E.J. Strait, M.S. Chu, C.M. Greenfield, L.L. Lao, B.W. Rice, E.A. Lazarus, "Prospects for Advanced Tokamak Scenarios of High Performance Tokamak Regimes," Bull. Am. Phys. Soc. **42**, 1980 (1997).

Wade, M.R., DIII–D Team, "Z-Dependence of Transport in the Core and SOL of DIII–D," Bull. Am. Phys. Soc. **42**, 1921 (1997).

Wade, M.R., D.L. Hillis, K.H. Burrell, T.C. Luce, R. Maingi, P.K. Mioduszewski, C.C. Petty, W.P. West, R.-M. Hong, D.H. Kellman, J.C. Phillips, DIII–D Team, "Experimental Evidence for the Suitability of ELMing H–Mode Operation in ITER with Regard to Core Transport of Helium," in Proc. 16th Int. Conf. on Plasma Physics and Controlled Nuclear Fusion Research, October 7–11, 1996, Montreal, Canada, Vol. 1, p. 801 (International Atomic Energy Agency, Vienna, 1997); General Atomics Report GA-A22473 (1996).

Wade, M.R., T.C. Luce, C.C. Petty, "Gyroradius Scaling of Helium Transport," in Phys. Rev. Lett. **79**, 419 (1997); General Atomics Report GA-A22530 (1997).

Walker, M.L., D.A. Humphreys, J.R. Ferron, "Multivariable Shape Control Development on the DIII–D Tokamak," in Proc. 17th IEEE/NPS Symp. on Fusion Engineering, October 6–11, 1997, San Diego, California (Institute of Electrical and Electronics Engineers, Inc., Piscataway, New Jersey, to be published); General Atomics Report GA-A22729 (1997).

Watkins, J.G., D.N. Hill, S.L. Allen, R. Maingi, R.A. Moyer, R. Lehmer, J.A. Boedo, C.M. Greenfield, "Comparison of Open and Closed Divertor Conditions in DIII–D," Bull. Am. Phys. Soc. **42**, 1920 (1997).

Watkins, J.G., R.A. Moyer, J.W. Cuthbertson, D.A. Buchenauer, T.N. Carlstrom, D.N. Hill, M. Ulrickson, "Reciprocating and Fixed Probe Measurements of Density and Temperature in the DIII–D Divertor," in J. Nucl. Mater. **241-243**, 645 (1997); General Atomics Report GA-A22362 (1996).

West, W.P., S.L. Allen, N.H. Brooks, D.A. Buchenauer, T.N. Carlstrom, J.W. Cuthbertson, E.J. Doyle, T.E. Evans, M.E. Fenstermacher, D.N. Hill, A.W. Hyatt, R.C. Isler, G.L. Jackson, R.A. Jong, C.C. Klepper, C.J. Lasnier, A.W. Leonard, M.A. Mahdavi, R. Maingi, G.R. McKee, W.H. Meyer, R.A. Moyer, D.G. Nilson, T.W. Petrie, G.D. Porter, T.L. Rhodes, M.J. Schaffer, R.D. Stambaugh, D.M. Thomas, S.N. Tugarinov, M.R. Wade, J.G. Watkins, D.G. Whyte, R.D. Wood, "Divertor Plasma Studies on DIII–D — Experiment and Modeling," in Plasma Physics and Controlled Fusion **39**, A295 (1997); General Atomics Report GA-A22461 (1996).

West, W.P., DIII–D Divertor Team, "Carbon Pathways to the Core Plasma in DIII–D," Bull. Am. Phys. Soc. **42**, 1919 (1997).

Whyte, D.G., J.N. Brooks, C.P.C. Wong, W.P. West, R.J. Bastasz, W.R. Wampler, J. Rubinstein, "DiMES Divertor Erosion Experiments on DIII–D," in J. Nucl. Mater. **241-243**, 660 (1997); General Atomics Report GA-A22342 (1997).

Whyte, D.G., T.E. Evans, A.G. Kellman, D.A.. Humphreys, A.W. Hyatt, T.C. Jernigan, R.L. Lee, S.L. Luckhardt, P.B. Parks, M.J. Schaffer, P.L. Taylor, "Energy Balance, Radiation and Stability During Rapid Plasma Termination Via Impurity Pellet Injections on DIII–D," in Proc. 24th European Conf. on Controlled Fusion and Plasma Physics, June 9–14, 1997, Berchtesgaden, Germany, Vol. 21A, Part III, p. 1137 (European Physical Society, 1997); General Atomics Report GA-A22639 (1997).

Whyte, D.G., M.R. Wade, D.F. Finkenthal, K.H. Burrell, P. Monier-Garbet, B.W. Rice, D.P. Schissel, W.P. West, R.D. Wood, "Measurement and Verification of Z_{eff} Radial Profiles Using Charge Exchange Recombination Spectroscopy on DIII–D," to be published in Nucl. Fusion; General Atomics Report GA-A22601 (1997).

Wolf, N.S., M.E. Rensink, G.D. Porter, M.E. Fenstermacher, D.N. Hill, "Modeling the Effect of Divertor Geometry on Radiative Divertor Plasma in DIII–D," Bull. Am. Phys. Soc. **42**, 1919 (1997).

Wong, C.P.C., R.J. Bastasz, D.G. Whyte, W.R. Wampler, W.P. West, "Results from the Divertor Materials Evaluation Studies (DiMES) at DIII–D," in Proc. 12th Top. Mtg. on The Technology of Fusion Energy, June 16–20, 1996, Reno, Nevada, Vol. 30 (3), Part 2A, p. 694 (American Nuclear Society, La Grange Park, Illinois, 1996); General Atomics Report GA-A22392 (1996).

Wood, R.D., S.L. Allen, M.E. Fenstermacher, D.N. Hill R.C. Isler, A.W. Leonard, W.P. West, "Measurements of Divertor Radiated Power Losses in the 170–1700 Å Spectral Region on DIII–D," Bull. Am. Phys. Soc. 42, 1844 (1997).